Volume 7, September 2023

AOFPR

Asian and Oceanic Forum for Paediatric Radiology

CONTENTS

CONTENTS

From the Guest Editors

Bernard F. Laya[1], Maria Lourdes B. Lacanilao[2], Maria Theresa T. Sanchez[3], Nathan David P. Concepcion[4], Joanna Marie D. Choa-Go[5]

It is a great honor for the Philippines to be the host country for the 7th issue of the Asian and Oceanic Forum for Paediatric Radiology (AO*f*PR). This is the second time that the Philippines is given such an opportunity, following a successful issue in February 2016.

Although Pediatric Radiology is already a well-established subspecialty in western nations and progressive Asian countries, it is still in its formative years in the Philippines. In spite of this, local Pediatric Radiology practitioners continue to raise the level of pediatric medical imaging. In June 25, 2017, the Philippine Society for Pediatric Radiology (PSPR) was born with the goal of enhancing healthcare of children through education, standardization of practice, and promotion of quality and safe imaging practices. This is made possible through PSPR's collaboration with the mother organization, the Philippine College of Radiology (PCR), as well as PCR local chapters including PCR-Southern Mindanao Chapter (PCR-SMC).

The Philippines hosted the Asian and Oceanic Society for Pediatric Radiology (AOSPR) Congress back in 2012. The city of Davao in the Philippines would have been the site of the AOSPR Congress 2020, but was hindered by the COVID-19 pandemic. Nevertheless, we were delighted that after 10 years, an opportunity to host the 20th AOSPR Congress on August 19-20, 2022 was again granted. This was a landmark event, being the first virtual AOSPR Congress due to the said pandemic. Once again, this was made possible through the joint efforts of the PSPR and PCR-SMC, with the support of the PCR. The theme was "Unifying Pediatric Clinical Imaging Across Asia and Oceania," with the aim of disseminating appropriate imaging practice standards, not only to radiologists, but also to clinicians.

[1] Immediate Past President, Philippine Society for Pediatric Radiology (PSPR)

[2] Immediate Past President, Philippine College of Radiology (PCR)

[3] Board Member, PCR, and Immediate Past President, PCR – Southern Mindanao Chapter, Inc.

[4] President, PSPR, and guest lay-out artist

[5] Board Member, PSPR

Following the theme of the 20th AOSPR Congress, the 7th issue of AO*f*PR features carefully selected articles that promote utilization of various imaging tools and techniques in diverse clinical applications. This was especially designed in order to cater to a wide range of participants, including Pediatric Radiology subspecialists, General Radiologists, Radiology trainees, and Clinicians.

In this issue of AO*f*PR, Dr. Mariaem Andres and colleagues give us a glimpse of what transpired during the 20th AOSPR Virtual Congress in the Philippines. The Pediatric Radiology Quiz, given by Dr. Jacqueline Austine Uy, is presented as an article in this issue. We also featured the three winning scientific papers presented during the AOSPR research competition, namely: "Challenges in

Diagnosis and Management of Pediatric Presacral Tumors: A Radiologist's Perspective" by Dr. Ebinesh from India; "Clinical Utility of the Diffusion Weighted Imaging (DWI) Ratio in Characterizing Primary Brain Neoplasms in Pediatric Patients: A 5-year Retrospective Study in a Tertiary Hospital in the Philippines" presented by Dr. Sheen Urquiza; and "Association between Germinal Matrix Hemorrhage at the First Week of Life and Perinatal Factors of Preterm Neonates" by Dr. Adrian Christopher Elio from the Philippines. In addition, we included research articles by Dr. Jerald Lim and colleagues entitled, "Chest Ultrasound and Contrast-enhanced CT in Detecting Pediatric TB Mediastinal Lymphadenopathy" as well as Dr. Karl Solidum and co-authors on "Pulmonary Imaging Findings of the Pediatric Novel Coronavirus Disease (COVID-19) in Two Tertiary Centers in the Philippines." Three local case reports were also included: (1) Dr. Florelyn Agravante and colleagues on the "Multi-modality Approach to an Adolescent Scrotal Arteriovenous Malformation", (2) Dr. Gia Marie Nicolasora and co-author on the "Intrathoracic Renal Ectopia with Congenital Diaphragmatic Hernia" and (3) Dr. Alexandra Rama-Estimo on the "Neonate presenting with Multiple Cardiac Masses". Lastly, a commentary by Dr. Justin Luke Yap was added, and entitled, "The Pediatric Radiology Journey of Northern Mindanao, Philippines: Insights and Experiences."

As the guest Editorial Team from the Philippines, we are thankful to the AOSPR leadership and the AO*f*PR Editorial Board for this wonderful opportunity. We would also like to thank all the contributing authors as well as Drs. Ronald de Castro, Cyrus Estrera and Princess Dawn Ybañez for this issue's cover art, without whom this issue would not be possible.

We hope that the articles in this AO*f*PR issue would be beneficial to all its readers.

Unifying Pediatric Clinical Imaging Practice Across Asia and Oceania: The 20th Virtual Annual Scientific Meeting of the Asian and Oceanic Society for Paediatric Radiology

Mariaem M. Andres[1,2,3], Joanna Marie D. Choa-Go[4,5,6], Nathan David P. Concepcion[1,2]

The Asian and Oceanic Society for Paediatric Radiology (AOSPR) is a society of Pediatric Radiologists in the Asian and Oceanic region stretching from Turkey and Jordan in the West, to Korea, Japan, Australia, New Zealand and the Philippines in the East, covering all countries in between. The Society aims to establish close ties with the many regional national societies and maintain close ties with the international Pediatric Radiology community. AOSPR is dedicated in promoting the Pediatric Radiology practice in the region and improve healthcare standards in the imaging of children through cooperative research, teaching and education.

The Annual AOSPR Congress has always been held face-to-face in various countries in the Asia-Oceania Region since the year 2000. However, due to the prevailing pandemic, the 2022 event was held virtually. The hosts of the AOSPR 2022 Congress were the Philippine Society for Pediatric Radiology (PSPR) and Philippine College of Radiology - Southern Mindanao Chapter (PCR-SMC), with support from the AOSPR and Philippine College of Radiology (PCR).

[1] Section of Pediatric Radiology, Institute of Radiology, St. Luke's Medical Center – Global City, Philippines

[2] Section of Pediatric Radiology, Institute of Radiology, St. Luke's Medical Center – Quezon City, Philippines

[3] Department of Radiology, St. Luke's Medical Center College of Medicine - William H. Quasha Memorial, Philippines

[4] Department of Radiology, The Doctors' Hospital, Inc., Bacolod City, Negros Occidental, Philippines

[5] Department of Diagnostic Imaging and Radiologic Sciences, Corazon Locsin Montelibano Memorial Regional Hospital, Bacolod City, Negros Occidental, Philippines

[6] Department of Radiology, University of St. La Salle College of Medicine, Bacolod City, Negros Occidental, Philippines

This two half-day academic activity with poster (Fig. 1) and theme, "*Unifying Pediatric Clinical Imaging Practice Across Asia and Oceania*", was held on August 19-20, 2022, comprising a mix of basic and advanced topics, which are meant to cater not only to pediatric radiology subspecialists and general radiologists, but also to clinicians, trainees, radiologic technologists and medical students.

The main objective is to promote and strengthen the practice of Pediatric Radiology in Asia and Oceania. The course also aimed to help standardize the practice by introducing recommended practice guidelines and algorithms in areas covered during the course, and to serve as an avenue for presenting and highlighting the advances in technology, resources, and capabilities pertaining to various imaging modalities in the pediatric population.

The congress was graced by the AOSPR President, Dr. Timothy Cain; PCR President, Dr. Imarzen V. Elepaño; PSPR President, Prof. Bernard F. Laya; PCR-SMC President, Dr. Maria Theresa T. Sanchez; and Immediate PCR President and Metro Davao Medical Society, Inc. (MDMSI) President, Dr. Maria Lourdes B. Lacanilao, who each gave their opening Keynote messages.

Fig. 1 Official poster of AOSPR 2022

THE EXPERTS AND THE AUDIENCE

AOSPR 2022 Virtual Congress was divided into four main sessions namely: Session 1 - Special Interest session moderated by Dr. Nathan David P. Concepcion (PSPR), Session 2 - Chest Imaging moderated by Drs. Ronald J. de Castro (PCR-SMC) and Mariaem M. Andres (PSPR), Session 3 - Gastrointestinal Imaging moderated by Drs. Maricar P. Reyes (PSPR) and Sagisag Dadap (PCR-SMC), and Session 4 - Genitourinary Imaging moderated by Dr. Maria Lourdes B. Lacanilao (PCR-SMC) and Prof. Bernard F. Laya (PSPR).

There was a total of 17 distinguished (15 international and two Filipino) pediatric imaging experts. Scientific presentations were delivered through a combination of lectures and case-based review, with emphasis on the importance of clinico-radiologic approach. The following were the guest speakers of AOSPR 2022 (Fig. 2) with their country of origin in parentheses and corresponding lecture topics:

Session 1 – Special Interest
Prof. Winnie Chu (Hong Kong) - Radiation Protection in Children;
Dr. Jaishree Naidoo (South Africa) - Artificial Intelligence in Pediatric Radiology
Prof. Dorothy Bulas (USA) - Advances in Fetal MRI
Prof. Kieran McHugh (UK) - Pitfalls in Pediatric Oncologic Imaging

Session 2 – Chest Imaging
Prof. Osamu Miyazaki (Japan) - Pediatric Chest Tumors
Prof. Pedro Daltro (Brazil) - Congenital Lung Malformations
Prof. Paul Guillerman (US) - Interstitial Lung Disease
Associate Prof. Supika Kritsaneepaiboon (Thailand) - Post-Operative Congenital Heart Disease

Session 3 – Gastrointestinal Imaging

Dr. Joanna Kasznia-Brown (UK) - Advanced Imaging of the Small Bowel
Prof. Yumin Zhong (China) - Appendicitis in Children: Ultrasound or CT?
Asst. Prof. Jeevesh Kapur (Singapore) - Jaundice in Children
Prof. Kushalhit Singh Sodhi (India) - Pancreatic Diseases in Children

Session 4 – Genitourinary Imaging

Dr. Angelo Don Grasparil II (Philippines) - Acute Pediatric Scrotal Abnormalities and Mimics
Prof. Hamzaini Abdul Hamid (Malaysia) - Imaging of UTI and Associated Anomalies in Children
Prof. Hye-Kyung Yoon (Korea) - Renal Masses and Mass-like Lesions

At the start of Session 4, a special feature was presented by Prof. Wendy Lam, MD (Hong Kong) on Radiographs to Photographs: Art and Hobbies as Expressions of Self Care; and before the closing ceremonies, Dr. Jacqueline Austine Uy (Philippines) discussed the answers of the Pediatric Radiology Quiz (*please see pages 52–59 of this volume*).

Fig. 2 Distinguished list of international and local Pediatric Radiologists

A total of 419 local (78%) and 136 delegates from various countries, 13% of which from Malaysia attended virtually. (Fig. 3)

Fig. 3 Distribution of attendees by country

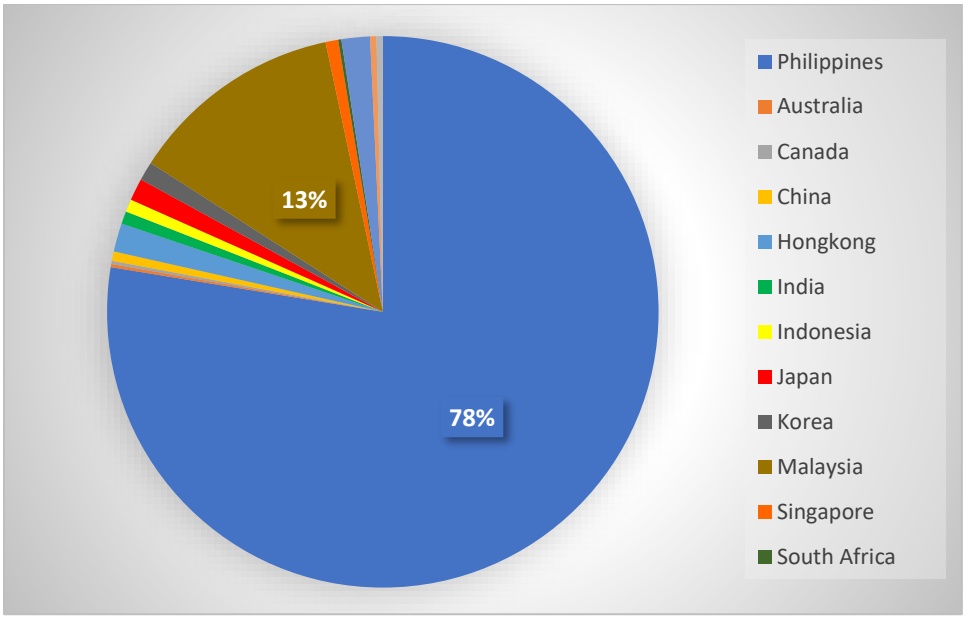

RESEARCH

A research competition was also held during the two-day event showcasing the varied cases and investigatory projects being conducted globally with regards to pediatric imaging. There were 21 papers accepted and designated as an oral (5) or poster (16) presentation based on the preliminary screening. Being a purely virtual platform, all poster submissions were electronic and the oral presentations were pre-recorded. The enthusiasm and creativity of the participants were well appreciated from the materials they have submitted to this congress.

Esteemed judges were invited to evaluate the submitted presentations. For the electronic scientific posters, the judges were Dr. Timothy Cain (Australia) as chairperson, Dr. Angela Villanueva (Philippines), and Dr. Ji Hye-Kim (Korea). For the oral paper presentation, the judges were Dr. Joanna Marie Choa-Go (Philippines) as chairperson, Dr. Nathan David Concepcion (Philippines), and Dr. Jaishree Naidoo (South Africa).

The 15 accepted poster presentations were made available for viewing in the AOSPR 2022 convention website during the event and were also presented briefly during the event itself. Only three pre-recorded oral paper presentations were submitted and shown during the first day of the conference, followed by a brief question-and-answer segment by the panel of judges.

The winners were announced by the chairperson of the research committee, Dr. Joanna Marie D. Choa-Go, during the closing ceremony. The winners of the research competition were the following:

ORAL PAPER PRESENTATION

First place: MR Imaging of the Neonatal Brain: Challenges, Perspectives, and Spectrum
Authors: Dr. A. Ebinesh A, Dr. A. Manchanda, Dr. R. Dixit, Dr. P. Das, Dr. G. Krishna, Dr. A. Kumar (India)

Second place: Clinical utility of the DWI ratio in characterizing primary brain neoplasms in pediatric patients: a 5-year retrospective study in a tertiary hospital in the Philippines
Authors: Dr. S. C. Urquiza, Dr. R. J. DL. Urgel, Dr. A. C. Camacho, Dr. R. E. Fragante (Philippines)

Third place: A series of pediatric presacral tumors with intraspinal extension: lessons from imaging
Authors: Dr. A. Ebinesh, Dr. A. Ashta, Dr. A. Prakash, Dr. A. Garg, Dr. P. Das (India)

ELECTRONIC SCIENTIFIC POSTERS

First place: Case Series: Synchronous Intracranial Atypical Teratoid/Rhabdoid Tumor (AT/RT) and Extracranial Malignant Rhabdoid Tumor
Authors: Dr. S. H. Ramli, Dr. C. Z. C. Daud, Dr. N. M. Said (Malaysia)

Second place: Tuberculous Immune Reconstitution Inflammatory Syndrome (TB-IRIS) in an Immunocompetent Child: A Case Report.
Authors: Dr. F. N. M. Nasir, Dr. C. Z. C. Daud (Malaysia)

Third place: Association between germinal matrix hemorrhage at the first week of life and perinatal factors of preterm neonates born at St. Luke's Medical Center
Authors: Dr. A. C. A. Elio and Dr. M. M. Andres (Philippines)

ORGANIZING COMMITEE

The Organizing Committee was composed of board members of the PCR-SMC and PSPR as well as IdeaHub IT Solutions Provider and residents of St. Luke's Medical Center.

Chairpersons	Maria Lourdes B. Lacanilao, MD Prof. Bernard F. Laya, MD, DO Maria Theresa T. Sanchez, MD
Scientific Programme	Prof. Bernard F. Laya, MD, DO
Ways and Means	Maria Theresa T. Sanchez, MD
Marketing and Promotions	Maria Lourdes B. Lacanilao, MD Mariaem M. Andres, MD
Registration	IdeaHub IT Solutions Provider
Continuing Professional Development	Mariaem M. Andres, MD
Research	Joanna Marie D. Choa-Go, MD Nathan David P. Concepcion, MD

Certificates and Awards	Marl Andrew B. Valdez, MD
Digital Art Directors	Kevin Ryan T. Yu, MD Joseph Marce P. Baluyut, MD Kevin Carlyle S. Vivar, MD

AOSPR 2022 organizing committee gratefully acknowledges and greatly appreciates the educational support of the following sponsors: Fujifilm, Elan Vita Diagnostic Solutions, IDSMed Philippines, Josmef Enterprises, Dryws Enterprise, Berovan Marketing, Medilines, Robustan, Arcorp Medical Enterprises, RBJ Comtrex and Shimadzu.

ORIGINAL ARTICLE

Concordance of Chest Ultrasonography with Contrast-Enhanced Chest Computed Tomography in the Detection of Mediastinal Lymphadenopathy among Pediatric Patients Clinically Diagnosed with Tuberculosis

Jerald Garvin S. Lim[1], Mariaem M. Andres[1], Marion O. Sanchez[2], Agnes R. Mendoza[2], Lady Anarose I. Regala[2], Bernard F. Laya[1]

ABSTRACT

Objective:
To determine the agreement of chest sonography with contrast-enhanced chest computed tomography scan in the detection of mediastinal lymphadenopathy in children with clinically diagnosed tuberculosis (TB)

Design setting and participants:
Twelve patients (5 females and 7 males) with age range of 8–17 years old, and with clinically diagnosed TB disease were prospectively recruited and underwent chest ultrasound using standard sonographic protocol. Computed tomography (CT) was used as gold standard to confirm the presence of mediastinal lymphadenopathy. The images were interpreted blindly by two pediatric radiologists.

Results:
Sonographic zones showing the highest concordance with CT include those taken in the transverse suprasternal and left parasternal views namely, zones B (prevascular/left upper paratracheal, 91.7%), C (subaortic/AP window, 100%), G (prevascular, 100%) & H (pericardial, cardiophrenic, 100%). The sonographic zones that show lower concordance are zone A (83.3%), as well as those taken in the suprasternal oblique views namely, zone E (retrotracheal, 75%) and zones D (prevascular) and F (retrotracheal/subcarinal), both at 83.3% concordance. Overall, the level of agreement of ultrasound findings with CT findings is moderate (89.6%, 95% CI Concordance = [0.835, 0.957] Cohen's Kappa = 0.535), and was statistically significant.

Conclusion:
Chest sonography shows moderate agreement with CT in detecting mediastinal lymphadenopathy in children with TB. Ultrasound may be used as an initial tool to detect enlarged lymph nodes in children clinically diagnosed with TB and to assess for disease progression.

[1] Institute of Radiology, St. Luke's Medical Center, Philippines

[2] Institute of Pediatrics & Child Health, St. Luke's Medical Center, Philippines

Corresponding Author:
Jerald Garvin S. Lim, MD
Institute of Radiology, St. Luke's Medical Center
279 E. Rodriguez Sr. Ave., Quezon City, Philippines
Email: *jgslim@stlukes.com.ph*

INTRODUCTION

Tuberculosis (TB) remains to have a significant burden worldwide. In 2015, the World Health Organization (WHO) declared TB to be responsible for more deaths than any other single infectious disease [1]. Children are included among the high-risk groups for developing TB and often pose a challenge to the clinicians in making a definitive diagnosis. Despite the global drop in the number of newly diagnosed TB cases as reported by the recent 2021 WHO report, children still accounted for 8% of all TB cases. The Philippines remains to be in the top 30 list of countries with high disease burden, which constitutes 6% of the total global TB cases [2].

On chest radiography, mediastinal lymphadenopathy with or without parenchymal involvement is the single most important diagnostic feature [3] and is regarded as the radiological hallmark of primary TB. Lymphadenopathy is also the most common abnormality noted in children with primary TB. However, this is not pathognomonic of TB because other infectious processes can also present with lymphadenopathy [4].

Marcet et al. generally recommend pediatric patients with a positive tuberculin skin test to undergo a chest radiographic study and mediastinal sonography. If both examinations are unrevealing, no additional imaging studies are needed. If radiographic findings are inconclusive and sonography is normal or confirms the presence of a hyperplastic thymus, no other diagnostic studies are needed [5]. In another study done in 2004 wherein they compared ultrasound with plain radiography and computed tomography scan for the detection of mediastinal TB lymphadenopathy in children [6], it showed that in 90.5% of children with chest x-ray images compatible with TB, coincident findings were also found in the mediastinal ultrasound study. In those with normal chest radiography, 66.7% had evidence of mediastinal lymphadenopathy on ultrasound. In all cases but one, ultrasound and computed tomography (CT) findings agreed. They concluded that mediastinal US is useful for the detection of enlarged lymph nodes in children with a positive tuberculin reaction and normal chest radiography.

In a study by Wernecke et al. in 1990, different proportion of diagnostic sonographic examinations varied for the different mediastinal compartments ranging from 85% (subcarinal region) to as high as 96% (supraaortic region). These results showed that sonography is superior to chest radiography in the diagnosis of mediastinal tumors. In certain mediastinal regions (supraaortic, pericardial, prevascular, and paratracheal), sonography was found to be more sensitive than that of CT [7]. Several more recent literatures depict that chest CT with contrast is the measure modality of choice to adequately assess mediastinal lymphadenopathies and/or masses and that chest sonography has good concordance with chest CT in detecting mediastinal lymphadenopathies.

However, sonography has limitations in assessing hilar involvement, because the hilum is surrounded by air in the lungs. Other limitations of using ultrasound include operator dependence and subjectivity, but these can be overcome with experience and procedure standardization [8]. Evaluation of primary progressive TB remains to be a combination of clinical, laboratory and imaging parameters. CT with contrast remains to be the gold standard and superior to all other imaging modalities in the detection of mediastinal lymphadenopathies, which is the imaging hallmark of primary progressive TB. The objective of this study is to determine the agreement of chest sonography with contrast-enhanced chest CT in the detection of mediastinal lymphadenopathy in children with clinically diagnosed TB disease.

METHODS

The legal guardians of all subjects participated voluntarily, and the participants/ representatives have provided written informed consent to participate in this study. This study was approved by the Institutional Review Board.

Eligible children aged 5–17 years old with clinical manifestations of TB (suspects/newly diagnosed untreated Category III pulmonary TB) who were referred for Chest CT for the evaluation of TB were prospectively enrolled. Such population was chosen since children in this age group can follow simple instructions, thereby waiving the need for sedation.

Children who have history of exposure to a patient with known active TB disease, positive Mantoux / tuberculin skin test, signs and symptoms suggestive of TB and/or abnormal chest X-ray were included. Meanwhile, children who were referred for other primary causes such as blood dyscrasia, autoimmune disease, other infections, neoplasms or who has moderate to high risk of developing iodinated contrast-media adverse reaction (e.g. renal disease/abnormal creatinine, allergy to contrast, food or medication allergy, asthma, congestive heart failure, thyroid disease, diabetes, seizure disorder, sickle cell trait and any pre-existing medical problem) were excluded in the study.

Prior to the CT procedure, serum creatinine and calculation of estimated glomerular filtration rate (eGFR) were obtained from all the participants to ensure adequate renal function. Computed tomography was performed on Siemens Somatom Force dual-source, dual-energy CT system. CT settings were adjusted to a low mAs and kVP, with less than 1 mm collimation, single breath hold and fast table speed. Scanning was performed from thoracic apex to the upper abdomen with ultra-high pitch and kVp of 120 (for body weight of more than or equal to 20 kg) and automated mAs. Non-ionic iodinated contrast media was administered at a dose of 1.2 cc/kg. Study was sent to a picture archive and communication system (PACS) for storage and interpretation.

The reference standard for the primary analysis was the presence of enlarged lymph nodes in chest CT, taken as any node measuring more than 1 cm in transverse or short axis dimension.

After performing the CT procedure, patients proceeded to ultrasound. A grey-scale and color doppler ultrasound machine (Hitachi Hi Vision Preirus) was utilized with small aperture phased array transducer having a center frequency of approximately 7.5 MHz (5.0 – 8.8 MHz) to access the mediastinum through the window of the suprasternal notch and the intercostal space left of the sternum. An experienced pediatric radiologist performed the ultrasound study, and the techniques are adapted from the study of Pool et. al. that was published in 2017 [9].

The four-view technique used the thymus as the acoustic window in all four predefined zones. The first predefined zone is noted in the transverse suprasternal view (Figs. 1–3) labeled as Zones A, B and C. Zone A is anterior to the right and left brachiocephalic vein within the thymic region, Zone B is seen between the left brachiocephalic vein and the aorta, while Zone C is between the aorta and the pulmonary trunk. The second predefined zone is obtained at the oblique suprasternal view (Fig. 4), and are labeled as Zone D, which is anterior to the left brachiocephalic vein within the thymic region, Zone E which is lateral to the arch of the aorta and posterior to the left subclavian artery, and Zone F is seen inferior and posterior to the aortic arch. The third predefined zone is seen at the transverse left parasternal view (Fig. 5) as represented by Zone G, which is anterior and to the left of the pulmonary trunk within the thymic region. The fourth predefined zone is identified in the longitudinal left parasternal view (Fig. 6), depicted as Zone H, which is seen at the anterior and to the left of the right atrium and ventricle within the thymic region.

The imaging studies were independently reviewed by two pediatric radiologists who are at least 8 years in practice. The official results of both ultrasound and CT were forwarded to the attending pediatrician's clinic for proper management.

Statistical analysis using SPSS software was utilized. Concordance rate (number of positive and negative concordance) using number and percent (%) with 95% confidence interval (CI) was calculated. Agreement between ultrasound and CT was measured using Kappa correlation coefficient.

RESULTS

A total of 12 patients (5 girls and 7 boys) were included with age ranging from 8 years old to 17 years old, with mean age of 11 years old (Table 1). 7 of 12 patients have 100% concordance rate, while 2 patients have only 5 of 8 concordant zones (Table 2).

Table 1 Descriptive statistics: Patient profile

Profile	Frequency	Percentage
Age (in years)		
8	2	16.7
9	4	33.3
10	2	16.7
12	1	8.3
15	1	8.3
17	2	16.7
Sex		
Female	5	41.7
Male	7	58.3
TOTAL	**12**	**100.0**

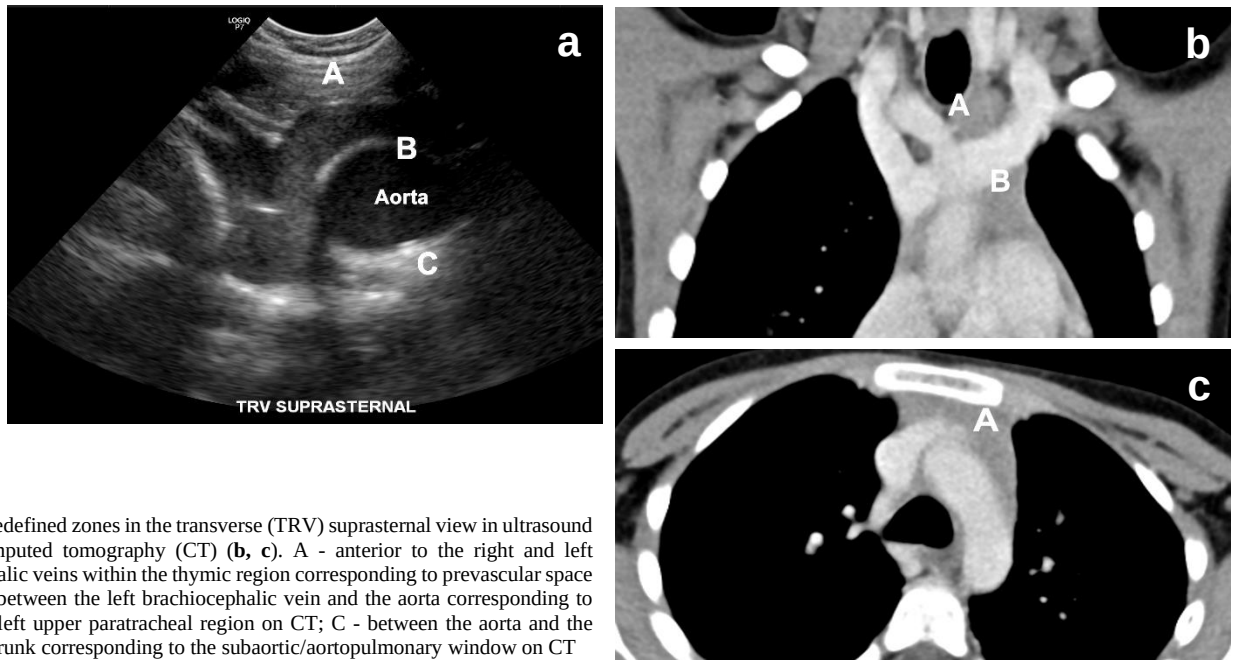

Fig. 1a-c Predefined zones in the transverse (TRV) suprasternal view in ultrasound (**a**) and computed tomography (CT) (**b, c**). A - anterior to the right and left brachiocephalic veins within the thymic region corresponding to prevascular space on CT; B - between the left brachiocephalic vein and the aorta corresponding to prevascular/left upper paratracheal region on CT; C - between the aorta and the pulmonary trunk corresponding to the subaortic/aortopulmonary window on CT

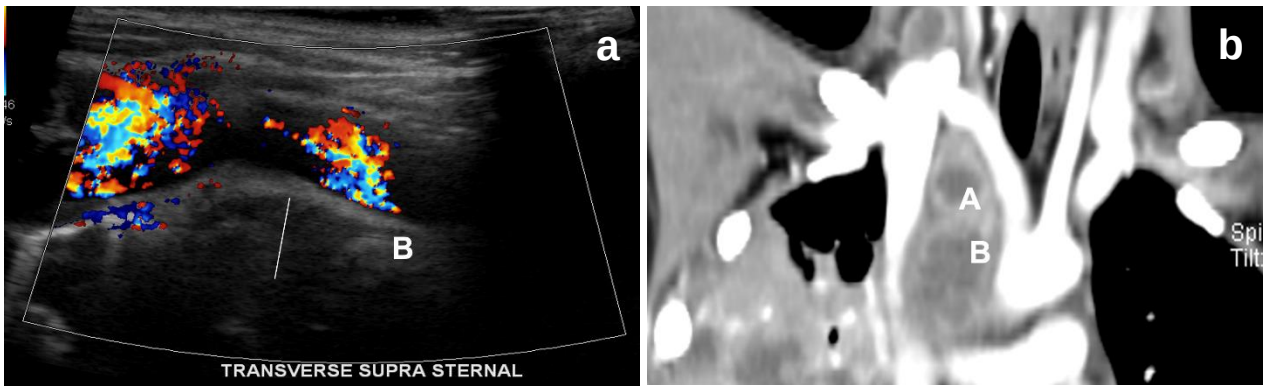

Fig. 2a–b Predefined zones in the transverse suprasternal view in ultrasound (**a**) and computed tomography (**b**). An enlarged lymph node (white line behind the colored brachiocephalic veins) is noted in zones A & B, with corresponding coronal CT image in soft tissue window setting

Table 2 Descriptive statistics: per patient finding

Patient # (Age in years)	No. of Concordant Zones (total of 8)	Concordant Zones	Concordance Rate (%)
Patient 1 (17)	8	A to H	100
Patient 2 (17)	8	A to H	100
Patient 3 (9)	5	A, C, F to H	62.5
Patient 4 (9)	8	A to H	100
Patient 5 (9)	8	A to H	100
Patient 6 (8)	8	A to H	100
Patient 7 (10)	6	A to D, G, H	75.0
Patient 8 (9)	8	A to H	100
Patient 9 (15)	8	A to H	100
Patient 10 (10)	7	B to H	87.5
Patient 11 (8)	7	A to D, F to H	87.5
Patient 12 (12)	5	B, C, F to H	62.5

Concordance rate was computed (Table 3). In Zone A, 5 patients were found positive for mediastinal lymphadenopathy in CT, but only 3 were positive in ultrasound. All 7 patients that were found negative in CT were properly identified in ultrasound but 2 patients were classified as "false negatives". Hence, concordance rate was computed to be equal to 83.3% (CI: 62.2 to 100%). The level of agreement of ultrasound findings with CT findings in Zone A using Cohen's Kappa statistic was equal to 0.636, which is classified as "substantial agreement", and was found to be statistically significant.

In Zone B, 2 patients were found positive for mediastinal lymphadenopathy in CT, but only 1 of them were positive in ultrasound. All 10 patients that were found negative in CT were properly identified in ultrasound but 1 patient was classified as "false negative". Hence, concordance rate was computed to be equal to 91.7% (CI: 76 to 100%). The level of agreement of ultrasound findings with CT findings in Zone B using Cohen's Kappa statistic was equal to 0.625, which is classified as "substantial agreement", and was found to be statistically significant.

In Zone C, all twelve (12) patients were found negative for mediastinal lymphadenopathy in CT and all were also found negative in ultrasound. Hence, concordance rate was at 100% (12 of 12 patients).

In Zone D, 3 patients were found positive for mediastinal lymphadenopathy in CT, but only 1 of them were positive in ultrasound. All 9 patients that were found negative in CT were properly identified in ultrasound but 2 patients were classified as "false negatives". Hence, concordance rate was computed to be equal to 83.3% (CI: 62.2 to 100%). The level of agreement of ultrasound findings with CT findings in Zone D using Cohen's Kappa statistic was equal to 0.429, which is classified as "moderate agreement", but was found to be not statistically significant.

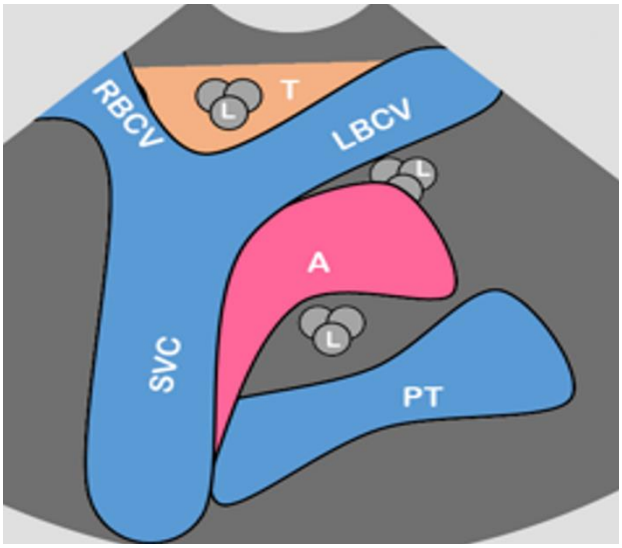

Fig. 3 Predefined zones in the transverse suprasternal view in ultrasound. A - aortic arch; L - lymph node; LBCV - left brachiocephalic vein; PT - pulmonary trunk; RBCV - right brachiocephalic vein; T - thymic region

Table 3 Zone A: Agreement of ultrasound (US) findings with computed tomography (CT) findings. * - not significant; † - significant at 5%; ‡ - significant at 1%

	US Zones	CT		Statistics
		Positive	Negative	
A	Positive	3	0	Concordance Rate = 83.3% 95% CI [0.622, 1.000]
	Negative	2	7	Cohen's Kappa = 0.636†
B	Positive	1	0	Concordance Rate = 91.7% 95% CI [0.760, 1.000]
	Negative	1	10	Cohen's Kappa = 0.625†
C	Positive	0	0	Concordance Rate = 100.0% 95% CI [1.000, 1.000]
	Negative	0	12	Cohen's Kappa = n/a
D	Positive	1	0	Concordance Rate = 83.3% 95% CI [0.622, 1.000]
	Negative	2	9	Cohen's Kappa = 0.429*
E	Positive	0	0	Concordance Rate = 75.0% 95% CI [0.505, 0.995]
	Negative	3	9	Cohen's Kappa = n/a
F	Positive	0	0	Concordance Rate = 83.3% 95% CI [0.622, 1.000]
	Negative	2	10	Cohen's Kappa = n/a
G	Positive	1	0	Concordance Rate = 100.0% 95% CI [1.000, 1.000]
	Negative	0	11	Cohen's Kappa = 1.000‡
H	Positive	1	0	Concordance Rate = 100.0% 95% CI [1.000, 1.000]
	Negative	0	11	Cohen's Kappa = 1.000‡

In Zone E, 3 patients were found positive for mediastinal lymphadenopathy in CT, but none of them were positive in ultrasound. All 9 patients that were found negative in CT were properly identified in ultrasound but 3 patients were classified as "false negatives". Hence, concordance rate was computed to be equal to 75.0% (CI: 50.5 to 99.5%).

In Zone F, 2 patients were found positive for mediastinal lymphadenopathy in CT, but none of them were positive in ultrasound. All 10 patients that were found negative in CT were properly identified in ultrasound but 2 patients were classified as "false negatives". Hence, concordance rate was computed to be equal to 83.3% (CI: 62.2 to 100%).

In Zone G, 1 patient was found positive for mediastinal lymphadenopathy in CT, and this was also found positive in ultrasound. All 11 patients that were found negative in CT were also properly identified in ultrasound. Hence, concordance rate was computed to be equal to 100% (12 of 12 patients). The level of agreement of ultrasound findings with CT findings in Zone G using Cohen's Kappa statistic was equal to 1.000, which is classified as "perfect agreement", and was found to be statistically significant.

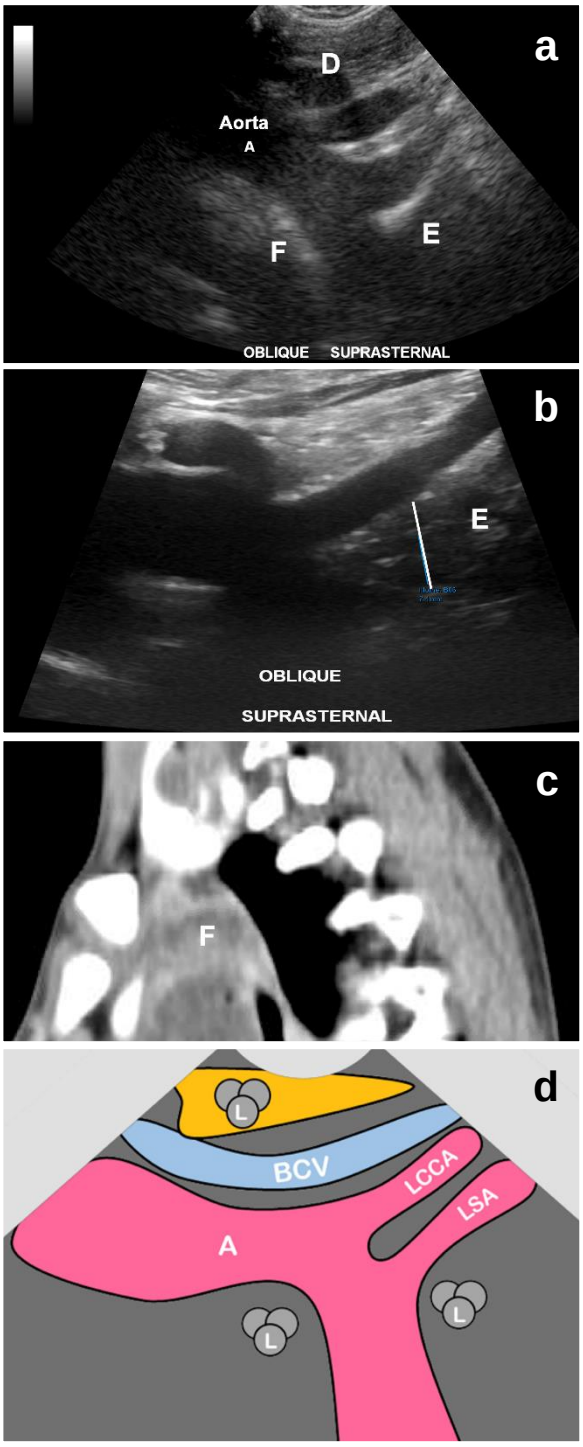

Fig. 4a–d Predefined zones in the oblique suprasternal ultrasound view (**a, b**), computed tomography (**c**) and in a schematic diagram (**d**). Enlarged lymph nodes are noted in a different patient (white line in **b**, and zone F in **c**). A - aortic arch; BCV - brachiocephalic vein; D - anterior to the left brachiocephalic vein within the thymic region corresponding to prevascular space; E - lateral to the arch of the aorta and posterior to the left subclavian artery corresponding to retrotracheal region; F - inferior and posterior to the aortic arch seen in the retrotracheal/subcarinal region; L - lymph node; LCCA - left common carotid artery; LSA - left subclavian artery

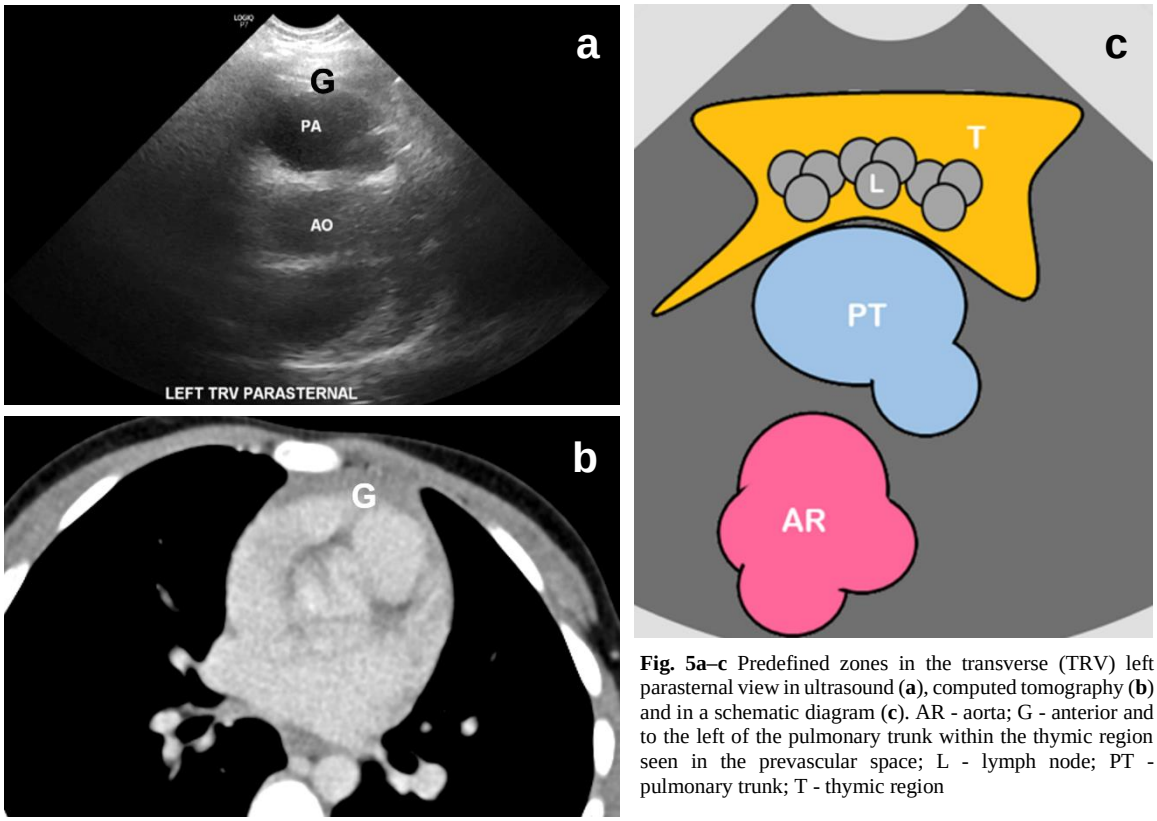

Fig. 5a–c Predefined zones in the transverse (TRV) left parasternal view in ultrasound (**a**), computed tomography (**b**) and in a schematic diagram (**c**). AR - aorta; G - anterior and to the left of the pulmonary trunk within the thymic region seen in the prevascular space; L - lymph node; PT - pulmonary trunk; T - thymic region

In Zone H, 1 patient was found positive for mediastinal lymphadenopathy in CT, and 1 was also found positive in Ultrasound. All 11 patients that were found negative in CT were also properly identified in Ultrasound. Hence, concordance rate was computed to be equal to 100% (12 of 12 patients). The level of agreement of ultrasound findings with CT findings in Zone H using Cohen's Kappa statistic was equal to 1.000, which is classified as "perfect agreement", and was found to be statistically significant.

The level of agreement of ultrasound findings with CT findings in Zone C, E, F using Cohen's Kappa statistic were not computed, due to insufficient information.

Overall (Table 4), 17 zones were found positive for mediastinal lymphadenopathy in CT, but only 7 of them were positive in ultrasound. All 79 zones that were found negative in CT were properly identified in ultrasound but 10 zones were classified as "false negatives". Hence, concordance rate was computed to be equal to 89.6% (CI: 83.5 to 95.7%).

Overall, the level of agreement of ultrasound findings with CT findings using Cohen's Kappa statistic was equal to 0.535, which is classified as "moderate agreement", and was found to be statistically significant.

Table 4. Overall agreement of ultrasound (US) findings with computed tomography (CT) findings. ***** - not significant; † - significant at 5%; ‡ - significant at 1%

	CT			Statistic
US	**Positive**	**Negative**	**TOTAL**	
Positive	7	0	**7**	Concordance Rate = 89.6.0%
Negative	10	79	**89**	95% CI [0.835, 0.957]
TOTAL	**17**	**79**	**96**	Cohen's Kappa = 0.535‡

DISCUSSION

In this cross-sectional study, the researchers determine the agreement of chest sonography with contrast-enhanced chest CT in the detection of mediastinal lymphadenopathy in children with clinically diagnosed TB. By adapting the standardized sonographic views developed by Pool et al. [9], the investigators were able to view the mediastinal lymph nodes and correlate to its corresponding CT planes. The sonographic zones showing the highest concordance with CT include those taken in the transverse suprasternal and left parasternal views namely, zones B (prevascular/ left upper paratracheal, 91.7%), C (subaortic/AP window, 100%), G (prevascular, 100%) & H (pericardial, cardiophrenic, 100%). The identification of these zones is most likely due to the accessibility of acoustic windows and lesser artifacts using the ultrasound techniques.

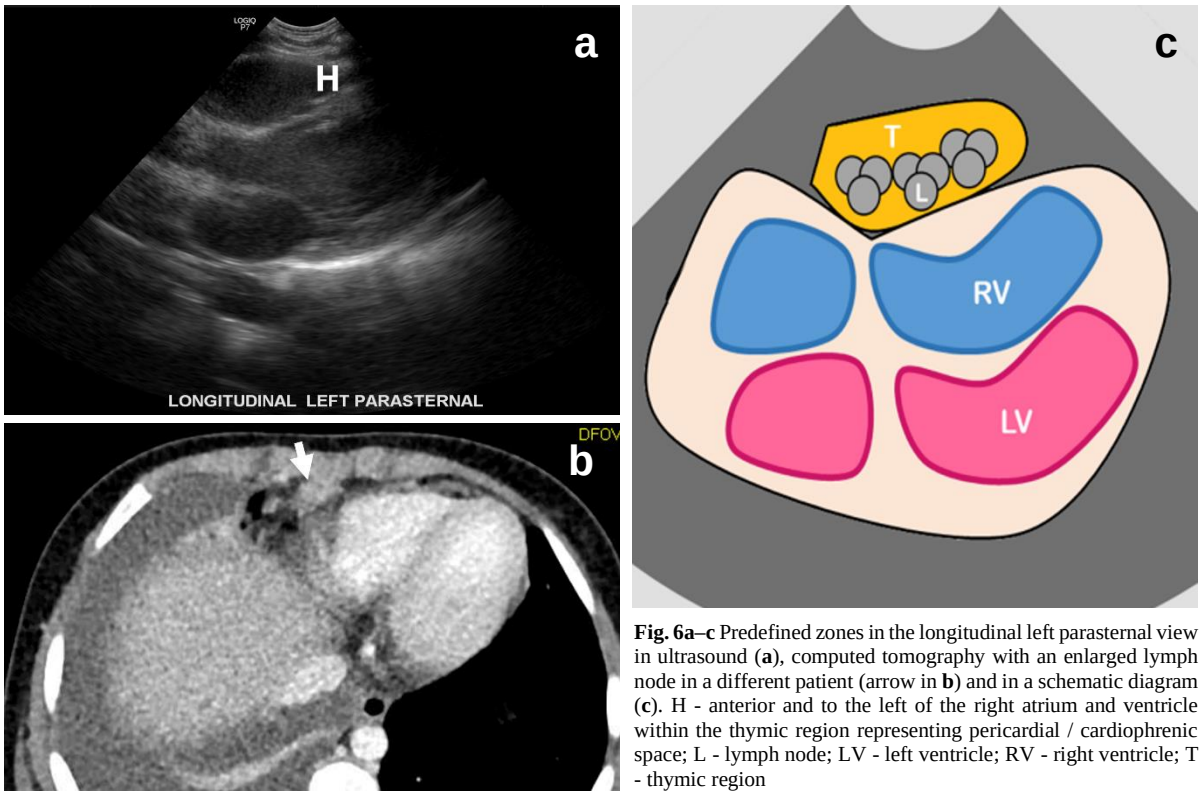

Fig. 6a–c Predefined zones in the longitudinal left parasternal view in ultrasound (**a**), computed tomography with an enlarged lymph node in a different patient (arrow in **b**) and in a schematic diagram (**c**). H - anterior and to the left of the right atrium and ventricle within the thymic region representing pericardial / cardiophrenic space; L - lymph node; LV - left ventricle; RV - right ventricle; T - thymic region

Meanwhile, sonographic zones which showed lower concordance include zone A (83.3%) as well as those taken in the suprasternal oblique views, namely, zone E (retrotracheal, 75%) and zones D (prevascular, 83.3%) and F (retrotracheal/subcarinal, 83.3%). These may be attributed to the limited views mostly due to poor acoustic window (zone D and zone A both corresponds to same prevascular spaces), deeper region of the mediastinum, and obscuration of the vascular landmarks in cases where lymph nodes are confluent and/or too large. Most of the discordant zones were negative on ultrasound but positive on CT. However, most of the positive findings on ultrasound were concordant with CT.

In a similar study by Wernecke [7] where ultrasound was compared with X-ray and CT for non-specific mediastinal masses, ultrasound also demonstrated high sensitivity at the paratracheal (89%), AP window (81%) and pericardial regions (100%), while ultrasound of the subcarinal region (69%) and posterior mediastinum (6%) also appears less sensitive. The prevascular (92%) space, meanwhile, yielded slightly higher sensitivity in the study.

Overall, the level of agreement of ultrasound findings with CT findings is "moderate" (89.6%), and was found to be statistically significant. This is congruent to the study done by Marcet [6] in a smaller group of six patients, which showed a concordance of (83.3%) between results of mediastinal ultrasonography and CT examination.

Despite the advances in modern medicine, diagnosis of childhood tuberculosis remains a challenge. The chest radiograph is one of the most commonly used tests in the diagnosis of TB, but it has its own inherent problems, as there is a high intra and inter-observer variability in interpretation of the radiograph. Furthermore, it is repeatedly stated in previous studies that although it achieves a moderate specificity of 74%, its sensitivity is low at 39% [10]. Computed tomography scan is an imaging tool with high accuracy and is considered the gold standard imaging test for primary pulmonary TB, capable of demonstrating abnormalities not readily seen in other imaging modalities [11, 12]. CT, however, is expensive and is not readily in low resource areas where TB is endemic. CT also poses radiation concerns especially in children.

The major factor encountered that decreased concordance of ultrasound findings with CT findings is obscuration of vascular landmarks (e.g., brachiocephalic vein, left common carotid and subclavian arteries) if the lymph nodes are too large or exhibits confluence. Operator expertise, dependence and subjectivity also come into play but may eventually be lessened with more experience.

A limitation of this study is its relatively small sample size. However, being a pilot study in the local setting, this can serve as a model for future research endeavors on this field.

CONCLUSION

Mediastinal ultrasound can be used as an initial imaging tool to detect enlarged lymph nodes in children clinically diagnosed with TB disease and to assess for progression. However, if found negative and clinically indicated, CT may still be done for further evaluation.

REFERENCES

1. Jenkins HE. Global Burden of Childhood Tuberculosis. Pneumonia (Nathan) 2016; 8.
2. World Health Organization, Global tuberculosis report 2013. ISBN: 978 92 4 156465 6
3. Mandal A, Sahi PK. Evaluation of Chest X-ray and Thoracic Computed Tomography in Patients with Suspected Tuberculosis: Correspondence. Indian J Pediatr 2017 Mar;84:254–5.
4. Concepcion ND, Laya BF, Andronikou S, Daltro PA, Sanchez MO, Uy JA, Lim TR. Standardized radiographic interpretation of thoracic tuberculosis in children. Pediatr Radiol 2017 Sep;47:1237–48.
5. Bosch-Marcet J, Serres-Créixams X, Borrás-Pérez V, Coll-Sibina MT, Guitet-Juliá M, Coll-Rosell E. Value of sonography for follow-up of mediastinal lymphadenopathy in children with tuberculosis. J Clin Ultrasound 2007 Mar;35(3):118–24.
6. Bosch-Marcet J, Serres-Créixams X, Zuasnabar-Cotro A, Codina-Puig X, Català-Puigbó M, Simon-Riazuelo JL. Comparison of ultrasound with plain radiography and CT for the detection of mediastinal lymphadenopathy in children with tuberculosis. Pediatr Radiol 2004 Nov;34:895–900.
7. Wernecke K, Vassallo P, Pötter R, Lückener HG, Peters PE. Mediastinal tumors: sensitivity of detection with sonography compared with CT and radiography. Radiology 1990 Apr;175(1):137–43.
8. Sodhi KS, Bhalla AS, Mahomed N, Laya BF. Imaging of thoracic tuberculosis in children: current and future directions. Pediatr Radiol 2017 Sep;47:1260–8.
9. Pool KL, Heuvelings CC, Andronikou S. et al. Technical aspects of mediastinal ultrasound for pediatric pulmonary tuberculosis. Pediatr Radiol 2017 Dec;47:1839–48.
10. De Villiers RV, Andronikou S, Van de Westhuizen S. Specificity and sensitivity of chest radiographs in the diagnosis of paediatric pulmonary tuberculosis and the value of additional high-kilovolt radiographs. Australas Radiol 2004 Jun;48(2):148–53.
11. Swaminathan S, Raghavan A, Datta M, Paramasivan CN, Saravanan KC. Computerized tomography detects pulmonary lesions in children with normal radiographs diagnosed to have tuberculosis. Indian Pediatr 2005;42(3):258–61.
12. Andronikou S, Joseph E, Lucas S, Brachmeyer S, Du Toit G, Zar H, Swingler G. CT scanning for the detection of tuberculous mediastinal and hilar lymphadenopathy in children. Pediatr Radiol 2004 Mar;34:232–6.

ORIGINAL ARTICLE

Pulmonary Imaging Findings of the Pediatric Novel Coronavirus Disease (COVID-19) in Two Tertiary Centers in the Philippines: A Local Experience

Karl Josef D. Solidum[1], Maria Angeline D.L. Nicandro[1], Rachel Q. Lacorte [2], Nathan David P. Concepcion[1,2]

ABSTRACT

Objective:
To describe the demographic and clinical profiles as well as the various pulmonary imaging findings of pediatric patients in St. Luke's Medical Center afflicted with SARS-CoV-2 infection (COVID-19)

Methods:
This descriptive, retrospective, cross-sectional study reviewed the hospital databases and pulmonary imaging studies of patients less than 19 years old who tested positive for SARS-CoV-2 infection based on viral RNA rt-PCR swab tests in St. Luke's Medical Center from March 1, 2020 to August 31, 2021.

Results:
A total of 196 patients were included in this study. The disease was most frequent in the adolescent age group (39%) with a slight male preponderance. Most common reported symptoms in decreasing order of frequency were cough, fever, and rhinorrhea. Leukocytosis and lymphopenia were the most common abnormal laboratory findings. 134 (68%) had normal chest radiograph findings. 62 patients (32%) were found to have abnormal radiographs with the most common showing bilateral ground-glass opacities.

Conclusion:
The majority of pediatric cases yielded normal chest radiograph findings and less extensive lung involvement, while those with abnormal radiographs most commonly showed bilateral ground-glass opacities. The results, along with the demographic and clinical profile in this population, are congruent with the findings in the literature. Through this study, further knowledge is gained on how the COVID-19 infection affects the pediatric population especially during the surge of cases in this time period. This also assesses the typical and atypical pulmonary imaging findings that radiologists and pediatricians should be aware of to ensure a prompt and accurate diagnosis.

Keywords: children, coronavirus infection, diagnostic imaging

[1] Institute of Radiology, St. Luke's Medical Center, Bonifacio Global City, Taguig, Philippines

[2] Institute of Radiology, St. Luke's Medical Center, Quezon City, Philippines

Corresponding Author:
Karl Josef D. Solidum, MD
Institute of Radiology, St. Luke's Medical Center
Rizal Drive cor. 32nd St. and 5th Ave., Taguig, Philippines
Email: *karlsolidum@gmail.com*

INTRODUCTION

Coronavirus disease 2019 (COVID-19) emerged in Wuhan, Hubei province, China in December 2019, and was caused by a novel coronavirus, since named severe acute respiratory syndrome - coronavirus 2 (SARS-CoV-2) [1]. SARS-CoV-2 is the seventh member of enveloped RNA coronavirus besides coronavirus 229E, OC43, NL63, HKU1, SARS-CoV and Middle East respiratory syndrome coronavirus (MERS-CoV) [2]. It is a highly infective disease which has rapidly spread all over the world, affecting both adults and children. The World Health Organization (WHO) declared the outbreak a global health emergency on January 3, 2020 [3]. Since then, the disease affected more than 177 countries globally [4].

Initially considered to primarily affect the elderly especially those with comorbidities, the virus has undergone several mutations over the subsequent several months with emerging variants that have become endemic to certain countries. In the late 2020 to mid-2021, more pediatric patients have been found to have been infected by the virus. It resulted in a spectrum of manifestations ranging from mild upper respiratory tract infection to severe pneumonitis, acute respiratory distress syndrome (ARDS), septic shock and even death [5]. Fortunately, the disease predominantly occurs in the milder end of the spectrum, with fewer symptoms in children compared to the adult counterparts [6,7]. The clinical presentation is non-specific, with the most common presenting symptoms including fever, cough, nasal congestion, and rhinorrhea [8-12].

Although the diagnosis of COVID-19 is primarily based on reverse transcription - polymerase chain reaction (rt-PCR) assay swab tests, imaging modalities including chest x-ray (CXR) and computed tomography (CT) are also used to detect abnormal lung changes [13]. The imaging features are diverse, ranging from normal to diffuse changes [14]. Because the time between onset of symptoms and the development of ARDS can be as short as 9 days among initial patients with COVID-19 pneumonia [15], early recognition of the disease is essential for the management of these patients.

While more data are emerging, the clinical presentation and course of COVID-19 as well as imaging findings in Filipino children remain poorly characterized since most reports in the literature dealt with foreign patients [16–21]. Knowledge of the imaging findings of COVID-19 is helpful in early detection of the disease process. Given the non-specific clinical presentation, imaging studies are likely to play an important role in diagnostic work-up for affected pediatric patients, especially in children with other co-morbidities such as congenital heart, lung and airway disease, malnutrition and tumors among others, who are vulnerable to severe infection [22].

The purpose of this study is then to describe the demographic and clinical characteristics of pediatric patients with COVID-19, as well as to characterize the different imaging findings among these patients. Given that this pandemic has been happening since the end of 2019, it has been observed that more cases have affected more pediatric patients in 2021. This therefore emphasizes the need for continued data gathering about the disease and to learn about any possible trend changes in the Philippine setting. Continuing surveillance is vital so that radiologists become aware of the latest updates on specific imaging findings to look for, especially since this viral disease continues to evolve. More importantly, this will also broaden the comprehension on how this disease affects the local pediatric population, and at the same time compare these findings to the relevant information being gathered in other countries.

METHODS

This was a descriptive, retrospective, cross-sectional study among pediatric cases from March 1, 2020 to August 31, 2021 in two tertiary hospitals in the Philippines. All patients less than 19 years old who tested positive for SARS-CoV-2 infection using the viral RNA rt-PCR test and who underwent chest imaging studies in this institution during the specified time period were included. Convenience sampling was utilized in this study.

Demographic data such as age and gender, type of imaging study performed, presenting signs and symptoms, pertinent laboratory findings and presence of co-morbidities were extracted from the hospitals' HealthCare System and Radiology Information System – Picture Archiving and Communication System (RIS-PACS). Patients were categorized by age into the following: newborn (<1 month), infant to toddler (1 month to <2 years), preschool child (2 years to <6 years), middle school child (6 years to <13 years) and adolescent (13 years to <19 years). These age categories were based from integrated age groups developed by Eunice Kennedy Shriver National Institute of Child Health and Human Development (NICHD) [23]. Pertinent complete blood count (CBC) findings were also collected.

The chest imaging findings were reviewed independently by pediatric radiology fellows-in-training, and a fellowship-trained pediatric radiologist practicing for 15 years, and a consensus was made if there is a discrepancy. These radiographs were assessed for certain findings such as lung parenchymal opacities including consolidation or ground-glass opacities, interstitial lung involvement and for pleural involvement.

Patients with incomplete medical records and those with suboptimal imaging studies, i.e. taken in obliquity, with motion artifact, and those with poorly visualized lungs, were excluded.

Categorical variables which include patient's demographic data, clinical presentation, and imaging findings were reported as frequency and percentage of findings among the study. Age was also reported as mean, median and interquartile range.

RESULTS

A total of 196 pediatric patients satisfied the criteria and were included in the study. Patient age ranged from newborn to 18 years old, with a mean age of 10 years and median age of 9 years (interquartile range, 5-16 years). COVID-19 was most frequently seen in the adolescent age group (n = 76/196, 39%), and slightly more in boys than girls with a male-to-female ratio of 1.4:1 (Table 1).

Table 1. Demographics of the 196 patients included in this study

Demographics	Frequency (n)	Percentage (%)
Age Distribution*		
Newborn (<1 month)	6	3
Infant to Toddler (1 mo. to <2 years)	29	15
Preschool to child (2 to 6 years)	31	16
Middle School (6 to 13 years)	54	28
Adolescent (13 to < 19 years)	76	39
Gender		
Male	116	59
Female	80	41

* Modified from integrated age groups developed by Eunice Kennedy Shriver National Institute of Child Health and Human Development (NICHD) [23]

Of the 196 pediatric patients, nine (4.5%) were asymptomatic, seven of which had known exposure to confirmed COVID-19 infected individuals, while the two had no known exposure but with recent history of trauma (Table 2). All asymptomatic patients had unremarkable chest radiographic findings.

The most common presenting symptoms were cough (44%), fever (41%) and nasal congestion or rhinorrhea (18%) (Table 2). Other symptoms that were manifested included ageusia, dyspnea, anosmia, sore throat, abdominal pain, and few with diarrhea, skin rashes, and headache/myalgia. There were no emergency warning signs for COVID-19 infection detected in any of the patients, such as cyanosis, inability to wake up, and swelling of the distal extremities [24].

Majority of the patients had no known co-morbidities (168/196, or 86%). The co-morbidities found among these cases were respiratory diseases (4) such as atypical Mycoplasma pneumonia, asthma and concomitant influenza A pneumonia, malignancy (3), heart disease (3), and prematurity (1). Others included one case each of seizure disorder, laceration, multiple fractures, arthrogryposis, and neuroleptic malignant syndrome. Six (3%) patients had concomitant dengue fever, one of which had the severe type, while the rest (5) had the mild form with no warning signs. Another six (3%) patients presenting with abdominal pain were found to have acute appendicitis (3) and mesenteric lymphadenitis (3). Chronic kidney disease and chronic liver disease, which are postulated to increase the risk for severe COVID-19 infection in pediatric patients [4, 23], were not recorded in this study.

Complete blood count (CBC) test was performed in 135 of 196 patients (69%), wherein 59 cases (43%) yielded normal results. The most common abnormal CBC findings were leukocytosis (33), lymphopenia (32), anemia (18), leukopenia (14), thrombocytosis (10), and thrombocytopenia (9). One patient with a known hematologic malignancy showed severe anemia with leukocytosis, lymphocytosis, and atypical mononuclear cells.

Table 2. Presenting symptom of the 196 cases

Presenting Symptom	Frequency (n)	Percentage (%)
Cough	86	44
Fever	80	41
Nasal congestion or rhinorrhea	36	18
Ageusia	25	13
Shortness of breath	23	12
Anosmia	20	10
Sore throat	9	4.5
Abdominal pain	8	4
Diarrhea	4	2
Skin rash	4	2
Headache	2	1
Muscle ache	1	1
Decreased sensorium	1	1
Asymptomatic	9	4.5

CHEST X-RAY FINDINGS

134 of 196 patients (68%) exhibited normal chest radiograph findings. The most frequent abnormal findings (Table 3) in decreasing order were bilateral ground-glass opacities (Fig. 1), subsegmental atelectasis or non-specific beginning pneumonia appearing as subtle haziness or linear opacities predominantly affecting one of the lower lobes (Fig. 2), air space consolidation or opacity, pulmonary hyperaeration, increased interstitial lung

markings with peribronchial cuffing, and minimal unilateral pleural effusion.

Table 3. Frequency of chest radiographic findings in the 196 patients

Findings	Frequency (n)	Percentage (%)
Bilateral ground-glass opacities	26	13
Subsegmental atelectasis or non-specific beginning pneumonia	17	9
a. Right upper lobe	2	1
b. Middle lobe	2	1
c. Right lower lobe	6	3
d. Left lower lobe	7	4
Air-space consolidation or opacity	9	5
a. Bilateral	4	2
b. Right lower lobe	3	1.5
c. Left lower lobe	2	1
Hyperaeration without focal opacities	6	3
Increased interstitial lung markings with peribronchial cuffing	3	2
Minimal pleural effusion, unilateral	2	1
Unremarkable	134	68

Fig. 1 A frontal view radiograph of a 5-year-old boy with known leukemia and COVID-19 shows ground-glass opacities and patchy consolidations in both lungs

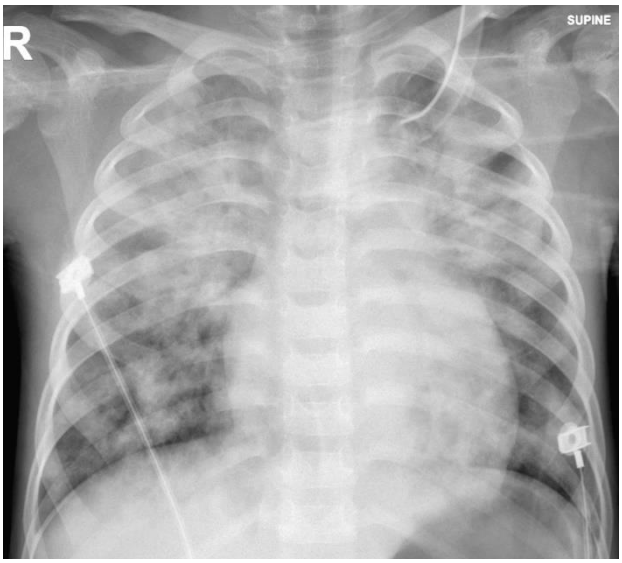

Among the 62 patients (32%) with symptoms and positive chest radiographic findings, 21 were adolescents, 14 infants, 14 middle-school children, 10 preschool, and 3 neonates. 12 patients had progression of the imaging findings. In these cases, fifty patients (81%) showed subsequent resolution or did not have any follow-up radiographs done in this institution.

Fig. 2 Two-year-old girl with confirmed coronavirus disease. Frontal view of the chest shows the atypical findings of atelectasis or beginning pneumonia (arrowheads) in the left lower lobe

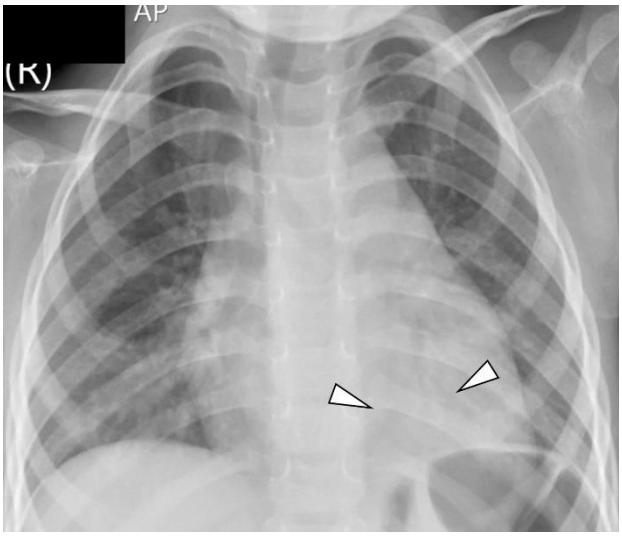

Among the remaining cases that had disease progression on follow-up x-ray, there were four notable patients worth mentioning in this paper. One adolescent, a 16-year-old boy, presented with difficulty of breathing. The chest radiograph initially showed hazy air-space and streaky lung opacities in both mid to lower lungs. Symptoms rapidly worsened and the patient was subsequently intubated. A chest CT scan was done which demonstrated multifocal bilateral ground-glass opacities and areas of consolidation in keeping with severe COVID-19 pneumonia possibly relating to acute respiratory distress syndrome (ARDS) (Fig. 3a–d).

Another 15-year-old boy, also with similar presentation of dyspnea, initially had diffuse hazy and confluent airspace opacities involving the middle and both lower lungs. Follow-up chest x-rays showed progression of these opacities, with subsequent development of minimal left-sided pleural effusion and pneumothorax. The patient was also categorized as having severe COVID-19 pneumonia with ARDS.

One patient, a 7-year-old girl, presented with decreased sensorium. Her complete blood count showed leukocytosis and lymphocytosis. Initial x-ray only showed minimal streaky opacities in the left retrocardiac region. Due to the altered level of consciousness, a brain MRI was also done which showed subtle frontoparietal leptomeningeal enhancement suggestive of an

inflammatory process. Follow-up chest radiographs only showed minimal progression of the lung disease. The patient was signed out with a diagnosis of COVID-19 infection with viral encephalopathy.

A 5-year-old boy known to have acute lymphocytic leukemia (ALL) presented with difficulty in breathing. His initial CXR showed patchy hazy opacities scattered in both lungs. The patient was intubated and had marked progression of the bilateral lung opacities on his subsequent radiographs. This patient eventually succumbed, and was the only casualty in this study.

DISCUSSION

Among the pediatric patients with coronavirus disease, majority belonged to the adolescent age group. This is similar to the data by Hasan, et al [4]. Increased incidence of COVID-19 was noted among male patients, with male-to-female ratio of 1.4:1, which is in close proximity to that from other previously published international studies from China by Dong and colleagues [25], and Lu and colleagues [26] with male-to-female ratio of 1.3:1 and 1.55:1, respectively.

Majority of the chest radiograph findings for children with COVID-19 were normal, as seen in 68% of 196 patients. This is likewise concordant with the single-center study done by Bayramoglu, et al. [27] wherein 81% of 69 patients had normal chest radiographs. These rates are also similar to the rates of normal chest CT findings in children with the same condition, as demonstrated in studies done by Steinberger and colleagues (77%) [28] and by Chen and colleagues (50%) [29]. Bayramoglu and colleagues analyzed the discrepancy between the findings on chest radiographs and chest CT studies of pediatric patients with COVID-19 and concluded that the majority of the causes for normal-appearing chest radiographs in COVID-19 infected patients with abnormal chest CT studies were attributed to low-density opacities, small-sized opacities, or basal opacities obscured by the diaphragm and hepatic dome on frontal chest radiographs [27].

Positive chest radiograph findings, such as nonspecific opacities suggestive of either subsegmental atelectasis or beginning pneumonia, and air-space consolidation or opacity, most frequently involved only one lobe. Among patients who demonstrated subsegmental atelectasis or beginning pneumonia, the lower lobes were the most commonly involved. According to the structured chest

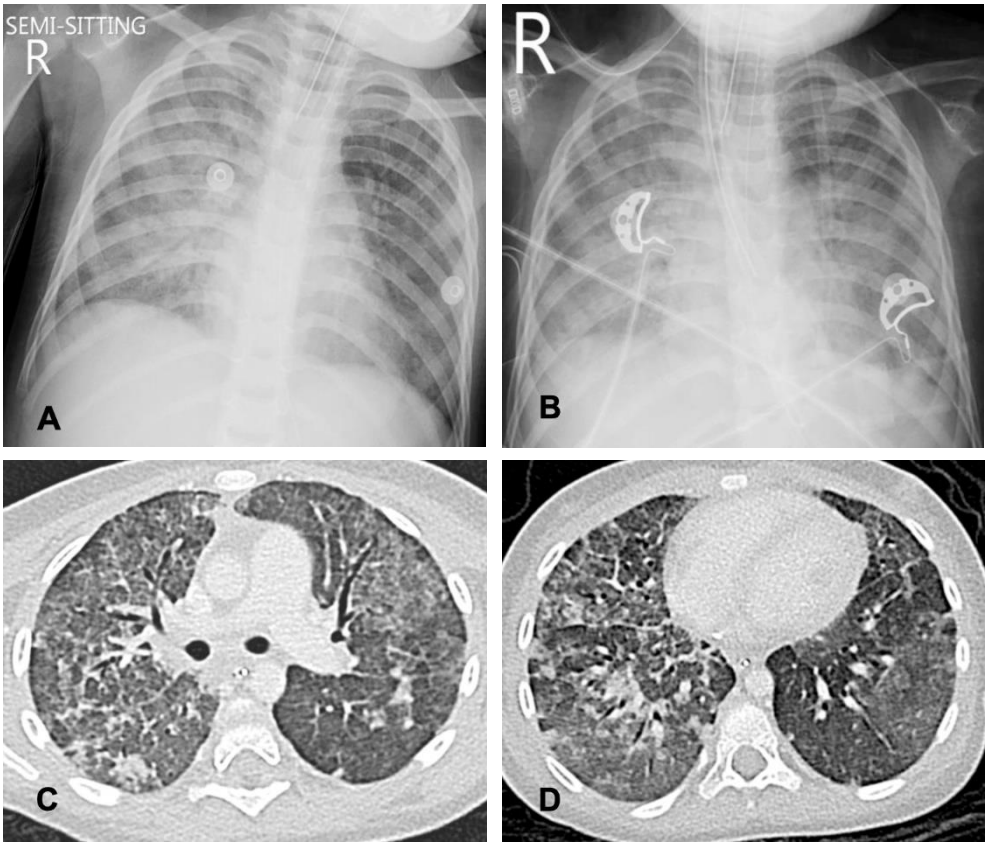

Fig. 3a-d Frontal view chest radiographs (**a**–**b**) and axial chest CT images in lung window setting (**c**–**d**) of a 16-year-old male show hazy air-space and streaky lung opacities with rapid progression in both mid to lower lungs in only two days (**a** to **b**) with extensive bilateral ground-glass opacities (**c** and **d**) compatible with the clinical impression of bilateral pneumonia with acute respiratory distress syndrome

radiographic reporting algorithm for pediatric COVID infection [21], lobar consolidation is uncommon and classified as atypical of COVID-19. This structured reporting system was adapted from the Radiological Society of North America expert consensus statement on reporting adult COVID-19. However, according to the study done by Bayramoglu, et al., this reporting system seems not to be applicable to children because imaging findings revealed different and heterogeneous opacity patterns compared to those in adults. It was also noted that pediatric COVID-19 related imaging findings were subtle or less extensive both on chest radiography and chest CT examinations [29, 30], as compared to those among infected adults.

A meta-analysis performed by De Rose and his colleagues among infants six months and below showed bilateral ground-glass opacities as a common imaging finding [5]. In this study, bilateral diffuse ground-glass opacities were noted in one patient who was born prematurely at 36 weeks. However, there was improvement after surfactant administration, with further regression after 4- and 11-day follow-up. Hence, this is more in keeping with surfactant deficiency, and less likely from COVID-19.

Two adolescent subjects developed severe pneumonia with imaging findings showing diffuse multifocal ground-glass opacities and consolidation in both lungs which raise the possibility of ARDS. The Pediatric Acute Lung Injury Consensus Conference (PALICC) has recommended the pediatric-focused definition and management for ARDS, in which the primary etiology is pneumonia [30, 31]. ARDS manifests as pulmonary inflammation, alveolar edema, and hypoxemic respiratory failure. It defines pediatric ARDS as those who develop respiratory failure and pulmonary edema within seven days of the known clinical insult, not fully explained by cardiac failure or fluid overload, and with chest imaging findings of new infiltrates consistent with acute pulmonary parenchymal disease. However, in contrast to the earlier adult-based definitions, the PALICC definition eliminates the requirement for bilateral pulmonary infiltrates on chest imaging due to a lack of evidence that etiology, management, and outcomes differ between patients with unilateral versus bilateral disease. Hence, ARDS remains primarily a clinical diagnosis.

Almost all of the patients with positive chest radiograph findings had at least one clinical symptom. Among the pediatric study population as well as among those with positive chest radiograph findings, the most common presenting symptoms encountered were cough and fever, consistent with the prior studies [2, 4, 10, 15], as well as nasal congestion or rhinorrhea.

There were nine patients who had an x-ray done but were asymptomatic. These COVID-19 positive cases had household exposure. The international consensus statement of the Radiological Society of North America on chest imaging in pediatric COVID-19 patients as postulated by Foust, et al. [21], states that imaging studies are actually not indicated for well-appearing immunocompetent patients greater than three months old who present with no symptoms. Initial imaging studies should only be reserved for those who have risk factors for disease progression or those with moderate to severe acute respiratory illness symptoms that are not responding to outpatient treatment and requiring hospitalization. This therefore emphasizes the importance of proper clinical history and physical examination to determine whether a chest radiograph is indeed warranted and in turn should obviate any unnecessary imaging studies. This decision-making becomes particularly important when considering cumulative radiation dose in pediatric patients. It is also important to keep in mind that the disease may still be in its early acute stages such that a normal CXR among positive COVID-19 patients does not essentially rule out pulmonary involvement at the time of examination. These asymptomatic cases yielded normal CXR results and had no disease progression, which did not necessitate any immediate follow-up imaging studies in our institution.

CONCLUSION

The COVID-19 pandemic, in the more recent years, has shown a surge of infection in pediatric patients. This emphasizes the need for further studies particularly in the field of pediatric radiology where it is crucial in finding a timely and accurate diagnosis.

In this series, adolescents were the most commonly affected followed by middle-school children, and is slightly more common in boys than in girls. Most common clinical symptoms presented were cough, fever, and nasal congestion or rhinorrhea, in decreasing order of frequency; lymphopenia and leukopenia were the predominant abnormal laboratory findings. Majority of pediatric patients with COVID-19 in this study exhibited normal chest radiograph findings. Among those with positive chest radiographic findings, initially bilateral ground-glass opacities were the most commonly seen. The lower lobes were most frequently affected.

Overall, these findings seen in children with COVID-19 infection in St. Luke's Medical Center are similar to the trends in the previously published international studies.

REFERENCES

1. Chiotos K, Hayes M, Kimberlin DW, et al. Multicenter Initial Guidance on Use of Antivirals for Children with Coronavirus Disease 2019/ Severe Acute Respiratory Syndrome Coronavirus 2. J Pediatric Infect Dis Soc 2020;9(6):701–15. doi:10.1093/jpids/piaa045.
2. Liu H, Liu F, Li J, Zhang T, Wang D, and Lan W. Clinical and CT imaging features of the COVID-19 pneumonia: Focus on pregnant women and children. J Infect 2020;80(5):e7–e13. doi:10.1016/j.jinf.2020.03.007.
3. Salehi S, Abedi A, Balakrishnan S, and Gholamrezanezhad A. Coronavirus disease 2019 (COVID-19): A Systematic Review of Imaging Findings in 919 Patients. AJR Am J of Roentgenol 2020;215:87–93. doi:10.2214/AJR.20.23034.
4. Hasan T, and Bedir Demirdag T. Novel coronavirus disease (COVID-19) in children. Turk J Med Sci 2020;50(3):592–603. doi:10.3906/sag-2004-174.
5. De Rose DU, Piersigilli F, Ronchetti MP, et al. Novel coronavirus disease (COVID-19) in newborns and infants: what we know so far. Riv Ital Pediatr 2020 Apr 29;46(1):56. doi:10.1186/s13052-020-0820-x.
6. She J, Liu L, Liu W. COVID-19 epidemic: Disease characteristics in Children, J Med Virol, 31 March 2020.
7. Liu H, Liu F, Li J, Zhang T, Wang D, and Lan W. Clinical and CT imaging features of the COVID-19 pneumonia: Focus on pregnant women and children. J Infect 2020;80(5):e7–e13. doi:10.1016/j.jinf.2020.03.007.
8. Lee B, Raszka, Jr, WV. COVID-19 Transmission and Children: The Child is Not to Blame, Pediatrics, June 10, 2020.
9. Kam KQ, Yung CF, Cui L, et al. A Well Infant with Coronavirus Disease 2019 (COVID-19) with High Viral Load. Clin Infect Dis. 2020 Feb 28. pii: ciaa201. doi: 10.1093/cid/ciaa201.
10. Cai J, Xu J, Lin D, Yang Z, et al. A Case Series of children with 2019 novel coronavirus infection: clinical and epidemiological features. Clin Infect Dis. 2020 Feb 28. pii: ciaa198. doi: 10.1093/cid/ciaa198. A
11. Wei M, Yuan J, Liu Y, Fu T, Yu X, Zhang ZJ. Novel Coronavirus Infection in Hospitalized Infants Under 1 Year of Age in China. JAMA. 2020 Feb 14. doi: 10.1001/jama.2020.2131.
12. Chen F, Liu ZS, Zhang FR, et al. [First case of severe childhood novel coronavirus pneumonia in China]. Zhonghua Er Ke Za Zhi. 2020;58:E005. doi: 10.3760/cma.j.issn.0578-1310.2020.0005.
13. Sun Z, Zhang N, Li Y, and Xu X. A systematic review of chest imaging findings in COVID-19. Quant Imaging Med Surg 2020 May;10(5):1058–1079. doi:10.21037/qims-20-564.
14. Shi H, Han X, Jiang N, et al. Radiological findings from 81 patients with COVID-19 pneumonia in Wuhan, China: a descriptive study. Lancet Infect Dis 2020 April; 20(4):425–434. doi:10.1016/S1473-3099(20)30086-4.
15. Huang CL, Wang YM, Li XW, Ren LL, Zhao JP, Hu Y, et al. Clinical features of patients infected with 2019 novel coronavirus in Wuhan, China. Lancet 2020; 395 (10223):497–506.
16. Kan MJ, Grant LMC, Muña MA, and Greenhow TL. Fever without a Source in an Infant Due to Severe Respiratory Syndrome Coronavirus-2. J Pediatric Infect Dis Soc 2021 February 13;10(1):49–51. doi:10.1093/jpids/piaa044.
17. Huang CL, Wang YM, Li XW, Ren LL, Zhao JP, Hu Y, et al. Clinical features of patients infected with 2019 novel coronavirus in Wuhan, China. Lancet 2020; 395 (10223):497–506.
18. Chen N, Zhou M, Dong X, Qu J, Gong F, Han Y, et al. Epidemiological and clinical characteristics of 99 cases of 2019 novel coronavirus pneumonia in Wuhan, China: a descriptive study. Lancet 2020 February 15;395(10223):507–513. doi:10.1016/S0140- 6736(20)30211-7.
19. Zhu N, Zhang D, Wang W, Li X, Yang B, Song J, et al. A Novel Coronavirus from Patients with Pneumonia in China, 2019. New Engl J Med 2020;382:727–733. doi:10.1056/NEJMoa2001017.
20. Chung M, Bernheim A, Mei X, Zhang N, Huang M, Zeng X, et al. CT Imaging Features of 2019 Novel Coronavirus (2019-nCoV). Radiology 2020;295:202–207. doi:10.1148/radiol.2020200230.
21. Foust AM, Philips GS, Chu WC, et al. International Expert Concensus Statement on Chest Imaging in Pediatric COVID-19 Patient Management: Imaging Findings, Imaging Study Reporting and Imaging Study Recommendations. Radiol: Cardiothorac Imaging 2020;2(2):e200214. doi:10.1148/ryct.2020200214.
22. She J, Liu L, and Liu W. COVID-19 epidemic: Disease characteristics in Children. J Med Virol 2020 July;92(7):747–754. doi:10.1002/jmv.25807. Epub 2020 April 15.
23. Williams K, Thomson D, Seto I, Contopoulos-Ioannidis DG, Ioannidis JPA, Curtis S,

Constantin E, Batmanabane G, Hartling L, and Klassen T. Standard 6: Age Groups for Pediatric Trials. Pediatrics 2012;129;S153. doi:10.1542/peds.2012-0055I.

24. Jiang L, Tang K, Levin M, Irfan O, Morris SK, Wilson K, Klein JD, and Bhutta ZA. COVID-19 and multisystem inflammatory syndrome in children and adolescents. Lancet Infect Dis 2020;20:e276–e288. doi:10.1016/S1473-3099(20)30651-4.
25. Dong Y, Mo X, Hu Y, Qi X, Jiang F et al. Epidemiology of COVID-19 among children in China. Pediatrics June 2020;145(6):e20200702. doi:10.1542/peds.2020-0702.
26. Lu X, Zhang L, Du H, Zhang J, Li YY et al. SARS-Cov-2 infection in children 2020. New Engl J Med 2000;382:1663–1665. doi:10.1056/NEJMc2005073.
27. Bayramoglu Z, Canipek E, Comert RG, Gasimli N, Kaba O, Yanartas MS, Torun SH, SomerA, and Ertuk SM. Imaging Features of Pediatric COVID-19 on Chest Radiography and Chest CT: A Retrospective, Single-Center Study. Acad Radiol 2021 January;28(1):18–27. doi:10.1016/j.acra.2020.10.002
28. Steinberger S, Lin B, Bernheim A, Chung M, Gao Y, Xie Z, Zhao T, Xia J, Mei Xueyan, and Little B. CT Features of Coronavirus Disease (COVID-19) in 30 Pediatric Patients. AJR Am J of Roentgenol 2020; 215:1–9. doi:10.2214/AJR.20.23145.
29. Chen A, Huang J, Liao Y, Liu Z, Chen D, Yang C, Yang R, and Wei X. Differences in Clinical and Imaging Presentation of Pediatric Patients with COVID-19 in Comparison with Adults. Radiol: Cardiothorac Imaging 2020;2(2):e200117. doi:10.1148/ryct.2020200117
30. Wang H, Qi Y, Qian L. Severe pediatric COVID-19 with acute respiratory distress syndrome: a narrative review. Pediatr Med 2021;4:27.
31. Bhowmick R, Gulla KM. Pediatric Acute Respiratory Distress Syndrome in COVID-19 Pandemic: Is it the Puzzle of the Century? Indian J Crit Care Med. 2022 Mar;26(3):264–265. doi: 10.5005/jp-journals-10071-24175. PMID: 35519936; PMCID: PMC9015922.

ORIGINAL ARTICLE

Clinical Utility of the Diffusion Weighted Imaging (DWI) Ratio in Characterizing Primary Brain Neoplasms in Pediatric Patients: A 5-year Retrospective Study in a Tertiary Hospital in the Philippines

Sheen C. Urquiza[1], Ryan Jason D.L. Urgel[1], Alvin C. Camacho[1], Rosanna E. Fragante[1]

ABSTRACT

Objective:
The goal of this study was to determine the accuracy of DWI ratio in characterizing primary brain tumors among pediatric patients in the Philippine General Hospital from January 2013 to July 2018.

Methods:
Magnetic resonance images of pediatric brain tumors were reviewed. Standardized ROI were placed at solid portion of the tumor that presented the highest signals on DWI (DWI T), at the normal appearing white matter of the contralateral frontal lobe (DWI WM), and at the normal-appearing homologous area of the ROI of the tumor in the contralateral hemisphere or adjacent region (DWI N). The DWI ratios were determined and analyzed. Data gathered were then subjected to statistical analysis to determine the accuracy of the DWI ratios.

Results:
Thirty cases of pediatric brain tumors were included in this study. Upon analysis, there was a significant difference in the median DWI(T/N) and DWI (T/WM) ratios between Grades II-IV neoplasms; with the Grade IV tumors exhibiting a higher median ratio compared to Grade II. There was significant difference in the median DWI (T/N) and DWI(T/WM) values between low- and high-grade neoplasms, with the median DWI (T/N) and DWI (T/WM) ratios significantly higher among those with high grade neoplasms.

Conclusion:
The DWI ratios presented relatively high sensitivity, high specificity, and relatively high diagnostic accuracies in grading or classifying pediatric intracranial tumors. This method shall be a useful additional non-invasive tool in the evaluation of tumor characteristics, which will guide clinicians in their therapeutic approach.

[1] Department of Radiology, College of Medicine and Philippine General Hospital, University of the Philippines, Manila

Corresponding Author:
Sheen C. Urquiza, MD
Department of Radiology, University of the Philippines – Philippine General Hospital
Email: *urquizasheen@gmail.com*

This paper won 2nd place in the oral research competition during the Asian and Oceanic Society for Paediatric Radiology 2022 Virtual Congress.

INTRODUCTION

Neoplasms are abnormal and uncoordinated proliferation of tissues from certain organs, which may be from previously normal cells in the organ or may be from inherent vessels or connective tissues [1]. This abnormal process does not occur in specific sites only but can affect any part of the body. It is of particular importance when a primary neoplasm occurs intracranially since a patient with such a condition can present with a variety of neurologic manifestations, sometimes life-threatening in the acute setting. Worldwide, intracranial neoplasms are estimated to have an annual incidence of 10–17 per 100,000 population; this is comprised of either primary neoplasms or metastasis from distant sites [2]. Primary neoplasms can occur at any age, with most cases seen among children and older adults; metastasis, on the other hand, is more common in adults than in children [3].

Although clinical diagnosis is very important in such cases, the need for radiologic imaging is emphasized since it may provide a useful set of differential diagnosis, exclude alternative diagnoses, and identify complications, all of which may greatly impact management.

Computed tomography (CT) and magnetic resonance (MR) imaging are the most common imaging modalities being utilized for evaluation of intracranial neoplasms or tumors. Between the two, MR imaging is preferred due to its ability to provide excellent anatomic information and better tissue characterization to ionizing radiation without exposure [2,4–7]. In both modalities, it is important for radiologist to look for characteristics that can help direct the correct diagnosis, as close as it can be to the histopathologic diagnosis - the latter remaining as the gold standard in such cases. Tissue characteristics such as the presence of calcifications, fat, cystic components, contrast enhancement, and signal intensity in the different MRI sequences, can assist the radiologist in narrowing down the differential diagnosis [8].

MR imaging is now being widely used, especially in pediatric patients. The most common sequences used for such cases are the T1- and T2-weighted imaging (T1WI and T2WI, respectively). Contrast enhancement is likewise being utilized for improved tumor characterization. Brain tumors usually exhibit low signal intensity on T1WI and high on T2WI [9]. However, contrast-enhancement level does not always correlate with tumoral grade as tumors can exhibit variable enhancement regardless of benignity or malignancy [10]. As such, DWI is suggested being used as an alternative, non-invasive modality to tissue diagnosis. This MRI sequence probes water molecular diffusion over distances that correspond to typical cell sizes, as well as the diffusivity of water diffusion across membranes (structures that are an integral part of the cell architecture). The effect of these membranes is expected to increase once there is increasing cell density, as seen in tumors.[6] Present research on DWI ratio has all been conducted internationally. Grading tumors based on the method proposed will provide more objective approach to management, whether to do surgical approach or medical tumor debulking, and diagnosis without doing biopsies.

This research was conducted to determine the accuracy of DWI ratio in characterizing primary brain tumors among pediatric patients in the Philippine General Hospital from January 2013 to July 2018. Specifically, it is made to determine the association between DWI ratio of pediatric brain tumors with its histopathologic diagnosis and to measure the diagnostic ability of DWI ratio using receiver operating characteristic (ROC) curve in identifying low- or high-grade neoplasms.

METHODS

This was a retrospective study reviewing the MR images of pediatric patients scanned in a tertiary hospital in Manila, Philippines, who were referred for possible intracranial tumors from January 2013 to July 2018. All pediatric patients with primary intracranial tumors were included in this study (image acquired using 1.5 Tesla MR unit, Magnetom Essenza; Siemens, Germany). The sequences used were T1WI, FLAIR and DWI (B1000) sequences. The histopathologic diagnosis was then obtained. The age of the patient and sex were also gathered.

Excluded in this study were patients with no preoperative MR imaging, or those who have had previous radiation and/or chemotherapy before the MRI. Patients with tumors composed mainly of cysts and without measurable solid components, and patients with tumor bleeding and calcifications on MRI (evidenced by the presence of magnetic susceptibility on the included susceptibility-weighted imaging), will not be included likewise in this study. Also excluded are patients with imaging that do not have histopathologic diagnosis. This study has been approved by the institutional ethics board.

Review of the images of said patients was done with two of the advisers of the study, who are fellows of the Philippine CT-MRI Society. One adviser had more than 10 years in CT-MRI imaging while the other adviser had pediatric neuroradiology subspecialty training. Non-concordance between the two advisers would warrant repeat reevaluation of the case. If after review, there is still non-concordance, the sample is to be discarded. The radiologists were blinded regarding the tissue diagnosis of each case.

The signal intensity of selected regions of interest (ROIs) on DWI was obtained at the b1000 value. Three standardized ROI's measuring 25 ± 5 mm^2 were placed at the solid portion of the tumor that presented the highest signals on DWI (DWI_T), at the normal appearing white matter of the contralateral frontal lobe (DWI_{WM}), and at the normal-appearing homologous area of the ROI of the tumor in the contralateral hemisphere or adjacent region (DWI_N) (Fig. 1). In acquiring the measurements, the ellipse/circle ROI was copied and moved to the areas of interest to standardize the size of the tissue to be analyzed and avoid sampling errors. Using the formulae below,

$$DWI_{T/WM} = DWI_T / DWI_{WM}$$
$$DWI_{T/N} = DWI_T / DWI_N$$

the ratios $DWI_{T/WM}$ and $DWI_{T/N}$ were computed. When artifacts are present in the areas of interest, the ellipse/

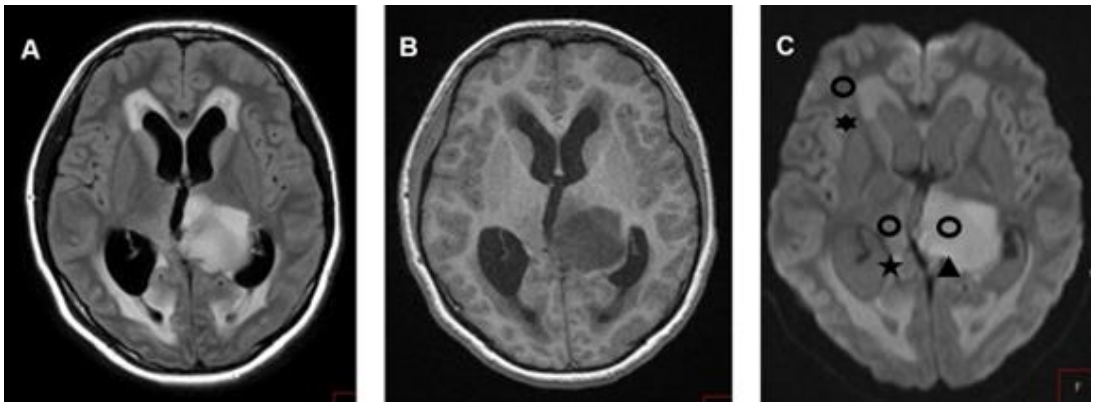

Fig. 1A–C Measuring signal intensities on DWI, with a tumor in the left thalamus (**A, B**). In order to obtain DWI values (**C**), three ROI's (black circles) are placed at the brightest solid portion of the tumor on DWI (▲), at the normal-appearing white matter of the frontal lobe (✶), and at the normal-appearing homologous area (★) of tumor ROI in the contralateral hemisphere on the axial DWI image. (Method adapted from Wu CC, et al., 2012) [4]

circle ROI was repositioned in areas without tumoral involvement, according to anatomical references.

Logistic regression was used to measure the association between DWI ratio and histologic diagnosis. Once computed, cases were categorized into low- or high-grade neoplasms, using $DWI_{T/WM}$ of 1.6 and $DWI_{T/N}$ of 1.5 as the cut-off values, with those equal to or less than the values considered as low-grade neoplasms. Categorizing into low or high-grade neoplasm is based on the 2016 WHO Classification of the Central Nervous System. Low-grade neoplasms include grade I and grade II, while high-grade neoplasms include grade III and grade IV [9]. After the initial analysis of the images, association was measured between the results and the histopathologic diagnosis to confirm whether the tumor grade.

Receiver operating characteristic (ROC) curve was used to determine the diagnostic ability of $DWI_{T/WM}$ and $DWI_{T/N}$ in identifying low- or high-grade neoplasms. The diagnostic ability was measured separately for $DWI_{T/WM}$ and $DWI_{T/N}$. The ROC curve was created by plotting the true positive rate (TPR) against the false positive rate (FPR) at various cut-off points of $DWI_{T/WM}$ and $DWI_{T/N.}$ An area of the ROC curve close to 1 suggests good diagnostic ability while an area close to 0 suggests poor diagnostic ability.

The test of normality of data was done using Shapiro-Wilk test. Since the data were not normally distributed, Kruskal-Wallis test was used to compare the median DWI ratios across the different tumor grades. Mann-Whitney U test was then used to compare the median DWI ratios between low-grade and high-grade neoplasms. Sensitivity and Specificity were calculated for $DWI_{T/WM}$ and $DWI_{T/N}$ in identifying low- or high-grade neoplasms.

Corresponding 95% confidence intervals were computed using Wilson Score Interval without continuity correction. The diagnostic accuracy was computed using the Youden Index (J), where,

$$J = \frac{\text{true positives}}{\text{true positives + false negatives}} + \frac{\text{true negatives}}{\text{true negatives + false positives}} - 1$$

to determine which cut-off points will yield the maximum predictive potential of $DWI_{T/WM}$ and $DWI_{T/N.}$

Encoding of needed data was done through Excel (Microsoft Office, USA) and all statistical tests used Stata 12.

RESULTS

Different cases of intracranial tumors included in this study were summarized in Table 1. Most of the included cases were low-grade gliomas; a few of these tumors were ependymoma and medulloblastoma.

Of the 52 pediatric tumor cases identified in MRI, 30 cases were included for analysis, given that 1 of the cases is that of tuberculoma, two have known histopathologic diagnosis but with unavailable MR images for review, and 19 which did not yield any available histopathologic results.

The DWI ratios were then computed and were categorized into low- or high-grade neoplasms, using $DWI_{T/WM}$ of 1.6 and $DWI_{T/N}$ of 1.5 as the cut-off values. Those equal to or less than these values were considered as low-grade neoplasms [4].

Table 1 Summary of included pediatric tumors done from January 2013 to July 2018

Disease	WHO Grade	Number	%
Ependymoma	II	5	16.7
Low-grade glioma	II	11	36.7
Non-germinomatous pineal gland tumor	II	1	3.3
Non-specific high-grade glioma	III	1	3.3
Anaplastic ependymoma	III	1	3.3
Medulloblastoma	IV	5	16.7
Glioblastoma	IV	2	6.7
Germ cell tumor	IV	2	6.7
Non-germinomatous germ cell tumor	IV	1	3.3
CNS embryonal tumor	IV	1	3.3
Total		30	100

There was a significant difference in the $DWI_{T/N}$ ratio between Grades II-IV neoplasms. Group IV exhibits a higher ratio compared to Group II; however, the ratios between Groups II and III, and III and IV were not significantly different. (Table 2)

Table 2 Median $DWI_{T/N}$ per WHO Tumor grade

Grade (n)	Median $DWI_{T/N}$ (Range)	p-value
II (17)	1.2 (0.5–1.9)	0.0119
III (2)	1.5 (1.5–1.6)	
IV (11)	1.8 (0.4–3.5)	

There was also a significant in the median DWI tumor:white matter ratios of Grades II-IV neoplasms (p-value=0.0150). Post-hoc analysis again showed that Group IV had significantly higher median $DWI_{T/WM}$ values than Group II. There were no significant differences in the median value of $DWI_{T/WM}$ between Groups II and III, and between Groups III and IV. (Table 3)

Table 3 Median $DWI_{T/WM}$ per WHO Tumor grade

Grade	Median $DWI_{T/WM}$ (Range)	p-value
II	1.3 (0.6–1.9)	0.0150
III	1.4 (1.4–2.0)	
IV	1.8 (0.5–3.2)	

The categorization of cases into low- or high-grade neoplasms was based on the 2016 WHO Classification of the Central Nervous System. Grades I and II were considered low-grade neoplasms, while Grades III and IV were considered high-grade neoplasm. There was a significant difference in the median $DWI_{T/N}$ values between low- and high-grade neoplasms (p-value = 0.003). Median $DWI_{T/N}$ was significantly higher among those with high-grade neoplasms. (Table 4)

Table 4 Median $DWI_{T/N}$ per WHO Classification of CNS Tumors

Classification (n)	Median $DWI_{T/N}$ (Range)	p-value
Low (17)	1.2 (0.5–1.9)	0.003
High (13)	1.7 (0.4–3.5)	

Table 5 showed a statistically significant difference in the median DWI tumor:white matter ratios between low- and high-grade neoplasms (p-value=0.004). The values were found to be higher among high-grade neoplasms (WHO Grades III and IV).

Table 5 Median $DWI_{T/WM}$ per the WHO Classification of CNS Tumors

Classification	Median $DWI_{T/WM}$ (Range)	p-value
Low	1.3 (0.6–1.9)	0.004
High	1.8 (0.5–3.2)	

It was also observed that the $DWI_{T/N}$ ratio had a relatively high sensitivity (69.23%) and high specificity (82.35%). The diagnostic accuracy of using DWI tumor:normal-appearing homologous area ratio in assessing low- and high-grade neoplasm was relatively high, with a computed accuracy of 76.67%. (Table 6)

Table 6 Diagnostic accuracy of $DWI_{T/N}$ in classifying low- and high-grade pediatric tumors

	Low $DWI_{T/N}$	High $DWI_{T/N}$
Low-grade neoplasm	14 (82.4%)	3 (17.6%)
High-grade neoplasm	4 (30.8%)	9 (69.2%)
Sensitivity	69.23% (95% CI = 42.37–87.32%)	
Specificity	82.35% (95% CI = 58.97–93.81%)	
Diagnostic Accuracy	76.67% (95% CI = 59.07–88.21%)	

On the other hand, it was observed that $DWI_{T/WM}$ had a relatively high sensitivity (61.54%) and a high specificity

(88.24%). The diagnostic accuracy of using the DWI tumor:white matter ratio in assessing low- and high-grade neoplasms was also relatively high, with a computed accuracy of 76.67%. (Table 7)

Table 7 Diagnostic accuracy of $DWI_{T/WM}$ in classifying low- and high-grade pediatric tumors

	Low $DWI_{T/WM}$	**High $DWI_{T/WM}$**
Low-grade neoplasm	15 (88.2%)	2 (11.8%)
High-grade neoplasm	5 (38.5%)	8 (61.5%)
Sensitivity	61.54% (95% CI = 35.52–82.29%)	
Specificity	88.24% (95% CI = 65.66–96.71%)	
Diagnostic Accuracy	76.67% (95% CI = 59.07–88.21%)	

DISCUSSION

Magnetic resonance diffusion-weighted imaging has been helpful in studying water mobility in normal brain tissue, cerebral infarction, multiple sclerosis, brain tumors and brain abscesses, and to differentiate between arachnoid cysts and epidermoid cysts and other diseases.[11] In the case of brain tumors, routine contrast-imaging studies alone may provide all the necessary information needed to differentiate between benign and malignant neoplasms.

Diffusion-weighted imaging (DWI) is one of the MR sequences utilized in determining hyperacute and acute infarcts in the first 6 hours after ictus, as it uses the diffusivity of the water molecules in the infarcted brain cells. The same principle can be used in the assessment of brain tumors, wherein signal characteristics are based on the alterations of the cellularity and of the extracellular spaces within the tumor. This specific procedure may provide qualitative and quantitative assessments of water diffusivity in brain tumors [5].

In most studies, pathological alteration of water diffusion in the brain tissues is illustrated by apparent diffusion coefficient (ADC) mapping. Most institutions use the ADCs to determine neoplastic density and proliferation indices. A previous study showed low ADC values in pediatric brain tumors suggesting high-grade hypercellular tumors, such as medulloblastoma, primitive neuroectodermal tumor, and glioblastoma; low-grade gliomas usually show high ADC values. However, there remains a considerable overlap of the ADC values between high- and low-grade tumors in both pediatric and adult patients, resulting in the limited clinical value of ADC for tumor grading [5]. As such, an ADC map alone is not totally sufficient in predicting the type and grade of intracranial neoplasms [2].

The use of DWI, particularly the DWI ratio, is another proposed and studied method in determining whether an intracranial tumor is high- or low-grade neoplasms. DWI ratio, is computed using the following formulae:

$$DWI_{T/WM} = DWI_T / DWI_{WM}$$
$$DWI_{T/N} = DWI_T / DWI_N$$

where DWI_T is the signal intensity value of the tumor, DWI_{WM} is the signal intensity value of the white matter of the contralateral frontal lobe, and DWI_N is the signal intensity value of the homologous contralateral normal brain tissue [4].

In a 2012 study, a higher DWI ratio ($DWI_{T/WM}$) was seen in high-grade gliomas. On the other hand, a lower DWI ratio was noted in low-grade tumors. This can be explained by the greater cellularity and fewer extracellular space in high-grade tumors, such as glioblastoma and lymphoma. In previous studies, homologous area in the contralateral hemisphere of the tumor was identified and used to determine the DWI ratio. Presently, cut-off values of 1.6 for $DWI_{T/WM}$ and 1.5 for $DWI_{T/N}$ have been used in pediatric neuro-oncological practice [4]. In this study, a significant difference in the DWI ratios of low- and high-grade tumors when comparing the DWI ratios between the tumor and the contralateral frontal lobe white matter and of the tumor with normal-appearing homologous area was determined. These results were congruent with the study by Wu, et al. in 2012 [4]. With a relatively high sensitivity and a high specificity, both the $DWI_{T/WM}$ and $DWI_{T/N}$ provided relatively high diagnostic accuracies in classifying low- and high-grade neoplasms, particularly gliomas. The results of this study indicate that a lower DWI ratio suggests a low-grade intracranial neoplasm, while a higher DWI ratio suggests otherwise.

However, the low sample size gathered in this study particularly in the homogeneity of the identified tumor grades, may not be statistical enough to generate a universal conclusion on the utility of the DWI to determine tumor grade. Determining the ADC values of pediatric intracranial tumors would still be of benefit, as seen in previous published studies where low ADC values in pediatric brain tumors suggest high-grade hypercellular tumors, such as medulloblastoma, and high ADC values suggest otherwise [4]. However, an ADC map alone is not sufficient in predicting the type and grade of intracranial neoplasms. A study in 2017 by Hyun Woo Goo, et al. showed a considerable overlap of the ADC values between high- and low-grade tumors in both pediatric and adult patients, resulting in the limited clinical value of ADC for tumor grading [5]. The information derived from determining the DWI ratio, on the other hand, may provide additional information to clinicians and surgeons.

The determination of the DWI ratio may be limited particularly after interventions (i.e. radiation, chemotherapy, or surgery) and which is beyond the scope of this study. This is to avoid potential confounding factors for tissue diffusion. Also, tumors with mostly cystic contents and patients with tumor bleeding and calcifications may provide inaccurate measurements on DWI. A prospective approach may provide improved results, considering that some of the possible cases that could have been included in this study did not have histopathologic results and did not have prior imaging studies for review.

CONCLUSION

The DWI ratios presented a relatively high sensitivity, high specificity, and relatively high diagnostic accuracies in grading or classifying pediatric intracranial tumors. This method shall be a useful additional non-invasive tool in the evaluation of tumor characteristics, which will guide clinicians in their therapeutic approach.

REFERENCES

1. Atlas of Pathology. Neoplasia (Tumor) [Internet]. Atlas of Pathology website. 2016 [cited 2017 June 15]. Available from: http://www.pathologyatlas.ro/tumors-neoplasia.php
2. Lavra F, Scartozzi M, Zaccagna F, Cartocci G, et al. Advanced magnetic resonance imaging in the study of primary intracranial brain tumors in adults: a state of art review. J Xiangya Med 2017;2:56.
3. American Brain Tumor Association. Brain Tumor Statistics. ABTA website. 2014 [cited 2017 June 15]. Available from: http://www.abta.org/about-us/news/brain-tumor-statistics/
4. Wu CC, Guo WY, Chen MH, Ho DM, et al. Direct measurement of the signal intensity of diffusion weighted magnetic resonance imaging for preoperative grading and treatment guidance for brain gliomas. JCMA [Internet]. 2017 [cited 2017 June 15]. Available from: https://www.sciencedirect.com/science/article/pii/S1726490112002225
5. Goo HW, and Ra Y. Advanced MRI for Pediatric Brain Tumors with Emphasis on Clinical Benefits. Korean J Radiol 2017;18(1):194–207.
6. Chedia S, Todua F. Differentiation between benign and malignant meningiomas using diffusion and perfusion MR imaging. Georgian Med News 2012;(206):16–22.
7. Maier SE, Sun Y, Mulkern RV. Diffusion Imaging of Brain Tumors. NMR Biomed 2010;27(7):849–64.
8. Smithuis R, and Montanera W. Brain Tumor – Systematic Approach. Radiology Assistant [Internet]. 2008 [cited 2017 June 15]. Available from http://www.radiologyassistant.nl/en/p47f86aa182b3a/brain-tumor-systematic-approach.htm
9. Louis DN, Perry A, Reifenberger G, von Deimling A, et al. The 2016 World Health Organization Classification of the Tumors of the Central Nervous System. Acta Neuropathol 2016;131(6):803–20.
10. Koob M, Girard N. Cerebral tumors: Specific features in children. DIII [Internet]. 2014 [cited 2017 June 15]; 95(10):965–83. Available from https://www.sciencedirect.com/science/article/pii/S2211568414002101
11. Kono K, Inoue Y, Nakayama K, Shakudo M, et al. The role of diffusion-weighted imaging in patients with brain tumors. AJNR Am J Neuroradiol 2001; 22(6):1081–88.

ORIGINAL ARTICLE

Challenges in Diagnosis and Management of Pediatric Presacral Tumors: A Radiologist's Perspective

A. Ebinesh[1]

ABSTRACT

Presacral tumors in pediatric patients pose unique diagnostic challenges due to their rarity, diverse histopathology, and complex anatomy of the presacral region. Accurate diagnosis and management of these tumors require a multimodal imaging approach and specialized expertise. This article explores the challenges encountered in imaging pediatric presacral tumors and emphasizes the importance of a comprehensive imaging strategy. The rarity and diverse histopathology of these tumors make accurate diagnosis challenging. The complex anatomy of the presacral space necessitates advanced imaging techniques such as magnetic resonance imaging (MRI) and computed tomography (CT) to visualize the relationships between the tumor and adjacent structures. Differentiating between benign and malignant tumors is crucial for treatment planning, but it can be challenging due to overlapping imaging features. Assessing the treatment response and detecting tumor recurrence require regular follow-up imaging, but post-treatment changes can mimic or mask tumor recurrence. A multidisciplinary approach involving radiologists, pediatric surgeons, pediatric oncologists, and pathologists is essential for accurate diagnosis and treatment planning. Effective communication and coordination among team members are necessary to overcome the challenges associated with managing these complex cases. Future research and advancements in imaging technology will further enhance the ability to diagnose and manage pediatric presacral tumors, ultimately improving patient outcomes.

Keywords: diagnostic imaging, neoplasms, pediatric, presacral

[1] Junior Consultant, Department of Radiology, Sri Narayani Hospital and Research Centre, Vellore, Tamil Nadu 632055, India
Email: *ebineshjezreel@gmail.com*

This was modified from the paper that won 3rd place in the oral research competition during the Asian and Oceanic Society for Paediatric Radiology 2022 Virtual Congress.

Acknowledgments:
Dr. Ebinesh is indebted to the contributions of the residents and faculty of Pediatric Surgery, Maulana Azad Medical College, New Delhi for their scientific input, feedback and follow-up. The author would also like to acknowledge the efforts of Dr. Anjali Prakash, Dr. Swarna Saxena, and Dr. Praislin for their valuable contributions.

INTRODUCTION

Presacral tumors are rare neoplasms that develop in the presacral space located between the rectum and sacrum. In pediatric patients, presacral tumors present unique diagnostic challenges due to their rarity, diverse histopathology, and complex anatomy of the presacral region. Imaging plays a crucial role in the diagnosis and management of these tumors, enabling accurate characterization, localization, and preoperative planning. However, the evaluation of pediatric presacral tumors requires a multimodal approach, combining various imaging techniques and expertise to overcome the diagnostic complexities. This article explores the diagnostic challenges encountered in imaging pediatric presacral tumors and highlights the importance of a comprehensive imaging strategy.

Pediatric presacral tumors are extremely rare, accounting for less than 1% of all pediatric tumors [1–3]. The wide range of histopathological subtypes further complicates their diagnosis. Common types include sacrococcygeal teratomas, neuroblastomas, Ewing sarcomas, rhabdomyosarcomas, and primitive neuroectodermal tumors [2]. Each subtype presents unique imaging features, making accurate diagnosis challenging. The radiologist's familiarity with these entities and their

imaging characteristics is essential for accurate interpretation.

Complex anatomy of the presacral space:

The presacral space contains various vital structures, including the rectum, sacrum, nerves, blood vessels, and adjacent pelvic organs [1]. The proximity of these structures to presacral tumors can influence the extent of disease and surgical planning [4]. Accurate delineation of tumor borders and their relationship with adjacent structures is crucial to determine the feasibility of complete resection and the potential for functional morbidity. Advanced imaging techniques, such as magnetic resonance imaging (MRI) and computed tomography (CT), with multiplanar reconstructions, help visualize these anatomical relationships.

The precise location of the tumor within this region provides important clues about its origin, relationship with nearby structures, and potential for invasion or compression of vital structures like the rectum, bladder, or blood vessels. Understanding the anatomical context helps in formulating a differential diagnosis and determining the appropriate diagnostic approach. Primary presacral tumors are more likely to arise from developmental remnants or embryonic tissues within the presacral region [1], whereas secondary tumors may indicate a primary tumor elsewhere in the body. Different types of tumors can occur in the presacral region, each with its own characteristic location and epicenter [4]. For example, sacrococcygeal teratomas primarily originate from the coccygeal region, whereas neuroblastomas tend to arise from the sympathetic ganglia. Identifying the specific location and epicenter of the tumor can help narrow down the possible tumor subtypes and guide further diagnostic tests. The location and epicenter of the tumor provide critical information about its extent of infiltration and potential involvement of nearby structures. For example, a tumor originating from the anterior presacral region may have a higher propensity to invade the bladder, while a tumor arising from the posterior presacral region may extend into the sacrum or coccyx. Evaluating the extent of infiltration and extension is essential for accurate staging and treatment planning. Certain tumor subtypes in the presacral region are associated with specific syndromes or congenital anomalies. For example, sacrococcygeal teratomas are often associated with chromosomal abnormalities or anomalies of midline structures [4]. Knowledge of the tumor's location and potential associated syndromes can aid in formulating the differential diagnosis and guide further genetic or syndromic evaluations.

Imaging modalities:

a) Ultrasonography: Ultrasonography is often the initial imaging modality used to evaluate pediatric presacral tumors due to its accessibility and lack of ionizing radiation. It aids in the assessment of tumor vascularity, tumor composition (solid vs. cystic components), and presence of calcifications. However, ultrasound has limited ability to evaluate deep pelvic structures and may not provide comprehensive anatomical information.

b) Computed Tomography (CT): CT is a standard tool for the evaluation of bony involvement and extent of the tumor. It is useful for evaluating bony structures and calcifications associated with presacral tumors. It provides detailed information on bone erosion, invasion, and potential complications such as pelvic abscess formation. CT is particularly valuable in cases where MRI is contraindicated or inaccessible. However, CT involves ionizing radiation and should be used judiciously, especially in pediatric patients.

c) Magnetic Resonance Imaging (MRI): MRI is considered the modality of choice for evaluating pediatric presacral tumors. It provides superior soft tissue contrast, multiplanar imaging capabilities, and the ability to characterize tumor components. MRI can accurately determine tumor extension, invasion of adjacent structures, and potential involvement of neural structures, aiding in surgical planning. Diffusion-weighted imaging (DWI) and dynamic contrast-enhanced MRI may provide additional information on tumor aggressiveness and vascularity.

d) Nuclear Imaging: PET-CT and PET-MRI play a significant role in the evaluation of pediatric presacral tumors. They provide functional information by detecting metabolic activity, aiding in differentiation between benign and malignant tumors, detecting lesions and metastases, assessing treatment response, differentiating residual tumor from post-treatment changes, and assisting in radiation therapy planning. These advanced imaging techniques provide valuable information that complements anatomical imaging, helping in accurate diagnosis, treatment planning, and monitoring of pediatric presacral tumors.

Differentiating benign and malignant tumors:

Accurate differentiation between benign and malignant presacral tumors is crucial for appropriate treatment planning [2]. Benign and malignant presacral tumors can often have similar imaging appearances, making it difficult to differentiate them based solely on imaging findings. Both types of tumors can present as well-defined

masses with heterogeneous internal characteristics, such as cystic or solid components, enhancing soft tissue, or necrotic areas. While certain imaging characteristics, such as invasion into adjacent structures or metastatic spread may suggest malignancy, these findings are not always present or definitive [5]. Additionally, some benign tumors can mimic malignant features on imaging, further complicating the differentiation.

Both benign and malignant presacral tumors can exhibit heterogeneity in terms of their internal composition, vascularity, and enhancement patterns. This heterogeneity can make it challenging to accurately characterize the tumor based on imaging alone. While larger tumors may raise suspicion for malignancy, small malignant tumors or benign tumors with aggressive features can be challenging to detect or differentiate from surrounding structures using imaging techniques. Some pathologic examples are presented in Figures 1 to 7.

Fig. 1 Immature sacrococcygeal teratoma in a 24-day-old neonate. Sagittal T2-weighted MR image shows a complex solid cystic tumor in the presacral space with extrapelvic extension and containing intralesional fat, soft tissue and hemorrhage

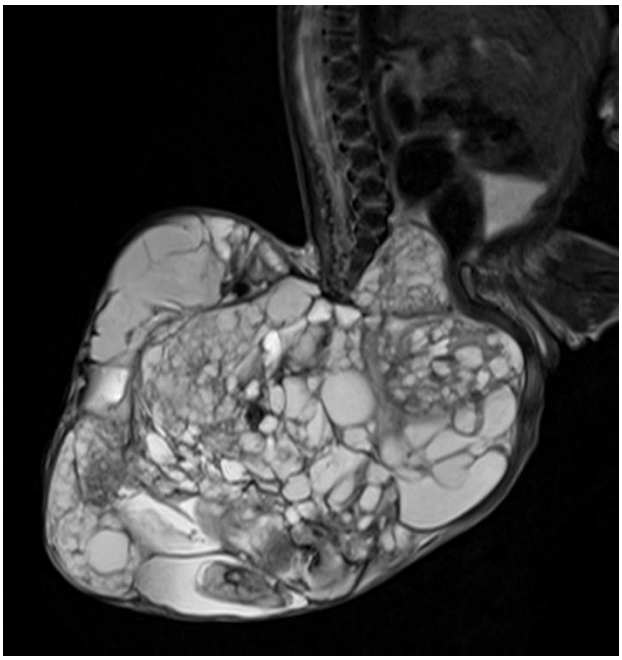

Advanced imaging techniques such as diffusion weighted imaging (DWI), dynamic perfusion imaging and nuclear imaging techniques such as positron emission tomography (PET) may aid in distinguishing between benign and malignant tumors by assessing cellular activity and metabolic characteristics [6].

Fig. 2 Malignant sacrococcygeal teratoma in a 5-year-old child. Sagittal reformatted contrast enhanced CT image shows a presacral tumor (asterisk) with heterogeneously enhancing solid component, intralesional fat and cystic areas. Associated destruction of the sacral vertebrae is also seen

Assessment of tumor response and recurrence:

Monitoring the response to treatment and detecting tumor recurrence are crucial aspects of managing pediatric presacral tumors. Imaging modalities, particularly MRI, play a vital role in assessing treatment response by evaluating changes in tumor size, vascularity, and necrosis after neoadjuvant therapy. In addition, regular follow-up imaging helps in early detection of recurrent disease, enabling prompt intervention and improving patient outcomes.

Presacral tumors are located deep in the pelvis, which makes them difficult to access and evaluate using conventional imaging techniques. Complex anatomical structures in the pelvic region, such as the bladder, rectum, and blood vessels, can further obscure the tumor boundaries and hinder accurate assessment. They can vary significantly in size and shape. Some tumors may be large and well-defined, while others can be small and irregularly shaped. This variability can make it challenging to accurately measure the tumor size and assess the response to treatment over time.

Fig. 3 Rhabdomyosarcoma in a 12-year-old girl. Sagittal reformatted contrast-enhanced CT image shows an infiltrative heterogeneously enhancing soft tissue tumor (asterisk) extending into the sacral spinal canal with destruction of the lumbar and sacral vertebrae

Currently, there is a lack of specific imaging biomarkers that can reliably indicate tumor response or recurrence in presacral tumors. Conventional imaging modalities, such as computed tomography (CT) and magnetic resonance imaging (MRI), primarily rely on changes in tumor size and morphology to assess treatment response. However, these changes may not always correlate with the actual tumor response, especially in cases where the tumor undergoes necrosis or fibrosis without significant reduction in size.

Following treatment, presacral tumors may exhibit various post-treatment changes, such as fibrosis, inflammation, or fluid collections. These changes can mimic or mask tumor recurrence, leading to false-positive or false-negative imaging results. Distinguishing between treatment-related changes and tumor recurrence can be challenging, requiring close collaboration between radiologists, oncologists, and surgeons. Functional imaging techniques, such as positron emission tomography (PET) and diffusion-weighted imaging (DWI), can provide valuable information about tumor metabolism and cellular activity. However, these techniques may not always be readily available in all healthcare settings or may have limited sensitivity and specificity in presacral tumors, further complicating the assessment of tumor response and recurrence.

Fig. 4 Clear cell sarcoma in a 10-year-old boy. Axial T2-weighted MR image shows a lobulated hyperintense tumor (asterisk) in the presacral space showing areas of necrosis and hemorrhage within and lytic destruction of the sacrum

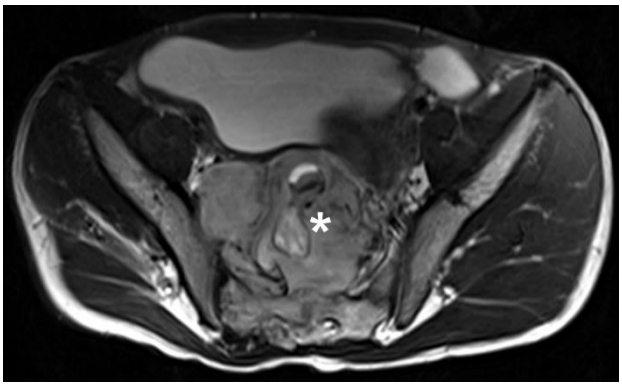

Fig. 5 Lymphoma in a 9-year-old child. Sagittal reformatted contrast-enhanced CT image shows multiple enlarged homogeneously enhancing lymph nodal masses (arrows) in the presacral region

Interdisciplinary approach and expertise:

Due to the complex nature of pediatric presacral tumors and the challenges associated with their imaging, a multidisciplinary approach is essential. Radiologists, pediatric surgeons, pediatric oncologists, and pathologists must collaborate to ensure accurate diagnosis, appropriate staging, and optimal treatment planning [7]. Each discipline brings unique perspectives and expertise to ensure a comprehensive evaluation of the tumor. Interdisciplinary collaboration facilitates the development of an optimal treatment plan. The expertise of radiologists with a strong understanding of the imaging characteristics of pediatric presacral tumors is crucial for accurate interpretation and guiding clinical decision-making. Pediatric oncologists contribute their expertise in systemic therapies, such as chemotherapy or targeted therapies, while surgeons determine the feasibility and extent of surgical resection. The combined knowledge and perspectives ensure a tailored approach to maximize treatment effectiveness. Regular imaging evaluations are necessary, and an interdisciplinary team can collectively interpret imaging findings and correlate them with clinical outcomes.

Fig. 6 Ewing's sarcoma in an 11-year-old child. Sagittal T1-weighted MR image shows an expansile lesion involving the sacrum (asterisk) with associated soft tissue extending anteriorly into the presacral space and posteriorly into the sacral spinal canal and the paraspinal soft tissue

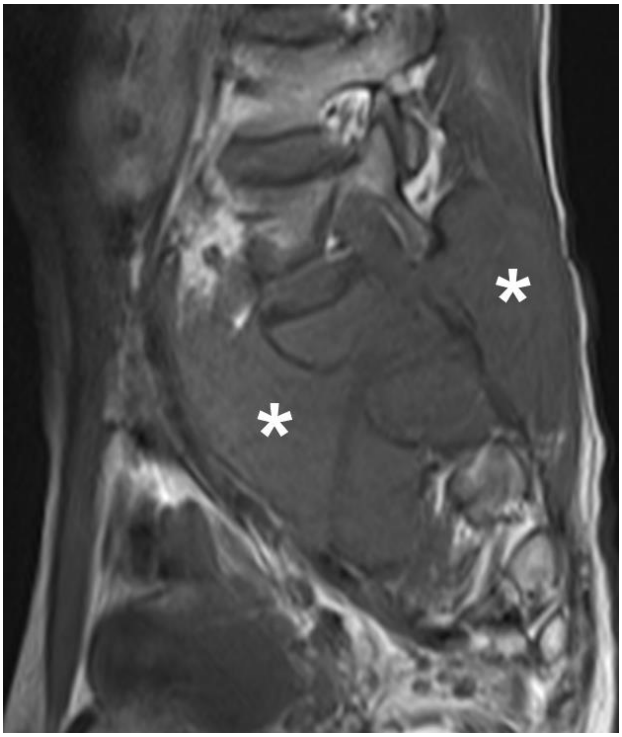

Effective communication and coordination among multiple specialists can be challenging, especially when managing complex cases. Different disciplines may use specialized terminology and have unique perspectives, necessitating clear and efficient communication to ensure a shared understanding of the case. Ensuring that all team members are up to date with the latest advancements and research in their respective fields is essential for optimal decision-making and patient care. Coordinating schedules and availability of team members can pose logistical challenges, particularly in time-sensitive cases. Achieving consensus in diagnosis and treatment planning is crucial to avoid conflicting recommendations and ensure consistent care for the patient. Addressing these challenges necessitates effective communication channels, regular team meetings, and a culture of collaboration and mutual respect. Continuous education and knowledge-sharing activities among team members can help mitigate differences in expertise. Emphasizing patient-centered care and shared decision-making further enhance the effectiveness of the interdisciplinary approach in managing pediatric presacral tumors.

Fig. 7 Neuroblastoma in a 5-year-old child. Axial contrast-enhanced CT image shows a heterogeneously enhancing infiltrative tumor in the presacral space (asterisk) towards the left of the midline with areas of necrosis within

CONCLUSION

Imaging pediatric presacral tumors presents several diagnostic challenges due to their rarity, diverse histopathology, and complex anatomy of the presacral space. An integrated imaging approach that combines various modalities such as ultrasound, MRI, and CT is crucial for accurate characterization, localization, and preoperative planning. Differentiating between benign and malignant tumors, assessing treatment response, and

detecting recurrence are additional challenges that require specialized imaging techniques. A multidisciplinary approach and the expertise of radiologists, along with other medical specialists, are vital for overcoming these diagnostic challenges and providing optimal management for pediatric patients with presacral tumors. Future research and advancements in imaging technology will further enhance our ability to accurately diagnose and manage these rare tumors, ultimately improving patient outcomes.

REFERENCES

1. Jao SW, Beart RW Jr, Spencer RJ et al. Retrorectal tumors. Mayo clinic experience. Dis Colon Rectum 1985;28:644–52.
2. Messick CA, Hull T, Rosselli G et al. Lesions originating within retrorectal space: a diverse group requiring individualized evaluation and surgery. J Gastrointest Surg 2013;17:2143–52.
3. Lu Z, Lu M. Presacral tumor: Insights from a Decade's experience of this rare and diverse disease. Front Oncol 2021;11:639028.
4. Hain SK, Pickhardt JP, Lubner GM et al. Presacral masses: Multimodality imaging of a multidisciplinary space. Radiographics 2013;33:145–67.
5. Bartels SA, van Koperen PJ, van der Steeg AF et al. Presacral masses in children: presentation, aetiology and risk of malignancy. Colorectal Dis 2011;13:930–4.
6. Kocaoglu M, Frush PD. Pediatric presacral masses. Radiographics 2006;833–57.
7. Patel N, Maturen KE, Kaza RK, et al. Imaging of presacral masses - a multidisciplinary approach. Br J Radiol 2016;89:20150698.

Association between Germinal Matrix Hemorrhage at the First Week of Life and Perinatal Factors of Preterm Neonates Born at St. Luke's Medical Center
(EP-007)

Authors:

Adrian Christopher A. Elio, MD
Radiology Resident
St. Luke's Medical Center – Quezon City, 279 E. Rodriguez Sr. Ave, Quezon City, Philippines
acelio1216@gmail.com and acaelio@stlukes.com.ph

Mariaem M. Andres, MD, FPCR
Pediatric Radiologist
St. Luke's Medical Center – Quezon City, 279 E. Rodriguez Sr. Ave, Quezon City, Philippines
St. Luke's Medical Center – Global City, 5th Ave., Taguig, Philippines
mariaem139@yahoo.com and mmandres@stlukes.com.ph

Association between Germinal Matrix Hemorrhage at the First Week of Life and Perinatal Factors of Preterm Neonates Born at St. Luke's Medical Center
(EP-007)
Adrian Christopher A. Elio, MD and Mariaem M. Andres, MD, FPCR

Introduction

In the Philippines, 13 out of 100 live births are preterm with complications of prematurity being the leading cause of neonatal deaths (31%)[1]. Germinal matrix hemorrhage (GMH) is one of common pathologies associated with prematurity due to the inability of the germinal matrix to compensate for the hemodynamic and oxygen tension changes during and after childbirth[2].

GMH is associated with degree of prematurity and is therefore associated with low birthweight and low Ballard score. Studies also show an association between GMH and poor Apgar scores and reduction of GMH risk with use of antenatal corticosteroids. Premature rupture of membranes and mode of delivery did not have any association with GMH while there are varying results in the association of GMH with maternal hypertensive disorder, gestational diabetes mellitus and multiple gestation.

Determining the risk factors for GMH is important since early detection and prompt and appropriate treatment are key in decreasing morbidity, such as the long term neurologic deficits, including poor cognitive outcomes and cerebral palsy.

For inquiries, please e-mail Adrian Christopher A. Elio, MD (acelio1216@gmail.com) and Mariaem M. Andres, MD, FPCR (mmandres@stlukes.com.ph)

Association between Germinal Matrix Hemorrhage at the First Week of Life and Perinatal Factors of Preterm Neonates Born at St. Luke's Medical Center

(EP-007)

Adrian Christopher A. Elio, MD and Mariaem M. Andres, MD, FPCR

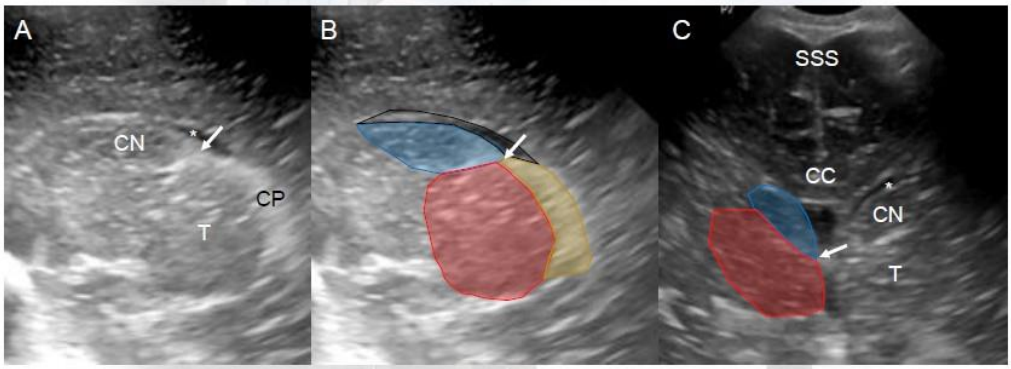

*Normal cranial ultrasound anatomy in sagittal (**A**,**B**) and coronal (**C**) planes showing the caudothalamic groove (→), caudate nucleus (CN), thalamus (T), lateral ventricle (*), choroid plexus (CP), corpus callosum (CC) and superior sagittal sinus (SSS)*

For inquiries, please e-mail Adrian Christopher A. Elio, MD (acelio1216@gmail.com) and Mariaem M. Andres, MD, FPCR (mmandres@stlukes.com.ph)

Association between Germinal Matrix Hemorrhage at the First Week of Life and Perinatal Factors of Preterm Neonates Born at St. Luke's Medical Center

(EP-007)

Adrian Christopher A. Elio, MD and Mariaem M. Andres, MD, FPCR

Methodology

This is a retrospective, cross-sectional study involving all preterm neonates who underwent cranial ultrasound from 2017 to 2020 at St. Luke's Medical Center in their first week of life, excluding those with congenital malformations, metabolic disorders, central nervous system infection, unknown perinatal data and unavailable cranial ultrasound images.

The presence and grading of GMH was evaluated independently by two pediatric radiologists who were blinded to the perinatal factors. A third pediatric radiologist also evaluated the images in cases of incongruent findings. The researcher, who is blinded to the cranial ultrasound findings, also determined the patient's sex, gestational age, birthweight, Ballard score, Apgar score in the 1st and 5th minute, mode of delivery, multiple gestation, presence of maternal hypertensive disorder, gestational diabetes mellitus, preterm premature rupture of membranes (PPROM) and use of antenatal corticosteroids through the medical records.

Determination of the association between GMH and perinatal factors was analyzed using univariate and multivariate statistics.

For inquiries, please e-mail Adrian Christopher A. Elio, MD (acelio1216@gmail.com) and Mariaem M. Andres, MD, FPCR (mmandres@stlukes.com.ph)

Association between Germinal Matrix Hemorrhage at the First Week of Life and Perinatal Factors of Preterm Neonates Born at St. Luke's Medical Center

(EP-007)

Adrian Christopher A. Elio, MD and Mariaem M. Andres, MD, FPCR

Operational Definitions

Germinal matrix hemorrhage grading by Papile, et al.

- Grade I: hemorrhage confined in the caudothalamic groove
- Grade II: hemorrhage extending to the ventricle without dilatation
- Grade III: hemorrhage extending to the dilated ventricle
- Grade IV: parenchymal hemorrhage secondary to venous infarction

Preterm: Birth before 37 weeks age of gestation

Maternal hypertensive disorder: blood pressure higher than 140/90 mmHg after 20 weeks of gestation

Gestational diabetes mellitus: fasting blood sugar > 92 mg/dL or 2 hour 75 gram oral glucose tolerance test > 140 mg/dL

For inquiries, please e-mail Adrian Christopher A. Elio, MD (acelio1216@gmail.com) and Mariaem M. Andres, MD, FPCR (mmandres@stlukes.com.ph)

Association between Germinal Matrix Hemorrhage at the First Week of Life and Perinatal Factors of Preterm Neonates Born at St. Luke's Medical Center

(EP-007)

Adrian Christopher A. Elio, MD and Mariaem M. Andres, MD, FPCR

Neonatal and Maternal Characteristics

Perinatal Factor		n (%) / Mean ± SD
GMH	Present	140 (37.6)
	Grade I	111 (29.8)
	Grade II	24 (6.5)
	Grade III	3 (0.8)
	Grade IV	2 (0.5)
	Absent	232 (62.4)
Sex	Male	195 (52.4)
	Female	177 (47.6)
GA (weeks)		33.1 ± 2.79
	Below 28	21 (5.6)
	28 to 31 6/7	74 (19.9)
	32 to 33 6/7	90 (24.2)
	34 to 36 6/7	187 (50.3)
BW (grams)		1829.1 ± 553.81
	Below 2,500	331 (89.0)
	2,500 and above	41 (11.0)
BS (weeks)		33.0 ± 2.84
	Below 28	20 (5.4)
	28 and above	352 (94.6)
APGAR 1'		7.9 ± 1.75
	0-3 (Concerning)	18 (4.8)
	4-6 (Moderately Abnormal)	31 (8.3)
	7-10 (Reassuring)	323 (86.8)
APGAR 5'		8.7 ± 0.94
	0-3 (Concerning)	2 (0.5)
	4-6 (Moderately Abnormal)	14 (3.8)
	7-10 (Reassuring)	356 (95.7)
Mode of Delivery	Vaginal	80 (21.5)
	Emergency CS	285 (76.6)
	Elective CS	7 (1.9)
Multiple Gestation	Singleton	268 (72.0)
	Multiple	104 (28.0)
Maternal Hypertension		105 (28.2)
GDM		127 (34.1)
PPROM		67 (18.0)
Antenatal Corticosteroids		159 (42.7)

Univariate Analysis in the Relationship between Perinatal Factors and Presence of GMH

Perinatal Factor	GMH Present n (%) / β coefficient	Odds Ratio (95% Confidence Interval)	p-value
Sex		0.98 (0.65 – 1.50)	0.934
Male, n=195	73 (37.4)		
Female, n=177	67 (37.9)		
GA	0.038	1.04 (0.96 – 1.12)	0.326
BW	0.000	1.00 (1.00 – 1.00)	0.307
BS	0.053	1.06 (0.98 – 1.14)	0.169
APGAR 1'		0.96 (0.51 – 1.78)	0.889
0 – 6, n=49	18 (36.7)		
7 – 10, n=323	122 (37.8)		
APGAR 5'		1.30 (0.48 – 3.58)	0.606
0 – 6, n=16	7 (43.8)		
7 - 10, n=356	133 (37.4)		
Mode of Delivery		1.00 (0.60 – 1.65)	0.978
Vaginal, n=80	30 (37.5)		
CS, n=292	110 (37.7)		
Multiple Gestation		1.05 (0.66 – 1.67)	0.837
Multiple, n=104	40 (38.5)		
Singleton, n=268	100 (37.3)		
Maternal Hypertension		1.03 (0.65 – 1.64)	0.908
Present, n=105	40 (38.1)		
Absent, n=267	100 (37.5)		
GDM		1.24 (0.80 – 1.92)	0.343
Present, n=127	52 (40.9)		
Absent, n=245	88 (35.9)		
PPROM		1.06 (0.62 – 1.83)	0.827
Present, n=67	26 (38.8)		
Absent, n=305	114 (37.4)		
Antenatal Corticosteroids		0.84 (0.55 – 1.28)	0.406
Given, n=159	56 (35.2)		
Not Given, n=213	84 (39.4)		

Association between Germinal Matrix Hemorrhage at the First Week of Life and Perinatal Factors of Preterm Neonates Born at St. Luke's Medical Center

(EP-007)

Adrian Christopher A. Elio, MD and Mariaem M. Andres, MD, FPCR

Results

140 out of the 372 subjects (37.6%) had germinal matrix hemorrhage, of which, 29.8% had grade I, 6.5% had grade II, 0.8% had grade III and 0.5% had grade IV GMH.

Univariate and multivariate analyses showed no statistically significant association between the presence of GMH and sex, gestational age, birthweight, Ballard score, Apgar score, mode of delivery, multiple gestation, maternal hypertensive disorder, gestational diabetes mellitus, PPROM, and use of antenatal corticosteroids.

Multivariate Analysis in the Relationship between the Perinatal Factors and Presence of GMH

Perinatal Factor	Odds Ratio (95% Confidence Interval)	p-value
Male Sex	0.95 (0.62 – 1.46)	0.831
Multiple Gestation	1.16 (0.69 – 1.93)	0.574
With Maternal Hypertension	1.16 (0.69 – 1.94)	0.581
With GDM	1.22 (0.78 – 1.91)	0.386
With PPROM	1.11 (0.63 – 1.96)	0.725
Given Antenatal Corticosteroids	0.81 (0.53 – 1.25)	0.348
APGAR 5' of 0-6	1.59 (0.55 – 4.55)	0.392
Vaginal Delivery	1.04 (0.60 – 1.78)	0.900
Birthweight less than 2,500 grams	1.00 (1.00 – 1.00)	0.215

For inquiries, please e-mail Adrian Christopher A. Elio, MD (acelio1216@gmail.com) and Mariaem M. Andres, MD, FPCR (mmandres@stlukes.com.ph)

Association between Germinal Matrix Hemorrhage at the First Week of Life and Perinatal Factors of Preterm Neonates Born at St. Luke's Medical Center

(EP-007)

Adrian Christopher A. Elio, MD and Mariaem M. Andres, MD, FPCR

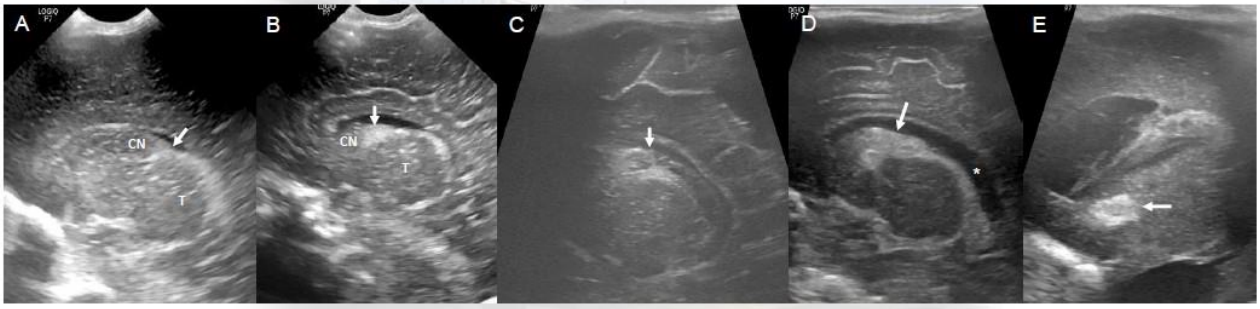

***A**. Normal sagittal cranial ultrasound showing the caudothalamic groove (→) between the caudate nucleus (CN) and thalamus (T); **B**. Grade I GMH showing hyperechoic focus localized in the caudothalamic groove (→); **C**. Grade II GMH showing extension of the hemorrhage (→) into the non-dilated ventricle; **D**. Grade III GMH showing intraventricular hemorrhagic extension (→) with ventricular dilatation (*); **E**. Grade IV GMH showing parenchymal hemorrhage at the caudate nucleus (→)*

For inquiries, please e-mail Adrian Christopher A. Elio, MD (acelio1216@gmail.com) and Mariaem M. Andres, MD, FPCR (mmandres@stlukes.com.ph)

Association between Germinal Matrix Hemorrhage at the First Week of Life and Perinatal Factors of Preterm Neonates Born at St. Luke's Medical Center

(EP-007)

Adrian Christopher A. Elio, MD and Mariaem M. Andres, MD, FPCR

Conclusion

Germinal matrix hemorrhage did not show any association with the various perinatal factors in this study.

Recommendations

We recommend further studies with a higher sample size and to consider evaluation of grades I and II versus the clinically significant grade III and IV GMH, as well as to look into the timing of and follow-up cranial ultrasound scans. The association between GMH and maternal COVID-19 infection during the perinatal period may also be a potential point of interest.

For inquiries, please e-mail Adrian Christopher A. Elio, MD (acelio1216@gmail.com) and Mariaem M. Andres, MD, FPCR (mmandres@stlukes.com.ph)

Association between Germinal Matrix Hemorrhage at the First Week of Life and Perinatal Factors of Preterm Neonates Born at St. Luke's Medical Center

(EP-007)

Adrian Christopher A. Elio, MD and Mariaem M. Andres, MD, FPCR

References

1. Healthy Newborn Network, "Philippines," 13 January 2020. [Online]. Available: https://www.healthynewbornnetwork.org/country/philippines/.
2. B. D. Coley, Caffey's Pediatric Diagnostic Imaging, 12th ed., Philadelphia, PA: Elsevier Saunders, 2013.
3. M. Castillo, Neuroradiology Companion: Methods, Guidelines, and Imaging Fundamentals, 3rd ed., Philadelphia, PA: Lippincott Williams & Wilkins, 2006.
4. A. M. Rudolph, C. D. Rudolph, M. K. Hostetter, G. Lister and N. J. Siegel, Rudolph's pediatrics, 21st ed., McGraw-Hill Professional, 2003.
5. A. Adefalujo, A. Yusuf, I. John, K. Soyebi and I. Fajolu, "Association between Germinal Matrix Hemorrhage and Perinatal Risk Factors in Preterm Neonates, in a Southwestern Nigerian Hospital," *Journal of Advances in Medicine and Medical Research,* pp. 1-11, 2018.
6. M. Fumagalli, L. A. Ramenghi, A. De Carli, L. Bassi, P. Fare, F. Dessimone, S. Pisoni, I. Sirgiovanni, M. Groppo, A. Ometto, D. Consonni, F. Triulzi and F. Mosca, "Cranial Ultrasound Findings in Late Preterm Infants and Correlation with Perinatal Risk Factors," *Italian Journal of Pediatrics,* 2015.
7. T. Wu, Y. Wang, T. Xiong, S. Huang, T. Tian, J. Tang and D. Mu, "Risk Factors for the Deterioration of Periventricular - Intraventricular Hemorrhage in Preterm Infants," *Scientific Reports,* 2020.
8. C. J. D. Gallaguez and N. D. P. Concepcion, "Association between Method of Delivery and Germinal Matrix Hemorrhage - Intraventricular Hemorrhage of Preterm Neonates," 2018.
9. Y. Pekcevik, A. Pasinli, E. A. Ozer and N. Erdogan, "Risk Factors of Germinal Matrix Intraventricular Hemorrhage in Premature Infants," *Iranian Journal of Pediatrics,* pp. 191-197, 2014.
10. A. J. Brouwer, F. Groenendaal, M. J. Benders and L. S. de Vries, "Early and Late Complications of Germinal Matrix-Intraventricular Haemorrhage in the Preterm Infant: What is New?," *Neonatology,* 2014.
11. K.-R. Kim, S.-W. Jung and D.-W. Kim, "Risk Factors Associated with Germinal Matrix Hemorrhage-Intraventricular Hemorrhage in Preterm Neonates," Journal of Korean Neurosurgical Society, 2014.

CASE REPORT

Multi-modality Approach to an Adolescent Scrotal Arteriovenous Malformation

Florelyn P. Agravante [1], Hance Rommel P. Panizales [1,3], Dennis C. Villanueva [1,2], Nathan David P. Concepcion[1,2]

ABSTRACT

Arteriovenous malformation (AVM) is a vascular abnormality that rarely affects the scrotum with only less than 20 reported cases in the literature. This is a retrospective review of an adolescent who complained of a slowly enlarging left scrotum initially thought to be due to a varicocele. Varicocelectomy was performed but the scrotal enlargement progressed. A testicular neoplasm was then considered. Imaging work-up using grey-scale ultrasound with color Doppler study and contrast-enhanced computed tomography scan however revealed a tangle of abnormal vessels reflective a scrotal AVM, confirmed and subsequently managed via conventional angiography with transcatheter embolization prior to eventual surgical excision. The use of various pre-operative imaging techniques for visualization, characterization and diagnosis of such anomalies are very critical to provide the appropriate management for these patients.

Keywords: adolescent, arteriovenous malformation, male genital disease

[1] Institute of Radiology, St. Luke's Medical Center, Bonifacio Global City, Taguig, Philippines

[2] Institute of Radiology, St. Luke's Medical Center, Quezon City, Philippines

[3] De La Salle University Medical Center, Gov. D. Mangubat Ave., Dasmariñas City, Cavite, Philippines

Corresponding Author:
Nathan David P. Concepcion, MD
Section of Pediatric Radiology, Institute of Radiology, St. Luke's Medical Center, Rizal Drive cor. 32nd St. and 5th Ave., Taguig, Philippines
Email: *npconcepcion@stlukes.com.ph*

INTRODUCTION

Vascular anomalies include varicocele, hemangioma, lymphatic malformation and arteriovenous malformation (AVM). Among these, arteriovenous malformations are the least common [1]. AVMs are generally considered to be congenital in nature, but it can be familial or sporadic. There are also reports of acquired AVMs diagnosed in older patients without being present at birth [2].

AVMs usually occur intracranially, and less commonly in the extracranial head and neck, extremities, truncal and visceral sites. Such vascular anomalies rarely involve the scrotum or its contents, presenting in a broad spectrum of symptoms mainly as paratesticular or intratesticular masses, which are detected during the evaluation of acute pain, swelling, infertility, and bleeding [3]. Scrotal AVMs are extremely rare, and there are only less than 20 cases of Scrotal AVM reported in the literature. These can cause oligo or azoospermia due to elevation in the scrotal temperature [4].

This paper presents a rare occurrence of a scrotal AVM in an adolescent, and the importance of multi-modality imaging techniques in the diagnosis and multi-disciplinary management of patients with such a condition. This was approved by the hospital's Institutional Ethics Review Board.

THE PATIENT

A 17-year-old Filipino male presented with a slowly enlarging left scrotum for five years. Initial diagnosis was a varicocele, for which he underwent varicocelectomy in 2017. However, the scrotal enlargement progressed prompting further evaluation two years after surgery.

Grey-scale ultrasound with color Doppler study was performed which demonstrated significant dilatation of pulsating peritesticular vessels bilaterally even at rest measuring up to 0.55 cm in maximum diameter (Fig. 1). The testicles were also smaller than usual. A scrotal AVM was considered.

Fig. 1 Ultrasound with color Doppler study of the patient in sagittal view shows significant dilatation of the peritesticular vessels (*arrowheads*). These were observed to be pulsatile (*not shown*) which suggests an arteriovenous malformation rather than a varicocele. The testicle (T) is also small for age

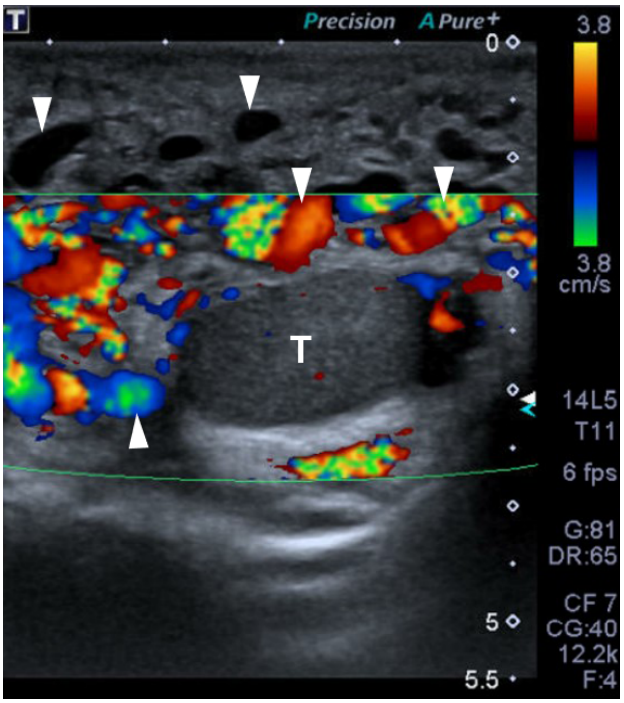

Contrast-enhanced lower abdominal computed tomography (CT) scan (Fig. 2) was also done which revealed a network of dilated serpiginous vascular structures in both scrotal sacs, left significantly more than right, with approximate aggregate measurement of 8.3 x 11.3 x 13.4 cm (anteroposterior x transverse x craniocaudal dimensions) in keeping with the sonographic consideration. The AVMs appeared to be supplied and drained by the internal and external iliac vessels.

Fig. 2 Axial contrast-enhanced lower abdominal CT image in soft tissue setting demonstrates the network of dilated serpiginous vascular structures in both scrotal sacs (*asterisk*), left significantly more than the right

Patient then underwent pre-operative conventional angiography (Fig. 3a) confirming the diagnosis with selective catheterization and embolization achieving significant devascularization (Fig. 3b). Ligation and excision of the AVM were performed with no complications.

Fig. 3a–b Conventional Angiography (**a**) with selective catheterization of the left internal iliac artery confirms the diagnosis of arteriovenous malformation (*asterisk*). Post-embolization (**b**) with alcohol and coils (*arrowheads*) resulted to significant devascularization of the lesion

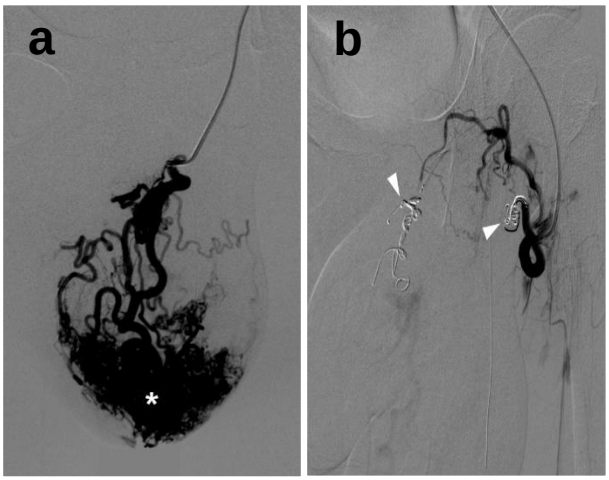

CONCLUSION

Although ultrasound and cross-sectional imaging are important tools to diagnose AVMs, transcatheter angiography is needed to better delineate the feeding vessels and draining veins [1,4], as in this case.

Embolization and surgical resection are the recommended options in patients with scrotal AVMs. Embolization is performed prior to surgical resection to minimize bleeding during the operation. Spermatogenesis has been shown to improve following surgery [4]. Thus, medical imaging using the various modalities play a critical role in the evaluation of patients with scrotal enlargement for proper diagnosis and appropriate management.

REFERENCES

1. Guerrera Avendaño GML, Enriquez García R, Saldivar Rodea CA, Sierra Juárez MÁ, Sotelo Cuéllar JS. Scrotal Arteriovenous Malformation: Case Report. Radiol Case Rep 2022;17(4):1266–1270. https://doi.org/10.1016/j.radcr.2022.01.055.

2. Tasiou A, Tzerefos C, Alleyne CH Jr, et al. Arteriovenous Malformations: Congenital or Acquired Lesions? World Neurosurg 2020 Feb;134:e799–e807. https://doi.org/10.1016/j.wneu.2019.11.001.

3. Mohammad A, Sahyouni W, Almeree T, Alsaid B. Angioembolization of Scrotal Arteriovenous Malformations: A Case Report and Literature Review. Case Rep Vasc Med 2020;2020:8373816. https://doi.org/10.1155/2020/8373816.

4. Zachariah JR, Gupta AK, Lamba S. Arteriovenous malformation of the scrotum: Is preoperative angioembolization a necessity? Indian J Urol 2012;28(3):329–334. https://doi.org/10.4103/0970–1591.102716.

CASE REPORT

Intrathoracic Renal Ectopia with Congenital Diaphragmatic Hernia

Gia Marie P. Nicolasora[1], Patricia Rose Dairo-Mabansag[1]

ABSTRACT

Congenital thoracic ectopic kidney is a very rare developmental disorder. It is often asymptomatic and discovered incidentally on chest radiography or ultrasonography. Symptoms can be present if it is associated with diaphragmatic defect and respiratory compromise. Herein is a case of a newborn male with cyanosis and respiratory distress since birth. Imaging eventually revealed the presence of intrathoracic ectopic left kidney with congenital diaphragmatic hernia. Radiological knowledge and increased awareness of this rare condition can avoid undue investigations and reduce patient morbidity.

Keywords: congenital, diaphragmatic hernia, renal ectopia

[1] Department of Radiology, Eastern Visayas Medical Center, Leyte, Philippines

Corresponding Author:
Gia Marie P. Nicolasora, MD
Department of Radiology, Eastern Visayas Medical Center, Tacloban City, Leyte, Philippines
Email: *g.nicolasora@gmail.com*

INTRODUCTION

Thoracic kidney is the rarest form of renal ectopia, with only about 200 cases reported and published in medical literature, and majority of them are in adults [1]. Most ectopic kidneys are found in the lower lumbar or pelvic region secondary to failure of ascent during fetal life. Intrathoracic kidney has the lowest frequency rate among all renal ectopias with a prevalence rate of about less than 0.01% [2]. The reported incidence is less than 5 per 1 million births [3]. It accounts for 5% of all renal ectopias and its association with congenital diaphragmatic hernia has been reported to have an incidence of only 0.25% [4,5].

Due to its rarity, literature on intrathoracic kidney, its management, prognosis and complications is sparse and is confined to case reports [5]. This paper presents a case of intrathoracic left kidney with congenital diaphragmatic hernia with review of literature on this condition.

THE PATIENT

Clinical Data

A full-term, male infant, from Leyte, Philippines, presented with respiratory distress. He was delivered via Cesarean section with appropriate weight for gestational age at a maternity clinic. Upon birth, the patient presented with cyanotic episodes, especially during crying, and had poor suck. Persistence of cyanosis prompted medical consultation and subsequent admission.

Physical examination showed decreased breath sounds in the left hemithorax and an apex beat heard at the right midclavicular line, level of 4^{th}–5^{th} intercostal space. Other physical examination findings were unremarkable. Patient was transferred to the neonatal intensive care unit for monitoring. Laboratory investigations were done and revealed *Staphylococcus haemolyticus* on blood culture and the patient was managed as a case of sepsis.

Diagnostic Imaging and Management

Chest and abdominal radiographs at 7 days old (Fig. 1a) showed multiloculated, large cystic lesions at the left hemithorax. Contralateral deviation of the mediastinal structures was noted. There is a focal, markedly dilated bowel loop in the abdomen. Lateral radiograph revealed a rounded opacity in the posterior part of the lower chest (Fig. 1b). Differential considerations at that time were congenital diaphragmatic hernia and congenital cystic adenomatoid malformation.

Ultrasound examination, at 12 days old, revealed absence of kidney in the left renal fossa and a normally placed right kidney. No ectopic kidney was visualized in the lower

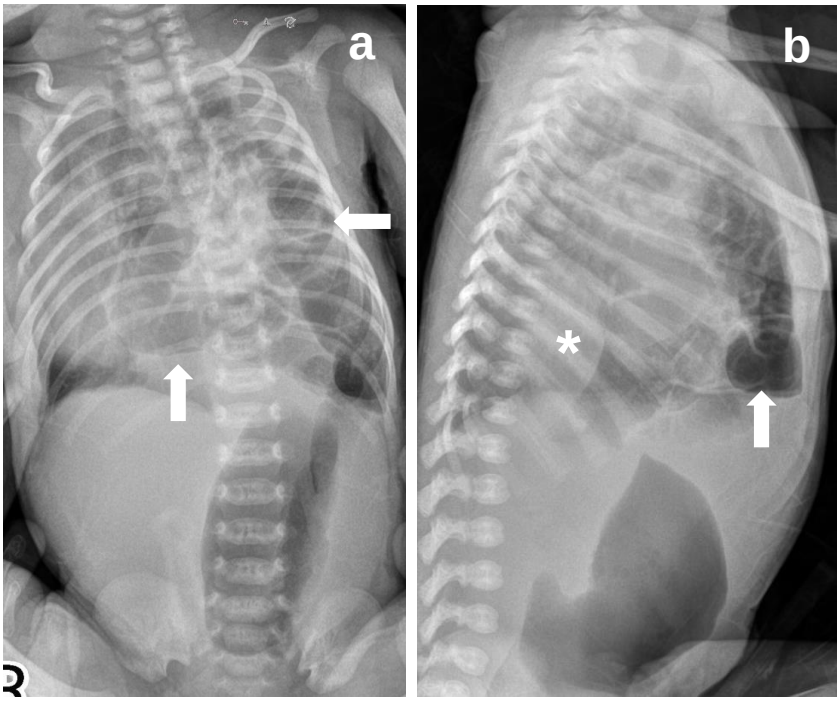

Figs. 1a–b Babygram at 7 days old. Frontal (**a**) and lateral (**b**) projections revealed multi-loculated large cystic lesions (arrows) in the left hemithorax with marked right-sided deviation of the mediastinal structures. A rounded opacity (asterisk) was also noted at the posterior part of the lower hemithorax

abdomen. Ultrasound was carried out in the intercostal region and revealed the left kidney in the left hemithorax (Fig. 2a) showing abnormal rotation, with its hila facing inferiorly, and has a lobulated echostructure. Medial deviation of the lower pole of the left kidney is also noted (Fig. 2b).

Contrast-enhanced computed tomography (CT) of the thorax and abdomen was also performed. This revealed a large left-sided diaphragmatic defect through which bowel loops are seen herniating through and occupying most of the left hemithorax, slightly extending to the right. The displaced left kidney is seen within the thoracic region (Fig. 3). The spleen is seen in the lateral aspect of the left hemiabdomen. No normal-looking reniform structure is appreciated in the left renal fossa. The right kidney is normal in size, shape, and position. The visualized collecting systems are not dilated (Fig. 4a–b).

The patient was referred to the pediatric surgery department and surgical intervention was done, with the herniated bowels reduced into the abdominal cavity. The ectopic left kidney was carefully reduced to the retroperitoneal cavity and the diaphragm was repaired. Post-operative course was uneventful with normal laboratory findings. The patient was discharged well and was advised for long-term follow-up.

Figs. 2a–b Ultrasound of the left hemithorax at 12 days old. Gray-scale sonographic images showed a left kidney located superior to the spleen with bowel loops in between (**a**). The left renal hilum is rotated inferiorly with medial deviation of the lower pole of the kidney (**b**)

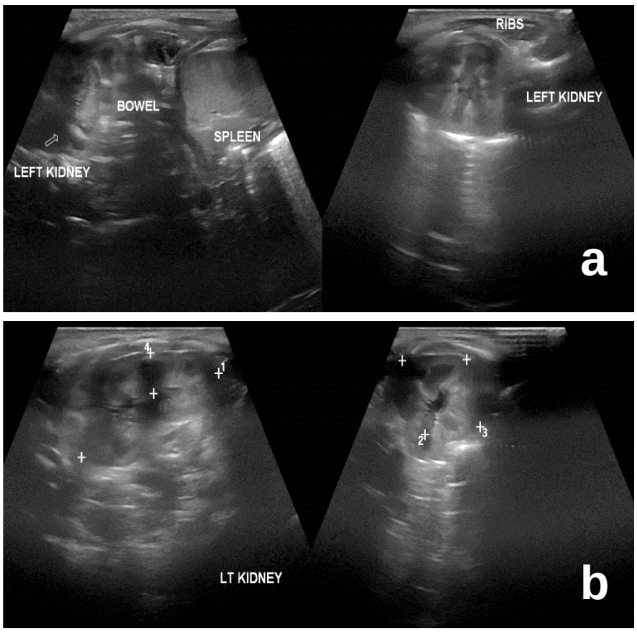

Fig. 3 Chest CT scan at 14 days old. Axial image in soft tissue window setting revealed herniated bowel loops (arrows) occupying left hemithorax. The displaced left kidney (arrowhead) is seen posteriorly

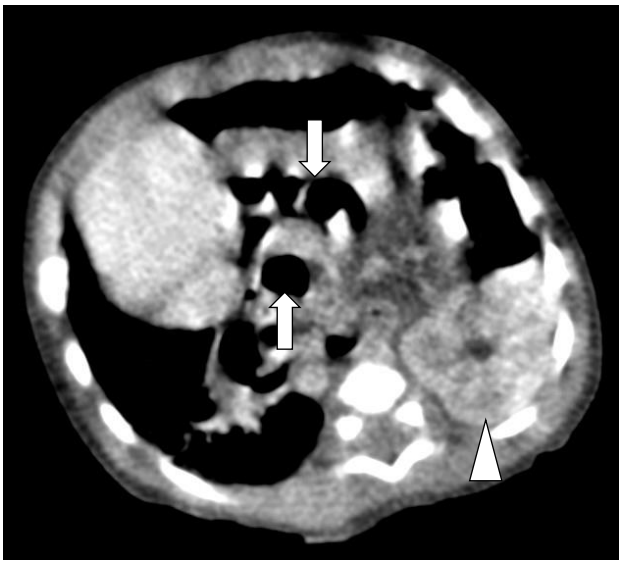

DISCUSSION

Ectopic kidney refers to a kidney located at any site other than the renal fossa [2]. The abnormality is found more commonly on the left (62%) than the right side (36%) and is rarely bilateral (2%). Males (63%) are affected more frequently than females (37%) [2]. About 60% of ectopic kidneys are placed in the pelvis minor, 35% paravertebrally, and less than 5% in the thoracic cavity [4]. With a prevalence rate of less than 0.01%, intrathoracic kidneys are extremely rare [2].

Intrathoracic kidney is not always associated with diaphragmatic hernia [2]. Studies showed an ectopic thoracic kidney that has not herniated through the diaphragmatic defect, but has been responsible for preventing closure of the diaphragm, which resulted in a diaphragmatic hernia [6]. Herniation of the kidney through the diaphragm is only possible if the kidney has a long renal artery and ureter. The renal vasculature and ureter on the affected side are usually significantly longer than those in the normally positioned kidney [7]. Intrathoracic ectopic kidneys do not show dysplastic parenchymal architecture and renal function is usually normal [8].

Various techniques have been used for the diagnosis of intrathoracic kidney. The radiographic appearance of a thoracic kidney may be similar to that of posterior mediastinal masses. In this case, a smooth round mass is seen extending into the chest near the midline on frontal chest radiograph and at the posterior aspect of the diaphragm on the lateral view [9]. Ectopic kidney is generally discovered accidentally during routine abdominal ultrasound [10]. In every case, when the kidney cannot be found in its typical location on ultrasound, it is necessary to look for it outside the lumbar area. Radiologists should consider examining the thorax before labeling a patient with unilateral renal agenesis [11]. On prenatal sonography, the kidneys can be seen as early as 12 weeks of gestation. True intrathoracic ectopic kidney presents during fetal life and has four characteristics: (1) a rotation anomaly with the hilum facing inferiorly, (2) structural abnormalities, such as lobulated or deformed shape (3) a long ureter, (4) anomalous high derivation of the renal vessels from the thoracic aorta, and (5) medial deviation of the lower pole of the kidney [13].

Fig. 4a–b. Abdominal CT scan at 14 days old. Coronal (**a**) and sagittal (**b**) images in soft tissue window setting show the liver (L) occupying most of the right hemiabdomen. The spleen (S) is seen in the lateral aspect of the left hemiabdomen and inferior to the displaced intrathoracic left kidney (arrows). Note the heart (H) is displaced to the right

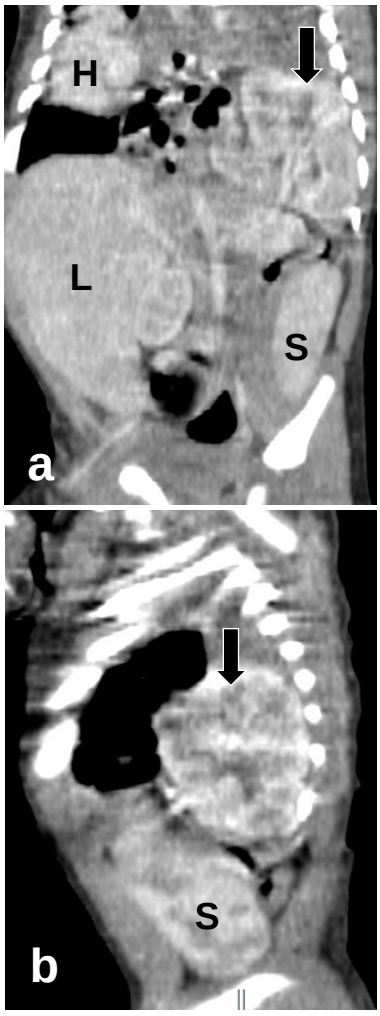

CT and MRI provide not only detection of a posterior mediastinal lesion but also visualization of its contour, extent, and size. CT urography is also helpful in confirming the diagnosis and in demonstrating the collecting system, vascular supply, and complications [9]. Renal scintigraphy with dimercaptosuccinic acid (DMSA) provides functional and anatomic information as well as perfusion of the kidneys [12].

Intrathoracic ectopic kidneys have been classified into four subtypes with different associations and approach to management: Group 1: Intrathoracic ectopic kidney associated with a closed diaphragm; Group 2: Intrathoracic ectopic kidney associated with diaphragmatic eventration; Group 3: Intrathoracic ectopic kidney associated with traumatic diaphragmatic rupture; and Group 4: Intrathoracic ectopic kidney associated with a congenital diaphragmatic hernia. The first two groups are usually asymptomatic and have a benign course, while the other two are often symptomatic and require therapeutic intervention [14].

Congenital diaphragmatic hernia associated with intrathoracic ectopic kidney have been reported to have ureters and vascular structures of adequate length, allowing reduction of the ectopic kidney into the abdominal cavity without hemodynamic impairment. Due to the ectopic nature of the kidney and the risk of complications, patients would benefit from long-term close monitoring and follow-up [15].

CONCLUSION

The association between intrathoracic renal ectopia and congenital diaphragmatic hernia is a very rare occurrence that poses diagnostic and management dilemmas for clinicians. When managing cases of intrathoracic kidney, it is crucial to accurately identify the specific subtype based on radiologic studies. This information is vital for determining the most appropriate treatment approach and devising an effective management plan. A meticulous approach and careful handling of the intrathoracic kidney are necessary to ensure optimal outcomes and preserve function. Radiologic imaging remains the main diagnostic tool for its detection.

REFERENCES

1. Lacasta Garcıa JD, Sanz Velez JI, Abad Roger J. Ectopic thoracic kidney. Actas Urológicas Españolas 1999;23(6):536–538.
2. Donat SM, Donat PE. Intrathoracic kidney: a case report with a review of the literature. J Urol 1988;140:131–2.
3. Sozubir S, Demir H, Ekingen G, Guvenc BH. Ectopic thoracic kidney in a child with congenital diaphragmatic hernia. Eur J Pediatr Surg 2005;15:206–9.
4. Fiaschetti V, Velari L, Gaspari E, Mastrangeli R, Simonetti G. Adult intrathoracic kidney: A case report of bochdalek hernia. Case Report Med 2010;2010. pii 975168.
5. Motiani PD, Gupta PK, Aseri KC, Agarwal KC. Bochdalek hernia on the right side in an adult - case report and review. Lung India 1991;9:63–5.
6. Fleischner FG, Robins SA, Abrams M. High Renal Ectopia and Congenital Diaphragmatic Hernia. Radiology 1950;55:24.
7. Karaoglanoglu N, Turkyilmaz A, Eroglu A, Alici HA. Right-sided Bochdalek hernia with intrathoracic kidney. Pediatr Surg Int 2006;22(12): 1029–1031.
8. Sarac M, Bakal U, Tartar T, Canpolat S, Kara A, Kazez A. Bochdalek hernia and intrathoracic ectopic kidney: presentation of two case reports and review of the literature. Niger J Clin Pract 2018;21:681–6.
9. Panossian DH, Thomas RD, Anholm JD. Roentgenogram of the month: asymptomatic mediastinal mass in an elderly man. Chest 1995;107:1165–6.
10. Sumner TE, Volberg FM, Smolen PM. Intrathoracic kidney − diagnosis by ultrasound. Pediatr Radiol 1982;12(2):78–80.
11. Allen D, Bultitude MF, Nunan T, Glass JM. Misinterpretation of radioisotope imaging in pelvic kidneys. Int J Clin Pract Suppl. 2005 Apr;(147):111–112.
12. Natarajan A, Agrawal A, Purandare N, Shah S, Rangarajan V. Rare case of thoracic kidney detected by renal scintigraphy. Indian J Nucl Med 2016;31:219–221.
13. Bronshtein M, Amit A, Achiron R, et al. The early prenatal sonographic diagnosis of renal agenesis: techniques and possible pitfall. Prenat Diagn 1994;14:291.
14. L. Pfister-Goedeke and E. Brunier. Intrathoracic kidney in childhood with special reference to secondary renal transport in Bochdalek's hernia. Helvetica Paediatrica Acta 1979;34(4):345–457.
15. Obatake M, Nakata T, Nomura M, et al. Congenital intrathoracic kidney with right Bochdalek defect. Pediatr Surg Int 2006;22:861–3.

CASE REPORT

Neonate Presenting with Multiple Cardiac Masses

Alexandra L. Rama-Estimo[1], Yvette G. Diola[2], April Jann Tutor-Malaza[2], Ann M. Co[1], Margaret. S. Modequillo[2]

ABSTRACT

This is a case of a neonate with multiple cardiac masses causing right ventricular outflow tract obstruction. Further work-up revealed presence of subependymal hamartoma, subependymal giant cell astrocytoma, cortical tubers and retinal astrocytic hamartoma in the right eye. Upon fulfillment of a set criteria, the patient was diagnosed with Tuberous Sclerosis Complex.

[1] Department of Radiology, Perpetual Succour Hospital, Cebu City, Cebu, Philippines

[2] Department of Pediatrics, Perpetual Succour Hospital, Cebu City, Cebu, Philippines

Corresponding Author:
Alexandra L. Rama-Estimo, MD
Department of Radiology, Medical Imaging Center, Perpetual Succour Hospital, Gorordo Avenue, Cebu City, Cebu, Philippines
Email: *alexandrarama1822@gmail.com*

INTRODUCTION

Tuberous sclerosis complex is a disease characterized by presence of benign hamartomas in multiple organs, cortical tubers, subependymal giant cell astrocytomas and renal angiomyolipomas [1]. It occurs in 1 in 6000 live births [2]. In utero, the earliest sign of tuberous sclerosis is rhabdomyoma. Cardiac rhabdomyoma is the most common pediatric cardiac tumor and 51–86% of cases are associated with tuberous sclerosis [1]. The presentation and clinical manifestations of tuberous sclerosis complex are diverse. Patients may be asymptomatic or present with intellectual disabilities and seizures [3].

THE PATIENT

This is a case of a neonate with multiple cardiac masses initially found during prenatal ultrasound and fetal 2D echocardiography. Patient was then worked up after delivery.

Patient was born via normal spontaneous delivery at 37 3/7 weeks of gestation with a normal birthweight and with an APGAR score of 7,9. Physical examination showed no head abnormality, acyanotic with good cry, and normal neurologic examination including reflexes. A grade 2 holosystolic murmur was identified at the second left intercostal space. No heredofamilial disease was noted.

Echocardiography was done revealing multiple homogeneous soft tissue masses within the right ventricular cavity and right ventricular lateral wall. There is also a 1.2 x 1.8 cm mass at the right ventricular outflow tract, partially obstructing the pulmonary outflow by more than 50%. Multiple similar masses are also detected at the left ventricular cavity, interventricular septum, and left ventricular lateral wall. The findings were suggestive of rhabdomyomas (Fig. 1).

The patient was referred to a pediatric neurologist and a cranial magnetic resonance imaging (MRI) was done revealing subependymal nodules/hamartomas, presumed subependymal giant cell astrocytoma, cortical/subcortical tubers, and obstructive hydrocephalus (Fig. 2). Referral to an ophthalmologist was also done wherein retinal astrocytic hamartoma was identified in the right eye.

A whole abdominal ultrasound was also performed with no remarkable findings.

The constellation of findings fulfilled the criteria for a diagnosis of Tuberous Sclerosis Complex.

DISCUSSION

Tuberous sclerosis complex, also known as tuberous sclerosis or Bourneville Disease, is an inherited autosomal dominant disease with a broad clinical spectrum [3]. Symptoms vary from severe intellectual impairment and uncontrollable epilepsy to normal intelligence and

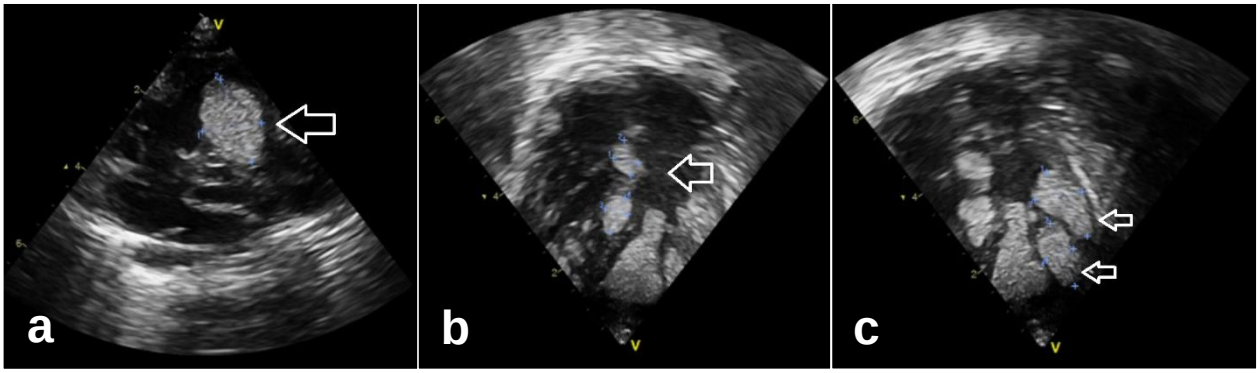

Fig. 1a-c Echocardiography revealed a homogeneous echogenic soft tissue masses (arrows) in the right ventricular outflow tract (**a**), interventricular septum (**b**) and left ventricle (**c**)

without seizures [3]. It is a multi-organ disease characterized by presence of hamartomas, cortical tubers, subependymal giant cell astrocytomas, and renal angiomyolipomas [1]. Its occurrence is attributed to mutation of the tumor suppressor genes TSC1 or TSC2, which encodes the proteins hamartin and tuberin, respectively, and affects 1 in 6,000 newborns [3]. There is few information on the disease's regional prevalence or trends but is perceived to be a rare disease by clinicians in Asia-Pacific countries [4].

According to the updated International Tuberous Sclerosis Complex Diagnostic Criteria and Surveillance and Management Recommendations [5], definite diagnosis of tuberous sclerosis complex is made when at least 2 major or one major plus two minor features are present (Table 1).

The hallmark of tuberous sclerosis complex is the involvement of the central nervous system [3]. Cortical tubers are characteristic brain lesions and are best seen on MRI [6]. Its appearance on MRI varies in age. In neonates and young children, these lesions are hyperintense to premyelinated white matter on the T1-weighted (T1W) sequence as in this case and hypointense on the T2-weighted (T2W) scans. In older children and adults, the lesions are iso-to hypointense on T1W and hyperintense to both gray and white matter on T2W images. Enhancement occurs in less than 5% of patients [7].

Aside from cortical tubers, subependymal nodules or hamartomas are also found in 95% of patients with tuberous sclerosis complex. They appear as irregular nodules protruding into the CSF-filled ventricles. In neonates, they usually appear hyperintense to adjacent unmyelinated white matter on T1W images [7].

Table 1 Diagnostic criteria for Tuberous Sclerosis. Adapted from the Updated International Tuberous Sclerosis Complex Diagnostic Criteria and Surveillance and Management Recommendations [5]. * These are present in this case

Major Criteria	Minor Criteria
Hypomelanotic macules (≥3; at least 5 mm in diameter)	"Confetti" skin lesions
Angiofibroma (≥3) or fibrous cephalic plaque	Dental enamel pits (≥3)
Ungual fibromas (≥2)	Intraoral fibromas
Shagreen patch	Retinal achromic patch
Multiple retinal hamartomas	Multiple renal cysts
Multiple cortical tubers and/or radial migration lines*	Nonrenal hamartomas
Subependymal nodule (≥2)*	Sclerotic bone lesions
Subependymal giant cell astrocytoma*	
Cardiac rhabdomyoma*	
Lymphangiomyomatosis (LAM)	
Angiomylipomas (≥2)	

Subependymal giant cell astrocytomas (SGCA) are also seen with an incidence of 15% in patients with tuberous sclerosis. They are located at or near the foramen of Monro and appear heterogeneous on cross-sectional imaging. They tend to enlarge and are associated with obstructive hydrocephalus [7].

White matter lesions presenting as straight or curvilinear bands, extending from the ventricle through the cerebrum toward the cortex, wedge-shaped lesions, nonspecific tumefactive or conglomerate foci or cerebellar radial

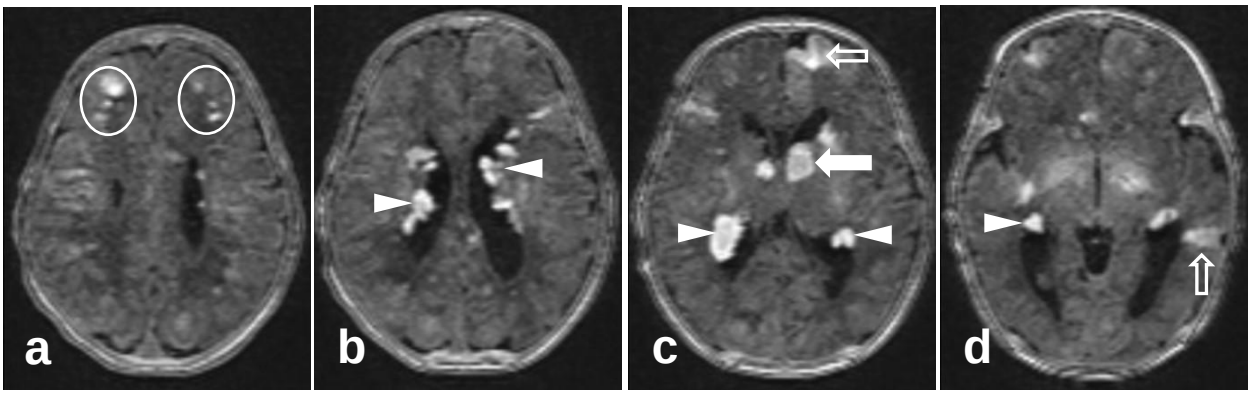

Fig. 2a-d Axial T1-weighted magnetic resonance images of the brain show white matter lesions (encircled), subependymal nodules (arrowheads), cortical tubers (open arrows) and subependymal giant cell astrocytoma (arrow)

bands can also be seen. In infants, they also appear as hyperintense lesions on T1W image and hypointense to unmyelinated white matter on T2W studies. In older children and adults, they are typically iso- to hypointense to white matter on T1W images and hyperintense to both gray and white matter on T2W scans. Twelve percent of the lesions show enhancement after contrast administration [7].

Another presentation of tuberous sclerosis is the presence of cardiac rhabdomyomas. Cardiac rhabdomyoma is the earliest clinical sign of tuberous sclerosis in utero. In ultrasound, it appears as rounded, homogeneous, hyperechoic areas within the myocardium. In contrast-enhanced CT, it is identified as low-density masses. Variable signal characteristics are seen on MRI but are often isointense or minimally hyperintense to the myocardium on T1W images and hyperintense on T2W images. Cardiac rhabdomyomas tend to increase in size until 32 weeks of gestation and progressively regress with observance of complete regression by 6 years of age [1].

Other lesions associated with tuberous sclerosis include presence of retinal hamartomas, vascular abnormalities such as aneurysm formation, skin lesions, renal angiomyolipomas and lymphangioleiomyomatosis [3].

CONCLUSION

Tuberous sclerosis complex is a rare multi-organ disease with a wide clinical spectrum that includes neurologic and cardiac manifestations. In this case, the earliest sign was the presence of cardiac rhabdomyoma. Through the aid of various imaging techniques, the diagnosis of tuberous sclerosis was made. Imaging played an integral role in the appropriate diagnosis and evaluation of the disease.

REFERENCES

1. Coley BD, ed. Caffey's Pediatric Diagnostic Imaging, 12th ed. Philadelphia: Elsevier Saunders; 2013.
2. Uysal SP, Sahin PU. Tuberous sclerosis: A Review of the Past, Present and Future. Turk J Med Sci 2020;50:1665–1676.
3. Kleigman RM, Stanton BF, St Geme JW, Schor NF, Behrman RE. Nelson Textbook of Pediatrics, 20th ed. Philadelphia: Elsevier; 2016.
4. Lawson J A, Chan C F, Chi C S, et. al. Managing tuberous sclerosis in the Asia-Pacific region: Refining Practice and the role of Targeted Therapy. J Clin Neurosci 2014;21:1180–1187.
5. Northrup H, Aronow M E, Bebin E M, et al. Updated International Tuberous Sclerosis Complex Diagnostic Criteria and Surveillance and Management Recommendations, Pediatr Neurol 2021;123:50–66.
6. Swischuk L E. Imaging of the Newborn, Infant and Young Child, 5th ed. Philadelphia: Lippincott Williams and Wilkins; 2004.
7. Osborn A G. Diagnostic Neuroradiology, 1st ed. Missouri: Mosby; 1994: 94–98.

Pediatric Radiology Case Challenge: An Educational Activity for AOSPR 2022 Attendees

Jacqueline Austine U. Uy[1,2]

ABSTRACT

The following cases presented in this article were originally part of an interactive online quiz for the participants of the 20th Asian and Oceanic Society for Paediatric Radiology (AOSPR) Annual Scientific Meeting held virtually on August 19 and 20, 2022. The objectives for the quiz were to direct self-education of the attendees, to introduce confounding cases and test diagnostic ability, and to review and discuss the pertinent findings of the selected cases.

Included are seven cases showing various cranial and abdominal computed tomography (CT) and magnetic resonance imaging (MRI) studies, which range from mundane to the complex. Each case is followed by a brief discussion of relevant findings and differential diagnoses.

[1] Institute of Radiology, St. Luke's Medical Center, Bonifacio Global City, Taguig, Philippines

[2] Institute of Radiology, St. Luke's Medical Center, Quezon City, Philippines

Correspondence:
Section of Pediatric Radiology, Institute of Radiology, St. Luke's Medical Center
Rizal Drive cor. 32nd St. and 5th Ave., Taguig, Philippines
Email: *jauuy@stlukes.com.ph*

CASE 1

A 12-day-old boy delivered term by cesarean section after prolonged labor was referred for a brain CT scan due to an enlarging head circumference.

Fig. 1A–B Non-contrast axial CT images of the brain show (A) hydrocephalus, and (B) heterogeneous extra-axial collection compressing the adjacent right cerebellum

Question: Which of the following is NOT true regarding the etiology of the imaging findings?

A. More common in term infants (correct answer)
B. Ultrasound could be used to make an early diagnosis
C. MRI can identify the anatomic structures better than CT
D. None of the above

Posterior fossa abnormalities are common in high-risk term infants, seen in about 66%, the most common of which is hypoxic-ischemic encephalopathy. Central nervous system (CNS) malformation, infection and posterior fossa hemorrhages are also commonly identified [1].

In the case presented, the collection at the right posterior fossa (Fig. 1B) shows mass effect on the cerebellum, for which mass lesion and hemorrhage are initially considered. The neonate was clinically suspected to have a bleeding disorder such as hemophilia and referred for genetic testing, which made posterior fossa hemorrhage the most likely diagnosis. Posterior fossa hemorrhage in term neonates is rare and more common in preterms, however incidence may range from 3.4% to 4% in hemophiliacs [2]. It is also difficult to detect since clinical symptoms are non-specific and may include increased head circumference, seizures or respiratory distress. Respiratory symptoms may occur when the medulla oblongata is involved. In neonates suspected with hemorrhage, cranial ultrasound would usually be the initial imaging examination of choice.

CASE 2

A 4-month-old boy was admitted for pneumonia. The infant was also assessed to have developmental delay; hence imaging was performed.

Fig. 2 Non-contrast axial CT image of the brain shows an unusual hyperdensity of the thalami

Question: Hyperdensity of the thalami can be seen in?

A. Profound perinatal ischemia
B. Krabbe disease
C. Gangliosidosis
D. Glioma
E. All of the above (correct answer)

All of the choices would result in the finding of thalamic hyperdensities (Fig. 2) in this infant. Differential diagnoses would include inherited metabolic disorders (Lysosomal storage disorders/gangliosidoses, Krabbe disease), acquired toxic/metabolic, infectious, neoplastic (glioma, lymphoma), or hypoxic-ischemic encephalopathy. Perinatal ischemia should be suspected since the deep brain structures, including the thalami and basal ganglia [3] are the most metabolically active and are therefore most vulnerable, especially in the first 3 days of life. Ischemia secondary to the patient's pneumonia is less considered since CT hyperdensity is considered a late finding, while acute hypoxic-ischemic changes should present as hypodensity. CT scan however is less sensitive and ideally MRI should be performed.

Lysosomal storage disorders such as Krabbe disease would present as bilateral thalamic CT hyperdensity [4] early on, as well as the caudate nuclei, corona radiata and the cerebellar dentate nuclei. MRI with diffusion tensor imaging and spectroscopy may also be useful for early diagnosis and to detect the extent of white matter involvement. Imaging findings may however overlap with other leukodystrophies and hypoxic-ischemic encephalopathy.

CASE 3

An 8-year-old boy who was previously diagnosed with neurofibromatosis type I (NF-1) underwent an MRI study due to a 6-week history of headache and blurring of vision.

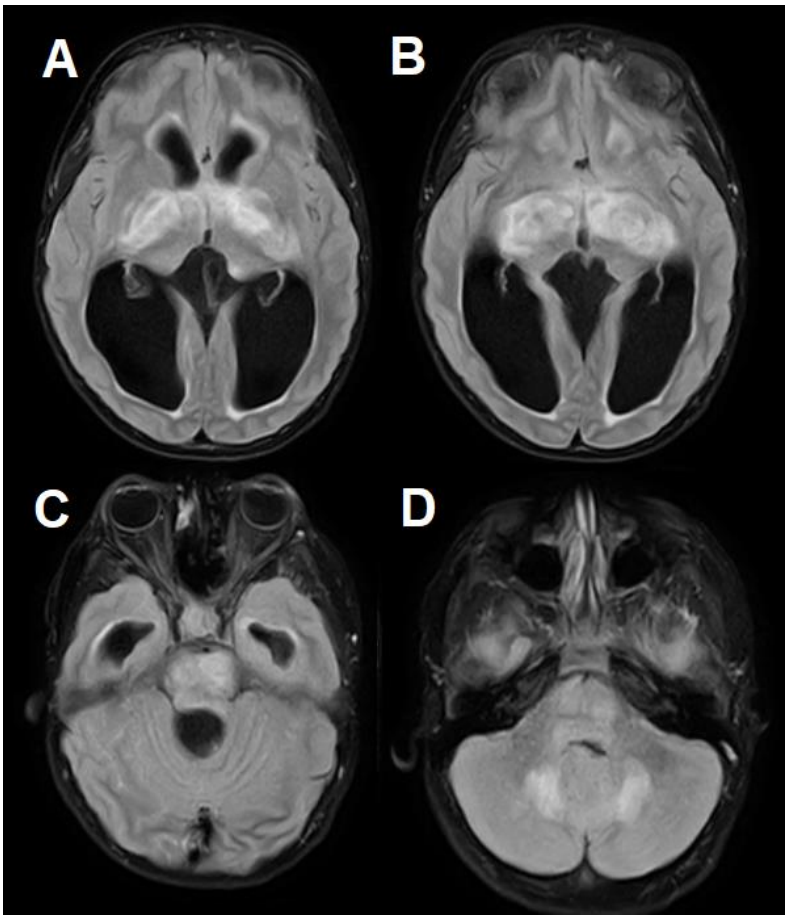

Fig. 3A–D Non-contrast axial MR images of the brain in fluid-attenuated inversion recovery (FLAIR) sequence show hyperintensities at the (A,B) bilateral globus pallidi, (C) midbrain, pons, and (D) dentate nuclei. Effaced fourth ventricle with hydrocephalus and transpendymal edema also detected

Question: What is the most commonly seen CNS MRI finding in Neurofibromatosis type I?

The most common brain lesions found in NF-1 on MRI are abnormal T2W hyperintensities, which are coined as focal areas of (high) signal intensity (FASI), without or with minimal mass effect. These rarely enhance after gadolinium infusion. These can be found in about 60% to 70% [5] or 60% to 80% [6] of pediatric NF-1 patients. MRI is the imaging modality of choice for detection of FASIs since these lesions are not usually seen on CT scan. The main differential diagnosis would be low-grade glioma which can present with more evident mass effect and enhancement.

The clinical significance of FASIs is largely unknown, and are believed to be caused by increased fluid accumulation in intramyelinic vacuoles. These lesions tend to decrease during adolescence, for which the reason remains unclear. The presence of concomitant optic gliomas within and outside the optic pathways may also muddle interpretation.

CASE 4

A 2-year-old girl presented with 4 days of abdominal pain and vomiting, and was admitted as a case of acute gastroenteritis. CT scan was done showing ileocolic intussusception.

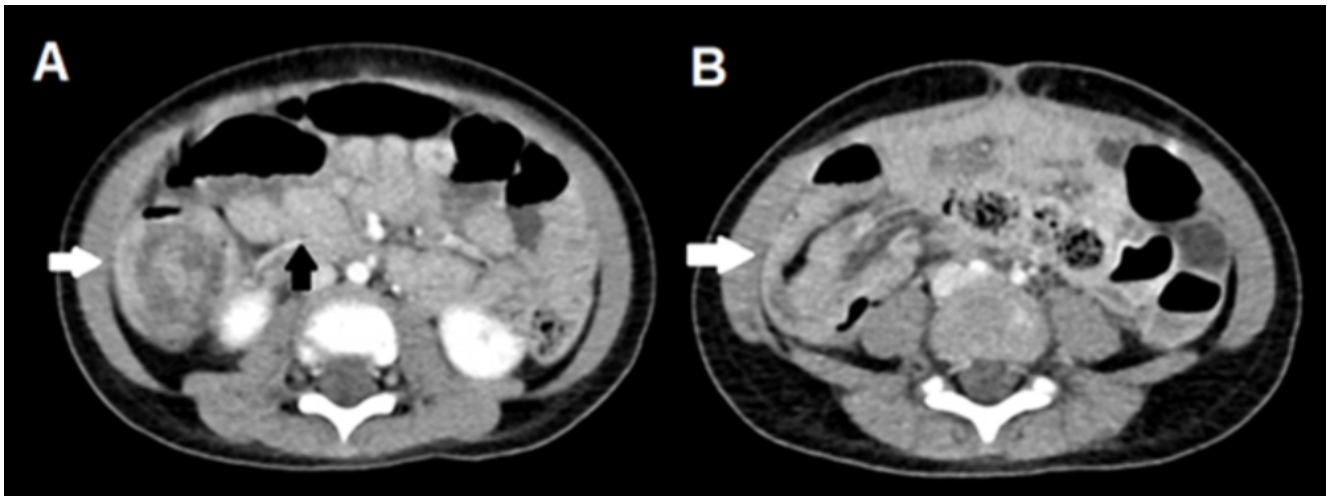

Fig. 4A–B Contrast-enhanced axial CT scan demonstrates (A) mesenteric adenopathy at the right hemiabdomen, with a 'target' lesion (A, B, white arrows) demonstrating ileocolic intussusception. There is (B) telescoping of the ileocecal region into the intussuscipiens

Question: The most likely lead point for intussusception is:

A. Lymphoid hypertrophy
B. Mesenteric lymph node
C. Juvenile Polyp
D. All of the above (correct answer)

Ileocolic intussusception is the most common type, seen in 75% to 95% of cases, with most of the causes being idiopathic. 1.5% to 12% [7] present with a pathologic lead point, while 90% of cases present with a lead point in adults. 66% of lead points are detectable during ultrasonography. The most common pathologic lead point is from Meckel diverticulum. The presence of a Meckel diverticulum is not a contraindication to air enema but there is an increased risk of recurrence of about 78.5%. Contraindications to fluoroscopic or ultrasound-guided reduction are the presence of pneumoperitoneum or peritonitis.

CASE 5

This is a case of a 12-year-old girl with 3-month history of abdominal bloatedness and discomfort.

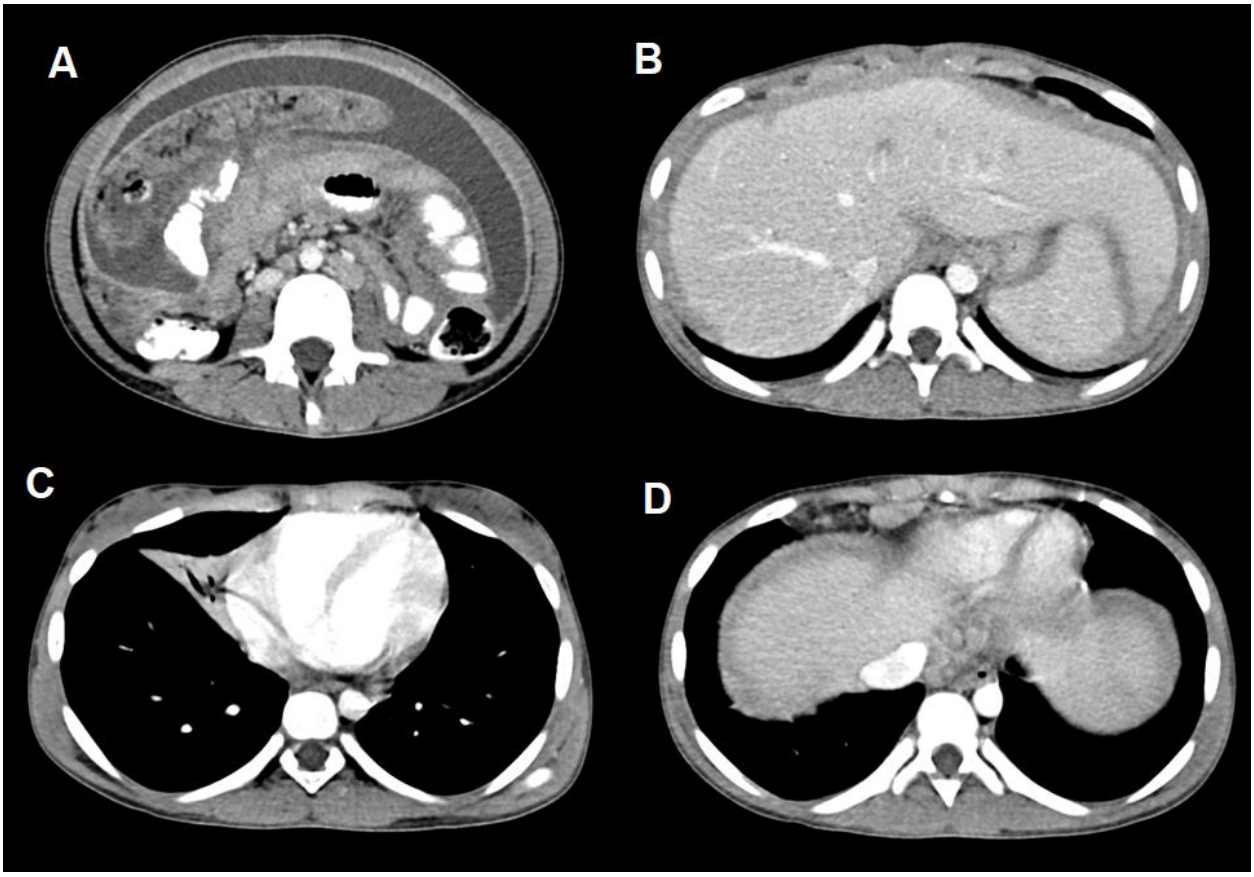

Fig. 5A–D Contrast-enhanced axial CT images demonstrate (A) ascites with smooth peritoneal thickening, as well and nodular mesentery. Other findings include (B) multifocal hepatic hypodense nodules, (C) incidental note of middle lobe atelectasis and (D) cardiophrenic lymphadenopathy

Question: What is the diagnosis based on the presented CT images?

A. Peritoneal carcinomatosis
B. Primary peritoneal mesothelioma
C. Peritoneal tuberculosis (correct answer)

Malignancy cannot be entirely ruled-out when faced with multi-organ involvement on imaging, particularly when presented with non-specific symptoms. Histopathologic findings in this patient would however prove the presence of extra-pulmonary tuberculosis. Abdominal involvement occurs in 11% to 12% of patients with extra-pulmonary tuberculosis [8], while peritoneal tuberculosis is the most common presentation. Based on the CT findings, a wet type of tuberculosis is considered, due to presence of ascites with peritoneal and mesenteric thickening.

Peritoneal tuberculosis would present as ascites, as seen in 70% to 90% [8], followed by peritonitis (38%), lymph node disease (23%), gastrointestinal (19%) and solid organ (10%) involvement. The most common solid organs involved are the liver and spleen in 70%, such as in our patient with hepatic nodules. The presence of mesenteric nodularity and peritoneal thickening in this case proved to be a diagnostic dilemna, since this mimics peritoneal carcinomatosis. With this in mind, the differential diagnoses of lymphoma and adenocarcinoma are not entirely ruled-out even in the pediatric population.

CASE 6

A 17-year-old boy with persistent abdominal pain despite endoscopic retrograde cholangiopancreatography (ERCP) for a known choledocholithiases.

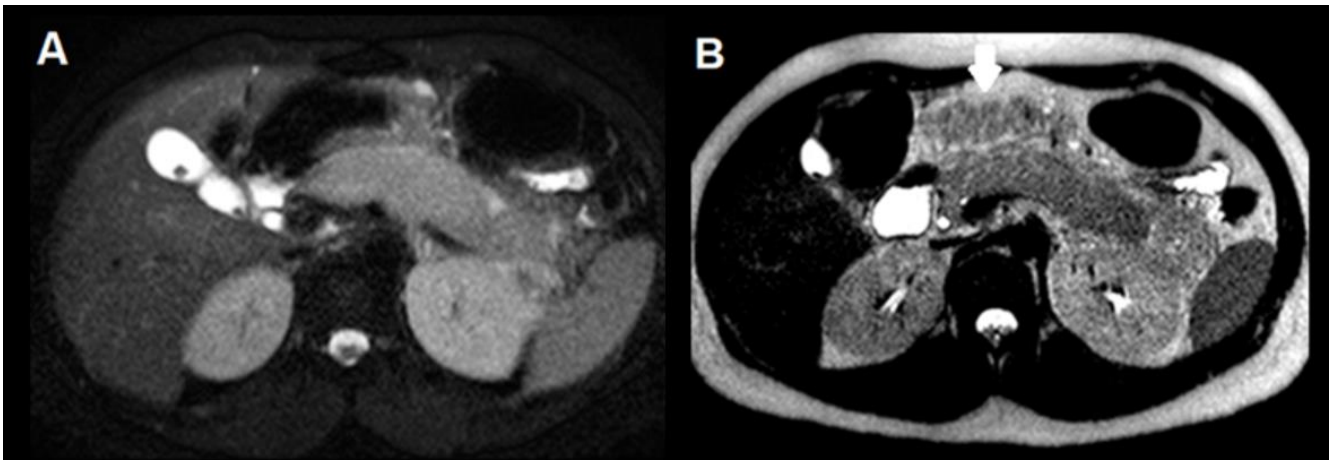

Fig. 6A–B Axial MRI of the abdomen reveals (A) cholelithiases and edematous pancreas with minimal peripancreatic fluid, while (B) there are also T2-weighted isointense and nodular peripancreatic and omental fat planes (white arrow)

Question: What would account for the unusual appearance of intra-abdominal fat?

A. Peritoneal carcinomatosis
B. Liposarcoma
C. Fat necrosis (correct answer)
D. Retroperitoneal fibrosis

The patient on MRI had findings suggestive for pancreatitis, therefore fat necrosis should be considered since this is a known complication of acute pancreatitis [9]. This is associated with low (12% mortality), and may develop over weeks to several months. The typical distribution of fat necrosis is peripancreatic, and extends to the fat planes of the transverse mesocolon, omentum and the mesenteric root. Fat necrosis is secondary to ghost fat cells damaged by pancreatic enzymes. Release of fatty acids precipitate with serum calcium, producing the phenomenon of saponification [10] of intra-abdominal fat.

Eventually when the acute phase of pancreatitis subsides, fat necrosis / saponification would take on the appearance of nodular lesions throughout the retroperitoneum and mesentery. Adding to confusion of those unfamiliar with the patient's history, imaging findings may mimic carcinomatosis while encapsulated fat necrosis can mimic liposarcoma.

CASE 7

A 15-day-old girl was known to have a hepatic mass seen during a congenital anomaly scan, likely a hemangioma. The baby was born with APGAR score of 6 and 8, and diagnosed with patent ductus arteriosus and congestive heart failure.

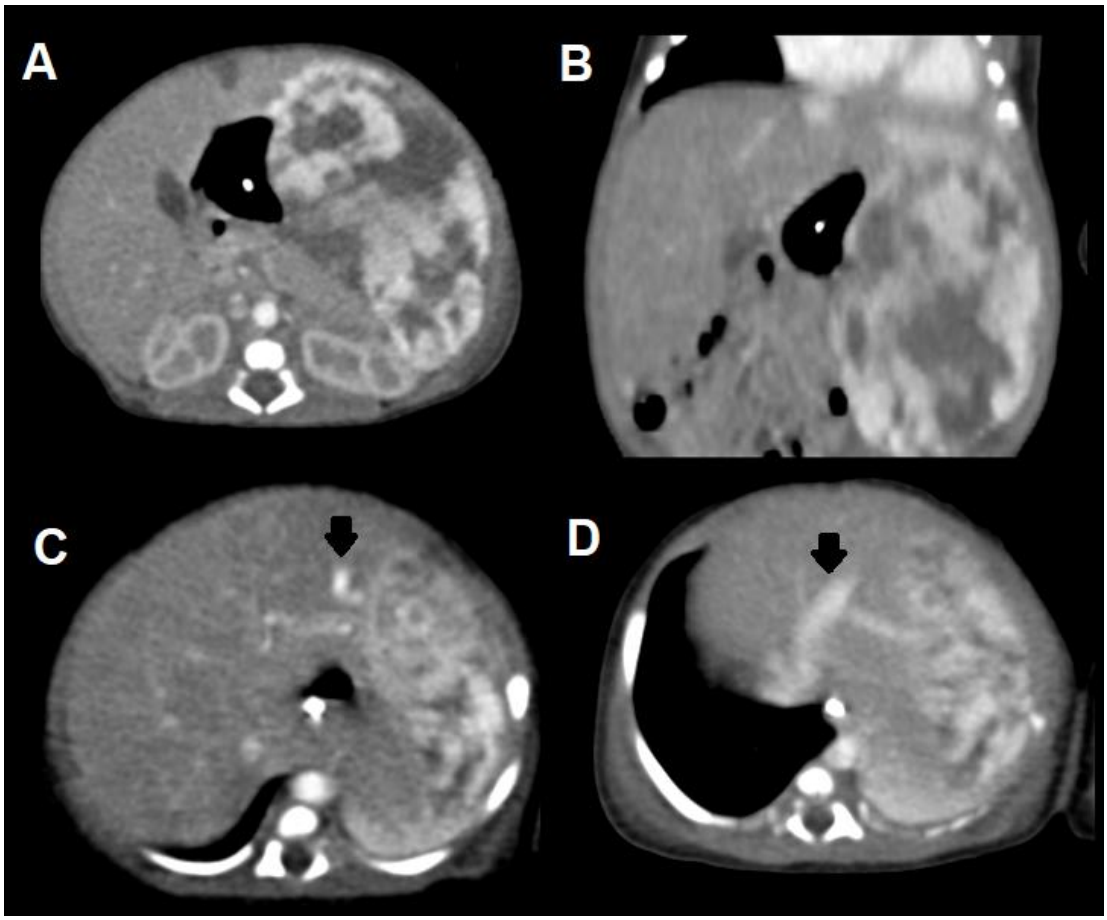

Fig. 7A–D Contrast-enhanced axial CT images of the abdomen show a (A,B) large vascular mass occupying the left hepatic lobe. (C) Arterial feeding vessels from the left hepatic artery (black arow), and (D) dilated draining left hepatic vein close to the lesion are identified, reflective of arteriovenous shunting

Question: Which imaging finding seen in this patient with Infantile Hepatic Hemangioma contributes to congestive heart failure?

Arteriovenous shunt (correct answer); An infantile hepatic hemangioma (IHH) is commonly asymptomatic, but 15% [11] of cases present with high-output cardiac failure with mortality of 70% to 90%. In the presented CT scan images, an arteriovenous shunt is present, which is the pathologic mechanism of congestive heart failure for patients with IHH. The shunt results in decreased systemic blood volume, with subsequent increased pulmonary blood volume (pulmonary hypertension) and resulting in cardiac output increase. 70% of all IHH-related deaths are caused by congenital heart failure [12], hence it is imperative that the arteriovenous shunts are reduced.

Treatment may be medical such as giving oxygen support, sedatives, diuretics and steroids. Transcatheter arterial embolism (TAE) is also strongly suggested for stabilization of heart failure in conjunction with pharmacologic therapy. For large hemangiomas and shunts however, these remain to be stop-gap measures with definite treatment being surgical resection and liver transplantation in some cases [11].

REFERENCES

1) Steggerda SJ, De Bruïne FT, Smits-Wintjens VE, Verbon P, Walther FJ, Van Wezel-Meijler G. Posterior fossa abnormalities in high-risk term infants: comparison of ultrasound and MRI. Eur Radiol 2015;*25*(9):2575–2583. https://doi.org/10.1007/s00330-015-3665-8.
2) Tsai P, Chen H, Ho C, Chiu N. Posterior fossa hemorrhage in a term neonate with hemophilia A. J Med Ultrasound 2018;26(1):56–58. https://doi.org/10.4103/JMU.JMU_10_18.
3) Heinz ER, Provenzale JM. Imaging Findings in Neonatal Hypoxia: A Practical Review. AJR Am J Roentgenol 2009;192(1):41–47. https://doi.org/10.2214/ajr.08.1321,
4) Van Cauter S, Severino M, Ammendola R, et al.. Bilateral lesions of the basal ganglia and thalami (central grey matter) — pictorial review. Neuroradiology 2020;62(12):1565–1605. https://doi.org/10.1007/s00234-020-02511-y.
5) Calvez S, Levy R, Calvez R, et al. Focal Areas of High Signal Intensity in Children with Neurofibromatosis Type 1: Expected Evolution on MRI. AJR Am J Neuroradiol 2020;41(9):1733–1739. https://doi.org/10.3174/ajnr.a6740.
6) Petrak B, Lisy J, Kraus J, Kyncl M, Zatrapa T. Focal areas of high-signal intensity on brain T2-weighted magnetic resonance imaging scans are significant for the diagnosis of neurofibromatosis Von Recklinghausen type 1. Pediatrics 2008;121(Suppl 2):S147. https://doi.org/10.1542/peds.2007-2022cccccc.
7) Dennis R, Anupindi S, Khwaja A. How to Diagnose Intussusception in Children. Appl Radiol 202150(1);19–27. https://doi.org/10.37549/ar2699.
8) Da Rocha EL, Pedrassa BC, Bormann RL, Kierszenbaum M, Torres L, D'Ippolito G. Abdominal tuberculosis: a radiological review with emphasis on computed tomography and magnetic resonance imaging findings. Radiologia Brasileira 2015;48(3):181–191. https://doi.org/10.1590/0100-3984.2013.1801.
9) Smith JR, Arnoletti JP, Varadarajulu S, Morgan DE. Post-pancreatitis Fat Necrosis Mimicking Carcinomatosis. Radiol Case Rep 2008;*3*(2):192. https://doi.org/10.2484/rcr.v3i2.192.
10) Devos H, Goethals L, Belsack D, et al. Fat misbehaving in the abdominal cavity: a pictorial essay. Pol J Radiol 2020;85(1):32–38. https://doi.org/10.5114/pjr.2020.93070.
11) Zhang X, Ren W, Song G, Xiao Y, Sun F, Wang N. Infantile hepatic hemangiomas associated with high-output cardiac failure and pulmonary hypertension. BMC Cardiovasc Disord 2019;19(1):216. https://doi.org/10.1186/s12872-019-1200-6.
12) Wang T, Wang Y, Liang Y, Lu G. Infantile Hepatic Hemangioendothelioma Associated with Congestive Heart Failure. Medicine (Baltimore) 2015;94(52):e2344. https://doi.org/10.1097/md.0000000000002344.

COMMENTARY

The Pediatric Radiology Journey of Northern Mindanao, Philippines: Insights and Experiences

Justin Luke D. Yap[1,2]

[1] Department of Radiology, Northern Mindanao Medical Center, Capitol Compound, Corrales Avenue., Cagayan de Oro City, Philippines

[2] Xavier University - Dr. Jose P. Rizal School of Medicine, Cagayan de Oro City, Philippines

Correspondence:
Department of Radiology, Northern Mindanao Medical Center, Capitol Compound, Corrales Avenue., Cagayan de Oro City, Philippines
Email: *justinyap21@gmail.com*

"It is not yet time." Too often, we try to rationalize situations that do not happen in our favor or meet our expectations with this statement. Some go as far as accepting that "it was not meant to be." Such was the case back in February 2020 when I had the opportunity to apply for the World Federation of Pediatric Imaging (WFPI) Observership Program [1] through the encouragement of my residency training officer, Dr. Roel Dilao, who introduced me to Prof. Bernard Laya - the country program coordinator. In the following month, the novel coronavirus disease (COVID-19) pandemic gripped the world and effectively postponed the applications for the program indefinitely. I thought**,** probably, it was not meant to be as the whole world was in a chokehold by a virus. It would take a two-year waiting period for the situation to normalize and the program to reopen.

I decided to apply after some soul-searching and knowing deep down I wanted to go into Pediatric Radiology. Thankfully, I was accepted into the said program for the Philippines. Prof. Laya and Dr. Nathan Concepcion, together with the entire St. Luke's Medical Center (SLMC) - Pediatric Radiology group (Fig. 1), gave me a warm welcome and offered to upgrade it further into a full fellowship, which I graciously accepted. I would go on to learn the intricacies of how to handle and approach pediatric imaging cases as well as realizing its uniqueness from adult imaging. I truly grasped the idea that children are definitely not small adults. We handled multiple pediatric imaging procedures daily and would come across one or two cases that would challenge us to read and study more. The routine cases also helped us master the techniques and protocols, which increased my confidence further along the way (Fig. 2).

Fig. 1 The St. Luke's Medical Center - Pediatric Radiology group (from right to left): Dr. Karl Josef Solidum, Dr. Marvin Bautista, Dr. Nathan David Concepcion, Prof. Bernard Laya, Dr. Mariaem Andres, Dr. Maricar Reyes, Dr. Jacqueline Austine Uy and Dr. Odina Gomez

Fig. 2 The author performing cranial ultrasound under the guidance of his mentor (not shown)

It was a dream come true. My days in training made me realize that the long wait was worth it. At the same time, I felt validated that this path I chose was indeed intended for me. The surprising thing was that it also became the path for my community. My practice is centered in Northern Mindanao, Philippines, which has a population of more than 5 million**,** wherein roughly 40% [2,3] of which are children, with no prior pediatric radiologist serving the area. With the guidance of my mentors, we were able to immediately impact the local community. A mere four months into my training, I was given the opportunity to share my learnings in pediatric radiology with the local radiologists through our organized chapter (Fig. 3). Key topics such as Image Gently were introduced

Fig. 3 The author giving a lecture for his local society of radiologists sharing his experiences and interesting cases gained from the World Federation of Pediatric Imaging (WFPI) observership

for the first time, which became an eye-opener to many. Monthly webinars prepared by the SLMC - Pediatric Radiology group were also shared with my local colleagues, which improved their understanding of important pediatric imaging topics such as white matter diseases and foreign bodies. Even after finishing the training program, my community is still reaping its benefits. We were able to produce a post-graduate course (Fig. 4) dedicated to both pediatricians and radiologists of

Fig. 4 Prof. Laya (center), the author (to his right) and Dr. Concepcion (to his left) together with the organizers and attendees of the 1st Pediatric Radiology post-graduate course held in Northern Mindanao, Philippines. The first of many scheduled lecture series all over the archipelago

Northern Mindanao, the first of its kind**,** and one that strengthened the partnership of doctors involved in the care of children. On a personal note, I was also given the opportunity to be a speaker at the Philippine Society for Pediatric Radiology mini-session during the Philippine College of Radiology Annual Convention discussing my research project done during fellowship training (Fig. 5).

Fig. 5 The author delivering his keynote presentation during the Philippine College of Radiology annual convention held February 2023

A lot has happened in just the past 12 months and I always find it amusing that we have accomplished so much for the country in the advancement of Pediatric Radiology, more so in the area of my practice. I have nothing but gratitude to WFPI and the *William Shiels* Memorial Foundation [1] for giving me an opportunity to carve my own path in this subspecialty while being ably guided by the greatest mentors in the country. I am beyond blessed to have met the likes of Prof. Laya, Dr. Concepcion, the rest of the SLMC - Pediatric Radiology group and their international counterparts, whom most have served as my inspiration in the pursuit of this craft. To paraphrase one of the biggest movie franchises, "the mission, if one should accept," is to image gently one child at a time. A mission I have wholeheartedly accepted and hopefully inspire more to do the same (Fig. 6).

Fig. 6 The author guiding the local radiology residents on how to perform ultrasound with special emphasis on pediatric imaging

REFERENCES

1. Observership - St. Luke's Medical Center, The Philippines. Available from: https://www.wfpiweb.org/Fellowships/ObservershipinthePhilippines.aspx. Accessed 10 July 2023.

2. Northern Mindanao. https://www.philatlas.com/mindanao/r10.html. Accessed 11 July 2023.

3. YAFS5 regional profile: Northern Mindanao. https://www.uppi.upd.edu.ph/sites/default/files/pdfyafs5-regional-profiles-NORTHERN-MINDANAO.pdf. Accessed 12 July 2023.